Master of Science Thesis

Characterization of Epoxy Nanocomposites by Space Charge Measurements and Breakdown Tests

Yonas T. Gebrekiros
1386085

Supervisor:
Dr. Ing. P.H.F. Morshuis

Thesis Committee:
Dr. Ing. P.H.F. Morshuis (TU Delft)
Prof. Dr. Ir. J. J. Smit (TU Delft)
Prof. Dr. M. Zeman (TU Delft)
Dipl. Ing. T. Andritsch (TU Delft)
Dipl. Ing. A. Lunding (Philips Healthcare DMC)

August 2009

Challenge the future

i. Summary

This thesis, *Characterization of epoxy nanocomposites with space charge measurements and breakdown tests*, tries to analyze the effect of introducing nanofillers of different types and fill grades in to neat epoxy and characterize them based on space charge measurements and breakdown tests. The thesis work was performed partly at TU Delft and partly at Philips Healthcare, Hamburg. Literature study of nanocomposites and space charge measurements, space charge measurements and analysis, preparation of nanocomposites, and preparation for the breakdown tests were performed at TU Delft. DC ramp breakdown tests and the analysis of the results were done at Philips Healthcare.

Approach:

A literature study was conducted on nanocomposites and their merit in improving the insulation characteristics of the base material. Basic understanding and possible improvements of insulation properties attributed to nanocomposites as employed for both DC and AC applications were also assessed. The mechanisms of space charge accumulation and the different procedures used to measure the amount and type of charges were dealt with in the literature study phase. Using the pulsed electro-acoustic (PEA) method, the space charge of about 13 samples of epoxy nanocomposites with Al_2O_3, AlN, MgO, and BN fillers containing different weight percentages was measured. The procedure was performed at field levels of 10, 15, and 18 kV/mm with about 1 hour of poling and depoling that ranged from 30 minutes to 90 minutes. The raw data was processed with a code written in MATLAB which basically performed denoising, deconvolution, correction for the attenuation and dispersion, and calibration. The final data contained information on space charge profile, field distribution, and potential profile throughout the thickness of the material. The results were then sorted out using time, amount of space charge, type of nanocomposites, weight percentage of nanocomposites, electric field, and approximate charging and discharging time constants as parameters.

For the break down tests that commenced at Philips Healthcare, Hamburg, a test cell was designed consisting of a set of two electrodes, to be immersed in oil to prevent an external flashover. As the electric field distribution in the case of DC application is dependent on the ratio of the conductivities of the insulator and the surrounding insulating medium, mineral oil in this case, conductivity measurements of the oil and the samples were performed. Conductivity values were obtained for the oil (Shell Diala B) with ample reproducibility. Still in the preparation phase for the breakdown testing, determining the number and size of the samples was of importance. Molds, good enough to prepare 4 samples at the same time, had to be designed and prepared. The last part in the preparation for the breakdown testing dealt with identifying the type of breakdown tests that need to be performed. Taking time in to consideration, it was decided to perform short time AC and DC breakdown tests. A ramp test was chosen over step-up test for both the DC and 600 Hz AC short time breakdown tests. As

dictated in the standards for AC and DC breakdown tests, 5 samples were needed from each batch of samples [1].

At Philips Healthcare, both DC and AC ramp breakdown tests were planned to be performed. The setup for the 600 Hz AC ramp test couldn't be realized in time, thus only DC tests were performed. DC ramp tests at 500 V/s on 25 batches with around 5 samples in each batch were first performed and the findings were analyzed. More DC ramp tests were later performed on the samples initially reserved for the AC tests. For the breakdown test, epoxy nanocomposites with Al_2O_3, AlN, MgO, SiO_2, SiO_2+Al_2O_3, SiO_2+AlN, and BN fillers were considered. The Weibull distribution was used to fit and analyze the breakdown results. The breakdown results were investigated to find possible correlation with the space charge characteristics of similar samples.

Results:

Some of the important results obtained from the space charge measurements and short time breakdown tests are summarized in the following.

From space charge measurements on epoxy nanocomposites with Al_2O_3, AlN, MgO, and BN fillers with varying loadings (0.5, 2, and 5wt%), and field strengths (10 kV/mm, 15 kV/mm, 18 kV/mm) the following main results were obtained.

- Homocharges were observed in all epoxy nanocomposites in the field levels considered during the full span of poling (1 hour).
- The average space charge was determined mainly by homocharges in front of the earth electrode, (i.e. space charge in the bulk of the samples was very small compared to peak homocharge.)
- MgO-Epoxy nanocomposites displayed very low homocharge peak at the earth electrode at all the field levels. At 18 kV/mm, and by the end of 1 hour of poling, the peak homocharge on all of the MgO nanocomposites was at least half of what was observed for neat epoxy (which was about 1.0 C/m^3). The average space charge followed a similar trend.
- For 5wt%_MgO-Epoxy nanocomposite, by the end of 1 hour poling, 37% decrease in the peak homocharge at the cathode was observed when the field was increased from 15 kV/mm to 18 kV/mm. This decrease was also observed in the average space charge.
- Epoxy nanocomposites, with MgO, BN, and (0.5, 2wt%)AlN fillers, where a rapid accumulation (to a stable value) of space charge was observed, a fast decay of space charge was also observed during depoling.

- Higher average space charge for higher wt% of AlN & Al_2O_3 fillers (5wt%), was observed as compared to 0.5 and 2wt% of the filler.

DC ramp breakdown results on epoxy nanocomposites with Al_2O_3, AlN, MgO, SiO_2, SiO_2+Al_2O_3, SiO_2+AlN fillers and fill grades of 0.5, 2, 5, 10, and 15wt% will be summarized. Besides, breakdown results for 10wt%_BN-Epoxy with filler sizes ranging 70 nm to 5 μm will be presented. In general, better DC ramp breakdown field strength was observed for the nanocomposites than neat epoxy.

- Nanocomposites with Al_2O_3, MgO, and SiO_2 fillers scored the highest DC ramp breakdown field strength for 0.5wt% filler content.

- For Al_2O_3-Epoxy nanocomposite, highest value of η (scale parameter), and hence higher breakdown field, was observed for 0.5wt% of the filler. Further increase to 2wt% resulted in lower field strength and the values were similar for the rest of the filler loadings above this value.

- In most of the cases, the dispersion of the breakdown data increased with increase of filler grade. This was observed for Al_2O_3, SiO_2, and Al_2O_3+SiO_2 fillers tallying decrease in β (shape parameter) with increase in filler grades.

- For 10wt%_BN-Epoxy, the increase in filler size from nano to micro resulted in a decrease in the breakdown field strength.

- Of all the batches, nanopox with 0.5wt% SiO_2 scored the highest scale parameter η=296.5 kV/mm with very narrow 90% confidence bound, hence, a high value of β=15.3.

ii. Acknowledgements

I would first want to thank TU Delft for offering me the scholarship to study at the university. My heartfelt gratitude goes to my supervisor Dr. Morshuis for being so helpful throughout the span of my thesis. I also want to thank Dipl. Ing. T. Andritsch for his help.

At this point I would like to thank members of the High voltage laboratory, TU Delft for their assistance. I also want to thank employees of Philips Healthcare in general and my special thanks go to Frank and my daily supervisor at Philips Dipl. Ing. K.M. Ress for being so cooperative and friendly.

I wouldn't close without passing my gratitude my parents in Ethiopia who have been morally on my side. Furthermore, I would like to thank Leake and Mulugeta for their kindness and being great friends. Last but not least I would like to thank my dearest, Rishie.

iii. List of abbreviations

AC	Alternating Current
AlN	Aluminum Nitride
Al_2O_3	Aluminum Oxide
BN	Boron Nitride
DC	Direct Current
DPZ	Damage Process Zone
EBM	Electron Beam Method
EPA	Environmental Protection Agency
HEPA	High Efficiency Particulate Air
HV	High Voltage
IEC	International Electrotechnical Commission
LDPE	Low-Density Polyethylene
LIM	Laser Intensity Modulation
LIPP	Laser Induced Pressure Propagation
MgO	Magnesium Oxide
nm	Nanometer
NMMC	Nano- and microfiller mixture composite
PD	Partial discharge
pH	Power of Hydrogen
PIPWP	Piezoelectric Induced Pressure Wave Propagation
PEA	Pulsed Electro-Acoustic
PMS	Philips Medical Systems
PPE	Personal Protective Equipment
PVDF	Polyvinylidene Fluoride
PWP	Pressure Wave Propagation
TEM	Transmission Electron Microscopy
TiO_2	Titanium Oxide
TPM	Thermal Pulse Method
TSM	Thermal Step Method
XLPE	Cross linked Polyethylene

Table of Contents

1. Introduction

In high voltage DC (HVDC) systems, one of the important parts worth a careful selection is the insulation material. As the demand for higher withstand voltages and smaller dimensions incessantly grows, the need for materials with improved properties rigorously rises. HVDC can be employed for energy applications like in high voltage cables and connectors or non-energy applications where insulation for HVDC application in X-ray systems can be cited as an example. Insulation properties for DC applications not as much investigated as for AC, added to the complications of designing for DC applications due to space charges, makes the area challenging.

Epoxy and epoxy based composites are preferred insulating materials for several electrical applications, such as printed circuit boards, bushings, GIS spacers, generator ground wall insulation systems, cast resin transformers. Excellent adhesive properties, resistance to heat and chemicals, good mechanical properties and very good electrical insulating properties make epoxy a favored insulating material [2]. Recently, epoxy based nanodielectric systems are being increasingly investigated for their electrical properties, since the introduction of nanofillers render several improvements in their properties. Compared with unfilled epoxy or epoxy systems with micrometer sized fillers, epoxy nanocomposites have displayed enhanced properties, as in e.g. [3].

From literature, it appears that investigation of DC properties focuses mainly on the introduction of nanofillers to XLPE. Besides, literature results on epoxy based nanocomposites circled around TiO_2, Silica, and Al_2O_3 fillers. As different filler materials were considered in this thesis, finding ample literature to compare measurement results was a challenge. Even though epoxy nanocomposites with various fillers types and weight percentages were considered, the space charge measurements being limited to very low field strengths, strong assertions on the space charge characteristics of the nanocomposites made at this stage could only be fairly plausible. However, space charge measurements for higher field strengths and more types and loading of nanofillers will be performed in a different package, separately from this thesis work. This will hopefully render a broader picture in the understanding of the DC insulation properties of the epoxy nanocomposites under consideration.

This introductory chapter has four sections. Description of the goal of the thesis is presented first. The scheme followed to attain the goal is then illustrated in the '*Approach'* section. To show the reason for the stay at Philips Healthcare, Hamburg, a subsequent section comes to being. The final section of this chapter illustrates the outline of the thesis.

1.1. Objective

The main goal of this thesis is:

> *Characterization of electrical insulation properties of epoxy nanocomposites with different filler types and fill grades by performing space charge measurements and DC ramp breakdown tests.*

The goal has the following sub-goals:

- ✓ To find out the space charge characteristics of epoxy nanocomposites
- ✓ To understand the DC ramp breakdown characteristics of epoxy nanocomposites
- ✓ To correlate the breakdown characteristics and the space charge behavior of epoxy nanocomposites

1.2. Approach

To attain the objectives of the thesis the following approach was adopted. To gain more insight about nanocomposites, space charges and space charge measuring techniques, an elaborate literature study was essential. For the nanocomposites at hand, space charge measurements were performed at TU Delft. Alongside to the space charge measurement, for the DC ramp tests that took place at Philips Healthcare, preparations were conducted. The major ones were conductivity measurement of samples, conductivity measurement of the oil to be used in the breakdown test setup, and design of electrodes that were to be used for breakdown tests. An important part of the thesis was the breakdown test. This part was executed in cooperation with Philips Healthcare and was performed at their site in Hamburg. After finishing the space charge measurements and all the necessary preparations at TU Delft, DC ramp breakdown tests were performed at the development department of Philips Healthcare, Hamburg. The test results were analyzed, and conclusions were made from the perspective of the space charge measurements and DC ramp breakdown test results. It was also tried to associate both results.

1.3. Stay at Philips Healthcare

Two types of tests have been performed in the characterization of epoxy nanocomposites. The first one was the space charge measurement that was executed at TU Delft. The breakdown tests, on the other hand were performed at Philips Healthcare in Hamburg. Travelling all the way to Germany to perform the breakdown tests was backed with the following reasons, among others:

- ✓ Due to the time limit and the number of samples considered, when the choice of performing short time breakdown tests was final, ramp test was favored and it could only be performed at Philips Healthcare due to the unavailability of the setup at TU Delft. This

was favored by the long and ongoing research cooperation between TU Delft HV group and Philips Healthcare.

- ✓ I was eager to do my thesis in a company so that I will get a feeling of how my work would be used to application, possibly in the long run.

Cognizant to the points above, a stay at Philips Healthcare was approved worthwhile and the following actions were planned to be performed:

- ✓ A familiarization to the premises and facilities of Philips Healthcare, especially, X-ray generator insulation and hybrid material.
- ✓ Preparing the setup for DC ramp test.
- ✓ Performing the DC ramp test.
- ✓ Preparing a setup for 600 Hz AC ramp breakdown test: this frequency was chosen to investigate the AC stress imposed on the samples while switching the DC generator (1 ms rise time).

The AC ramp test was not carried out due to problems of preparing the setup. Hence, more DC tests could be performed on the samples that were supposed to be stressed with AC. It was unfortunate that a change of plan had to be made in the last stage of the project. On the other hand, performing more DC ramp breakdown tests helped to follow the IEC 60243 standard [1, 4] well. As prescribed in the standard, the test should be performed on 5 samples and if any one of the results deviates from the mean value with more than 15%, that result should be discarded and 5 more samples tested. This rule was not strictly followed in the first round due to the limitation in the number of samples. Samples that were reserved for the AC ramp tests were then used for the DC ramp tests.

1.4. Outline

This thesis has 6 chapters and two appendices. In this section the structure of the thesis is outlined.

Chapter 2 discusses nanocomposites: definition, properties, applications, preparation procedures and safety issues related to nanocomposites (during application and preparation). Chapter 3 starts with theoretical description of space charges, and space charge measurement techniques and goes on to the analysis and presentation of space charge measurement results.
Chapter 4 begins with the preparation undertaken for the breakdown tests that took place at Philips Healthcare; it then discusses the measurement protocol and presents the results of the breakdown test in the last section.
Chapter 5 hosts the conclusions drawn from the space charge measurements and breakdown tests and winds up with a recommendation and proposal for further work.
Different figures/plots and tables are presented in the appendices.

2. Nanocomposites

Nanotechnology, sometimes shortened as '*nanotech'*, deals with the manipulation and manufacturing of structures of which at least one of the dimensions is less than 100 nanometers [5, 6]. Nanotechnology has the potential to create and is creating many new materials and devices with wide-ranging applications, such as in medicine, electronics, and energy production. On the other hand, nanotechnology raises many of the same issues as with introduction of any new technology, including concerns about the toxicity and environmental impact of nanomaterials.

Nanocomposites can be found naturally or, as is mostly the case, prepared artificially. Spider silk can be mentioned as an example of naturally occurring organic nanocomposite [5]. Owing to their nanometric sizes, the nanofillers yield higher interfacial areas as compared to microfillers of the same volume. Dielectric properties of a nanofilled material are therefore commonly characterized by the interface regions, rather than by the filler [7]. The true start of nanocomposites history is in 1990 when Toyota first used clay/nylon-6 nanocomposites for Toyota car in order to produce timing belt covers. Today, nanocomposites are used in various applications. A brief look at new, common commercial uses reveals automotive panels for sports utility vehicles, polypropylene nanocomposites for furniture, appliances, and bulletin board substrates. Advanced technologies implemented include magnetic media, bone cement, filter membranes, aerogels, and solar cells. Table 2.1 [8], presents some of the nanocomposites and their characteristics in comparison to the base material.

Table 2.1 Commercial polymer nanocomposites [8]

Product	**Characteristics**	**Applications**	**Producer**
Nylon Nanocomposites	improved modulus, strength, heat distort temperature, barrier properties	automotive parts (e.g. timing belt cover, engine cover, barrier, fuel line), packaging , barrier film	Bayer Honeywell Polymer RTP Company Toyota Motors Ube Unitika
Polyolefin nanocomposites	stiffer, stronger, less brittle, lighter, more easily recycled, improved flame retardancy	step-assist for GMC Safari and chevrolet Astro vans, heavy-duty electrical enclosure	Basell, Blackhawk Automotive, Plastics Inc, General Motors, Gitto Global Corporation, Southern Clay Products
M9	High barrier properties	Juice or beer bottles, multi-layer films, containers	Mitsubishi Gas Chemical Company

Durethan KU2-2601 (nylon 6)	Doubling of stiffness, high gloss and clarity, reduced oxygen transmission rate, improved barrier properties	Barrier films, paper coating	Bayer
Aegis NC (nylon 6/barrier nylon)	doubling of stiffness, higher heat distort temperature, improved clarity	medium barrier bottles and films	Honeywell Polymer
Aegis TM OX	Highly reduced oxygen transmission rate, improved clarity	High barrier beer bottles	Honeywell Polymer
Forte nanocomposite	improved temperature resistance and stiffness, very good impact properties	automotive furniture appliance	Noble Polymer

2.1. The role of the interface

It is now well recognized that composite properties are typically more than the sum of the individual components because of interfacial interactions. Hence, as the size of the composite component phases is reduced, the extent to which interfacial interactions contribute to materials' properties increases. Indeed, materials at interfaces can constitute a separate phase, sometimes called the 'interphase' [9]. This approach helps to understand why this significant variation (improvement) in electrical and/or other behaviors is observed with the addition of a very small percentage of nanofiller into the base material. The explanation is as follows: as the size of the nanofiller becomes smaller, the surface interaction becomes dominant and the nanofiller affects the electrical properties even at very small weight proportions. This increased interfacial area, however, is not the only factor that brings about the changes in electrical properties. The improvements in dielectric properties observed for nanofilled polymers could also be due to the following factors: the large surface area of nanoparticles which creates a large 'interaction zone' or region of altered polymer behavior, changes in the polymer morphology due to the surfaces of particles, and/or a reduction in the internal field caused by the decrease in size of the particles [10]. It is stated in [11] that interface properties become increasingly prominent if the

first phase is a particle of finite size and surrounded by a host material. This is the situation for a composite dielectric and, as shown in fig. 2.1, the total interface contribution can become very significant as the particle diameter is reduced. This effect is graphically portrayed in fig. 2.2 of [5].

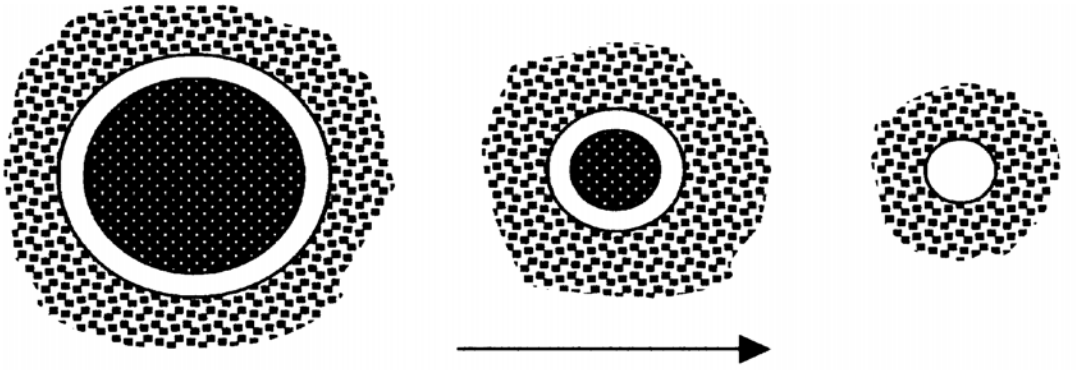

Fig.2.1 Interface properties become increasingly dominant as the particle size is reduced [11].

It must be noted at this point that one of the challenges with Nanocomposites is developing synthetic approaches that precisely define the size of particular phases, their periodicity, and the interfaces between components [10].

2.2. Improved electrical insulation properties of nanocomposites

As many improvements in material properties are harnessed from using nanocomposites, a lot of electrical properties are also seen to have been enhanced making use of nanocomposites. Quite a few literature results show enhancement of electrical properties using nanocomposites. One of the significant advantages of using nanoscale fillers instead of micrometer-scale fillers may be an increase in the breakdown strength. Ajayan [5] mentions that, the permittivity of polymers can be increased with the addition of many metal oxide fillers, on both the micro- and nanoscale. The use of micrometer-scale fillers, however, might result in a significant decrease in breakdown strength due the field concentration created by the particles.

Due to the improvement of the electrical properties of insulating materials, attributed to the introduction of nanofillers, for both DC and AC applications special attention is drawn to this field and a lot of research is being conducted in selecting the right filler materials and ways to homogenously disperse the filler. In the subsequent subsections, summary of improved electrical properties both for DC and AC applications due to the introduction of nanocomposites will be given.

2.2.1. Nanocomposites for AC applications

Treeing resistance, resistance to surface degradation due to surface discharges, breakdown strength, and loss coefficient (tan-δ), among others, are used to describe AC electrical properties. Generally, some nanocomposites show improved electrical properties as compared to the base material.

Nanocomposites can be designed to be more resistant to treeing and hence the life of the insulator will be longer than for the base material alone or the microcomposite counterparts. Expectations that a fundamental change in the material properties arises becomes obvious if one considers an electrical tree channel propagating through the material which is interacting with many nanoparticles instead of only a few microparticles [7]. Particles introduce submicron-defects to be generated around the dispersed particles, which expands the tip of the tree (expansion of the Damage Process Zone, DPZ) that in turn renders higher treeing resistance and hence the insulator lifetime fig. 2.2. When a tree encounters the filler, it propagates along the interface between resin and filler. This propagation is repeated until the tree reaches the ground electrode and breakdown occurs. The increased frequency of these encounters in nano- and micro-filler mixture prevents treeing from propagating effectively [12].

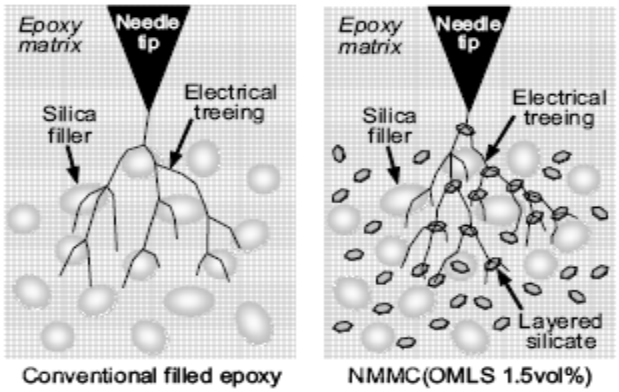

Fig. 2.2 Expansion of the Damage Process Zone (DPZ) [11]

Another important effect observed was that the ratio of lifetime of the nanocomposite to the base epoxy resin increases with temperature. This can be attributed to the decrease in internal stress due to the rise in temperature of the nanocomposite. Besides, adding small weight percentage of a nanocomposite, the peak value of tan-δ is shifted to a higher temperature. Addition of small amount of micro particles with the same percent weight didn't change results from the original base material [7].

The introduction of both nano- and microfiller mixture (NMMC) to an epoxy matrix has a profound effect on insulation breakdown strength and time to breakdown. The NMMC shows densely packed structure in comparison to conventional filled epoxy. This increases the breakdown strength and insulation lifetime but tends to increase resin viscosity and cost [12].

Several dielectric properties of epoxy nanocomposites have been evaluated in the last couple of years and the permittivity and tan delta values in some nanocomposites are reported to be lower than that of base epoxy and microcomposites when insulating oxides are used as the fillers. A similar reduction in the values of permittivity and tan delta were also observed when layered nanosilicates were dispersed in epoxy [3]. Similarly, a higher ac electrical breakdown time is recorded in epoxy composites with Al_2O_3 nanofillers as compared to unfilled epoxy [2, 12].

Some other strong suits of nanocomposites for AC application are listed in the following lines.

- ✓ Surface treated nano particles incorporated in XLPE eliminate the dispersion in the relative permittivity observed in the base resin at 1 Hz [13].
- ✓ TiO_2 nanocomposites are more resistant to PD (erosion) than epoxy without fillers or with micro-fillers [14].
- ✓ Surface roughness of Polyamide nanocomposites caused by partial discharge was far smaller than in specimens without the nanofiller, i.e. Polyamide with nanofiller is more resistant to PD than the specimen without [15].

2.2.2. Nanocomposites for DC application

The most significant DC electrical properties are space charge accumulation, DC breakdown strength, and volume conductivity. Apart from other factors, the DC breakdown strength could be affected by the accumulation of space charges and might be improved with the addition of nanofillers depending on the type of the filler material. Some examples that witness improvement of the DC insulating characteristics by using nanocomposites will be shown in the following paragraphs.

LDPE_MgO-nanocomposite at 5wt% of the filler, showed an increase in volume resistivity by about two orders of magnitude as compared to the LDPE base. Besides, the amount of space charge in LDPE under high electric field is reduced due to the addition of nano sized MgO-filler [16].

It is suggested in [7] that micro-sized TiO_2 particles incorporated in LDPE increase electronic charge injection from the electrode, and also act as charge traps in the bulk. Consequently, the density of space charge in the bulk and its electrical conductivity increased. Nanoparticles on the other hand don't act as efficient charge traps in the bulk. They appear to render the electrode/LDPE interfaces partially blocking, causing heterocharge formation adjacent to the electrodes.

The introduction of nanofillers increases the accumulation of space charges at low DC fields whereas an increase is observed at medium voltages. This is advantageous if used for HVDC applications [17]. As space charge accumulation causes field enhancement in some parts of the insulation system, it could be fatal for HVDC systems.

Introduction of industrially produced layered silicate, nanofiller, to LDPE increased space charge density considerably. The composites, however, showed improved AC performance [7]. In epoxy nanocomposites filled with TiO_2 fillers, the AC voltage endurance, short-term DC and AC dielectric strengths and impulse breakdown strengths are found to be higher as compared to microcomposites [3].

2.3. Safety issues

Health and environmental issues related to the use and preparation of nanomaterials is a very broad topic. In this section, a summary of the concerns mentioned in the whole life cycle of nanomaterials will be presented.

The threats of using nanomaterials can be assessed using the *risk assessment paradigm* or the *life cycle perspective*. In the first case, the risk is characterized by making use of exposure assessment and dose-response assessment. The dose-response assessment is obtained from the hazard identification phase, where chemical and physical properties of the nanomaterials are identified. The second method of assessment, life cycle perspective, makes use of the life cycle of the material where the effects of preparation of the nanomaterials (worker exposure), industrial emissions, consumer exposure, disposal by the end of life are all boiled down to human and ecological hazards. One of the main challenges in assessing the risks associated with using nanomaterials, however, is the diversity and complexity of nanomaterials which makes the chemical identification difficult [18].

The following major effects can be considered regarding to the effects of nanomaterials on the environment [18]:

- ✓ *Nanomaterials in air:* particles in the range of (80- 2000) nm, are described as being in the accumulation mode and can stay in the air for as long as weeks. They can be inhaled or ingested.
- ✓ *Nanomaterials in soil:* chemical and physical properties dictate the rate of sorption.
- ✓ *Nanomaterials in water:* their fate is controlled by aqueous solubility, interaction with chemicals in the system, and the biological and abiotic[1] processes.
- ✓ *Bioavailability and bioaccumulation of nanomaterials:* Consumption of nanosized particles by bacteria and living cells which might be a potential for bioaccumulation in food chain.

[1] Abiotic describes the physical and chemical aspects of an organism's environment

Human exposure to nanomaterials is another important issue. There are a lot of potential sources and mechanisms by which humans may be exposed to nanomaterials: some of them are summarized below[18].

- ✓ *Occupational exposure:* workers can be exposed to nanomaterials during synthesis of nanoscale materials, while working with nanopowders, during disposal of products containing nanoscale materials.
- ✓ *Release and general population exposures*: environmental releases from the production and use of nanomaterials and direct of use products containing nanomaterials.

As the horizon of use of nanomaterials expands, the ways of exposure to humans diversifies. The following list highlights possible path ways of exposure:

- ✓ Inhalation exposure
- ✓ Ingestion exposure
- ✓ Dermal exposure
- ✓ Ocular exposure

Good understanding of the chemical behaviors and their adversities to humans or the ecosystem in general is the first step in mitigating the problem of nanotoxicity. Methods identified in controlling exposures to nanomaterials include [19]: use of HEPA filters, enclosures, local exhaust ventilation, fume hoods, and magnetic filter systems for magnetic oxide nanofillers can be mentioned among the control methods. Besides, while working with nanocomposites, it is advisable to use properly fitted respirators with a HEPA filter as personal protective equipment (PPE).

2.4. Preparation of epoxy nanocomposites

A lot has been said about nanocomposites and the improvements they render in their respective areas of application: mechanical, thermal, electrical, and some more. How well the nanofiller is distributed and dispersed in the matrix of the base material, determines the expected improvement. The enhanced properties, if any, would then be liable to how well the preparation procedure is executed. Ajayan [5], explains the dispersion and distribution of the nanofiller as follows: Distribution describes the homogeneity throughout the sample and dispersion describes the level of agglomeration. Lack of proper dispersion and distribution of the filler, the high surface area is compromised and the aggregates can act as defects, which limit properties. Cognizant to this fact, the processing of nanocomposites stays to be a bottle neck in the commercialization process.

To date, several methods for the preparation of nanocomposite are recognized: intercalation, Sol-gel, molecular composite and direct dispersion, table 2.2. *The intercalation method* is the

most popular for polymer nanocomposite formation where polymers are intercalated between layers of inorganic layered substances to cause to disperse them into polymers during polymerization. The *sol-gel* method, which presently is attracting a lot of attention, might be easily modified to suit to industrial manufacture. This method is characterized by the fact that inorganic or composite organic-inorganic materials are made at relatively low temperatures, and in principle, consists of hydrolysis of the constituent molecular precursors and subsequent polycondensation to glass-like form [20]. In the direct dispersion method, which was used to create specimens for this thesis, nanoparticles are chemically modified to increase compatibility with polymers, and are subsequently mixed with a polymer and dispersed homogenously without agglomeration. Summary of the preparation methods is presented in table 2.2, details about the methods can be found in [5].

Table 2.2 Nanocomposite preparation methods

(1) Intercalation method (a) Polymer or pre-polymer intercalation from solution (b) In-situ intercalative polymerization (c) Melt intercalation
(2) Sol-gel method
(3) Molecular composite formation method
(4) Nanofiller direct dispersion method
(5) Other methods

2.4.1. Choice of filler materials

It is reported that the major role in improvement of the material properties (electrical, mechanical, and thermal) is played by the size of the filler more than by the chemistry of the particles [21]. Hence, different nanofillers with different filler sizes have been investigated for this thesis. The base material used for all the nanocomposites was an epoxy resin, bisphenol-A type resin (CY231) and anhydrite hardener (HY925) from Huntsman. The specification of the type of nanofiller and their average particle size are given in table 2.3.

Table 2.3 Nanofillers and particle sizes used for the thesis

Nanofiller	***Average particle size according to TEM (nm)***
Al_2O_3	*30-50*
Al_2O_3(Conventional)	*4000*[2]
AlN	*60*
BN	*20*
MgO	*22*

In his report, Andritsch [22] mentions the reasons for selecting the nanofillers that are used now.

[2]Primary particle size from datasheet

Al_2O_3: Common material both nanoscale and conventional size, proof of concept for comparison with work from others
MgO: Indications that the nanoparticles can reduce the amount of space charges
BN: Similar structure to MgO, and high thermal conductivity
AlN: Semiconducting material with high heat transfer rate, used for comparison with alumina

2.4.2. Choice of filler percentages

For small particle sizes, a large surface area is already reached for small percentages of the filler. Filler concentration of even less than 1% in weight, therefore, might already bring a significant change in the properties of the base material [3]. On the other hand, lower concentrations of the filler material might pose difficulty in the dispersion process. The explanation to this effect might be that the lower the filler content is, the smaller the amount of particles that shear against each and the less effective the mixing process, resulting in agglomerations [22]. It is, therefore, important to consider a wide range of filler percentages and try to investigate the dispersion mechanism and the electrical properties. For this thesis, a wide range of weight percentages has been considered: 0.5, 2 and 5wt% of the nanofiller were typically used for the space charge measurements and 10 and 15wt% were used in addition to the above percentages for the breakdown tests.

2.4.3. Preparation of nanocomposites at Delft ChemTech.

In this section, the steps practiced at Delft ChemTech to prepare MgO-Epoxy nanocomposite will be discussed. The preparation of MgO-Epoxy nanocomposites consisted of two parts. The first part included the dispersion of the nanocomposite powder in ethanol and making sure the alcohol is fully removed from the solution. The second part incorporates the mixing of the (nanofiller + epoxy resin mixture) with a hardener and putting the solution in a mold and finally obtaining the desired shape.

Step 1:
The MgO nanofiller (powder form), with average size of less than 22 nm, is first dispersed in ethanol and put in an ultrasonic bath. This step prevents the nanocomposites from sticking to each other. This was followed by the addition of formic acid so as to reach a ζ-potential[3] (zeta-potential) approximately 0. This is done by adjusting the pH of the solution, where 3 is the value needed for MgO [22]. To disperse the nanoparticles, the solution is put in an ultrasonic bath for about 1.5 hours. The next step was addition of s*ilane (3-Glycidoxypropytrimethoxysilane)* for surface functionalization of the filler. The surface functionalization procedure can be similarly applied to Al_2O_3 filler. Surface functionalization process for aluminum oxide [23] is illustrated in fig. 2.3.

[3] ζ-Potential: the potential difference between the dispersion medium and the stationary layer of fluid attached to the dispersed particle.

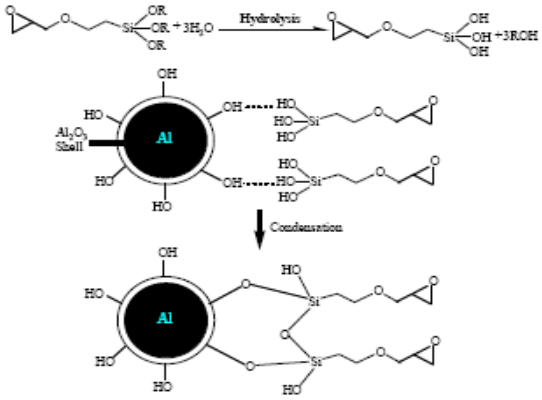

Fig. 2.3 Schematic showing the reactions of silane coupling agent with aluminum particle surface [23]

The solution is then put in an ultrasonic bath. At this point it can be said that the molecules of the nanofiller are well dispersed in the ethanol solvent. After this step, epoxy resin (CY231), is added to the mixture and the solution is mixed in a high shear mixer with a rotational speed of typically 3000 rpm for about 15 minutes and put in an ultrasonic bath before the solution is put in a vacuum oven. This step is necessary to avoid overflow of the mixture as it tends to highly expand. Finally the ethanol- epoxy resin-nanofiller mixture is put in a vacuum oven and heated to a temperature of 90^0C, above the boiling point of ethanol. It stays in the oven from 2-3 days until all the ethanol has evaporated.

Step 2:

The second part of the preparation is performed as follows. The alcohol free solution is mixed with a hardener (HY925) and put in a mixer with a speed of 6000 rpm for about 15 minutes. The mixture is then degassed as follows. First it is put in an ultrasonic bath (*Branson 2510* with mean frequency of 42 kHz). This was an immediate step to prepare the solution for vacuum degassing. The solution is then put in vacuum for some time before it is poured in to a mold. Finally, the solution is cured in an oven at 140^0C for about 3 hours. The samples considered in this thesis had a diameter of 56 mm, an average thickness of 0.6 mm. A typical sample is shown in fig. 2.4.

Fig. 2.4 5wt% Al_2O_3-Epoxy nanocomposite

3. Space charge characterization of epoxy nanocomposites

In high voltage DC, both for energy and non-energy applications, a design that doesn't incorporate the effect of space charges is almost unthinkable. Accumulation of space charges in the insulation system makes the electric field distribution non-Laplacian. In other words, the *Laplacian field* distribution equation 3.1a (distribution where space charges do not exist) becomes *Poissonian* equation 3.1b. This results in field concentrations in some parts of the DC insulation system. This might in turn create a weakest link for dielectric breakdown, and hence a partial or total failure of the insulation system. This might become very severe in case of polarity reversal where the field due to the space charge adds up to the applied field.

$$\frac{dE(x)}{dx} = 0 \tag{3.1a}$$

$$\frac{dE(x)}{dx} = \frac{\rho(x)}{\varepsilon_0 \varepsilon_r} \tag{3.1b}$$

Equations 3.1a and 3.1b represent Laplacian and Poissonian field in one dimension respectively. $E(x)$ represents the electric field, ε_0 the permittivity of free space, ε_r the relative permittivity of the material, and $\rho(x)$ represents the space charge along the thickness of the material.

This chapter starts with how these space charges are formed in solid insulating materials under the application of DC voltage. In the subsequent sections, highlights of different space charge measurement techniques with detailed discussion of the PEA method and the results obtained using this setup at the HV laboratory of TU Delft are discussed. The analysis of the results and discussions close the chapter.

3.1. Space charge formation

Complex physical processes are associated with this topic and it will be instructive to have a look at [24] for the details. Some basic points about the formation and types of space charges will be discussed in this subtopic.

Important points in the study of generation of space charges are the following: [24]

- ✓ *Injection*: Emission or extraction of charges from the electrodes.
- ✓ *Conduction*: Movement of charges in the dielectric
- ✓ *Trapping*: Locking of charge carriers in discrete locations in the polymer chains.

Accumulation of space charges occurs at locations where the current density is divergent. This means, when the flow of charged particles into a region of space differs from the flow out of that region, a net charge will build up in time in this region. This divergence in current density is exhibited in a lot of cases some of which are dielectric-electrode interface, dielectric-

dielectric interface, when a temperature gradient is present, and in case of inhomogeneity. For this thesis, since single flat samples are considered, electrode-dielectric interface and inhomogeneity are of importance.

Based on the difference between injection and transport currents, three conditions can occur. When the injection and transport of charge carriers are equal, the interface is considered ohmic and space charge build up is not observed. In the case when more charge carriers are injected than transported, a space charge with the same polarity as the electrodes is generated. This type of charge is called homocharge. Depending on the depth and distribution of traps, some time is needed till this charge vanishes when the applied voltage is removed. A sample with homocharges is illustrated in fig. 3.1. On the other hand, when charge carriers move faster along the dielectric than the electrodes can supply, space charge with opposite polarity of the electrodes, heterocharges, develop on the interface. Heterocharge in a sample is schematically shown in fig. 3.2. Compared to the Laplacian field, a decrease in the field along the electrode sample interface is observed. The bulk of the sample on the other hand, is stressed with a field higher than the Laplacian field. The opposite is true in the case of heterocharges.

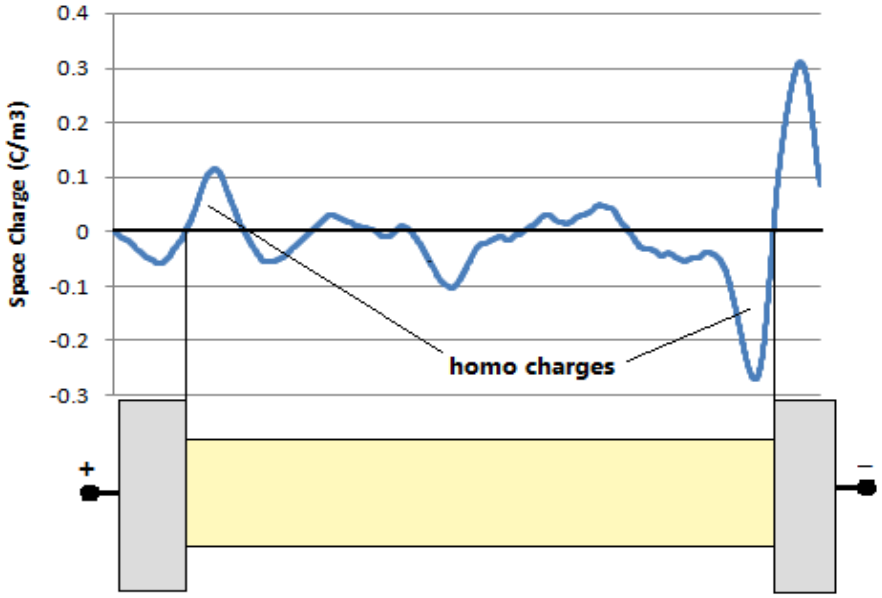

Fig. 3.1 Homocharges on 0.5wt%_MgO-Epoxy Nanocomposite (1 hr poling at 18 kV/mm)

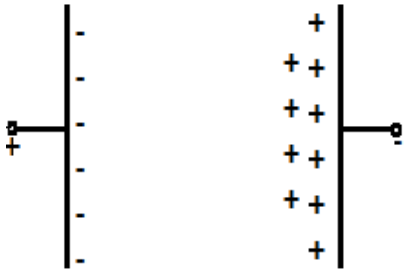

Fig. 3.2 Heterocharges on the electrode dielectric interface

3.2. Space charge measurement techniques

A deep interest in space charges has led to the development of a number of methods to measure their amount, polarity, and location in a dielectric. It would be important to understand why the knowledge of the amount and location of space charges does any good. As mentioned in the start of the chapter, the existence of space charges distorts the electric field and creates field enhancements in some parts of the insulation. Thus, knowing how much charge is trapped and where it is trapped will tell us the areas of the insulation system where field enhancements are likely to occur and hence the location(s) that is (are) likely to be the weakest points in the insulation system.

Space charges, unlike surface charges, are more difficult to measure, especially in solid dielectrics. The easiest and destructive way to measure space charges would be, cutting of slices from the dielectric and measuring the charge on each slice [24]. This, however, is not an effective method as there could be discharging through the cutting instrument apart from its being destructive. In the course of time, a number of nondestructive measurement methods were developed. Table 3.1 summarizes the excitation and outputs of the space charge measurement methods commonly used in on solid dielectrics.

Table 3.1 Measurement methods for space charge distribution [25]

Measurement Method	**Excitation Method**	**Measurement Signal**
PIPWP	Nanosecond pressure pulse	Nanosecond electric signal
LIPP	Nanosecond pressure pulse	Nanosecond electric signal
PEA	Nanosecond electric pulse	Nanosecond pressure signal
TSM	Thermal step	Electric current
TPM	Thermal pulse	Electric signal
LIM	Modified thermal pulse	Electric current
EBM	Electron beam irradiation	Electric current

In PIPWP and LIPP, collectively called the PWP method, the charge moves as the acoustic wave propagates. This movement causes a change of surface charge on the electrodes. By measuring the displacement current between the electrodes, the charge distribution is obtained [26]. In the PEA method, which will be discussed in detail in the next section, narrow electric pulses are applied to the sample and the interaction between the electric pulses and the internal charges in the sample creates an acoustical wave in the insulation which is detected by a piezoelectric transducer. The response signal carries the information of the space charge distribution but is a convoluted function of space and time and requires the use of appropriate mathematical methods to obtain space charge and electric field distributions [27]. A brief explanation and references for detailed explanations of the other methods of space charge measurement mentioned in table 3.1 can be found at [25].

3.3. Space charge measurement using the PEA method

The PEA method was developed in 1987 [28], and it was shown theoretically that this method can be used to measure the space charge profile. But due to the limited frequency band of the ceramic piezo-electric transducer used by that time, the detected signal did not directly indicate the space charge profile. The ceramic piezo-electric transducer was then replaced by a PVDF transducer. Certain properties of the polymer piezoelectric transducer, such as high sensitivity, a wide frequency range, a broad dynamic response, and a low acoustic impedance, make it possible to overcome the disadvantage of the ceramic transducer in frequency characteristics [28]. The PEA technique is more common than other techniques due to its simplicity in structure, low cost and easy to implement for both plaque and cable samples [29]. The schematic of the PEA measurement setup is illustrated in fig. 3.3.

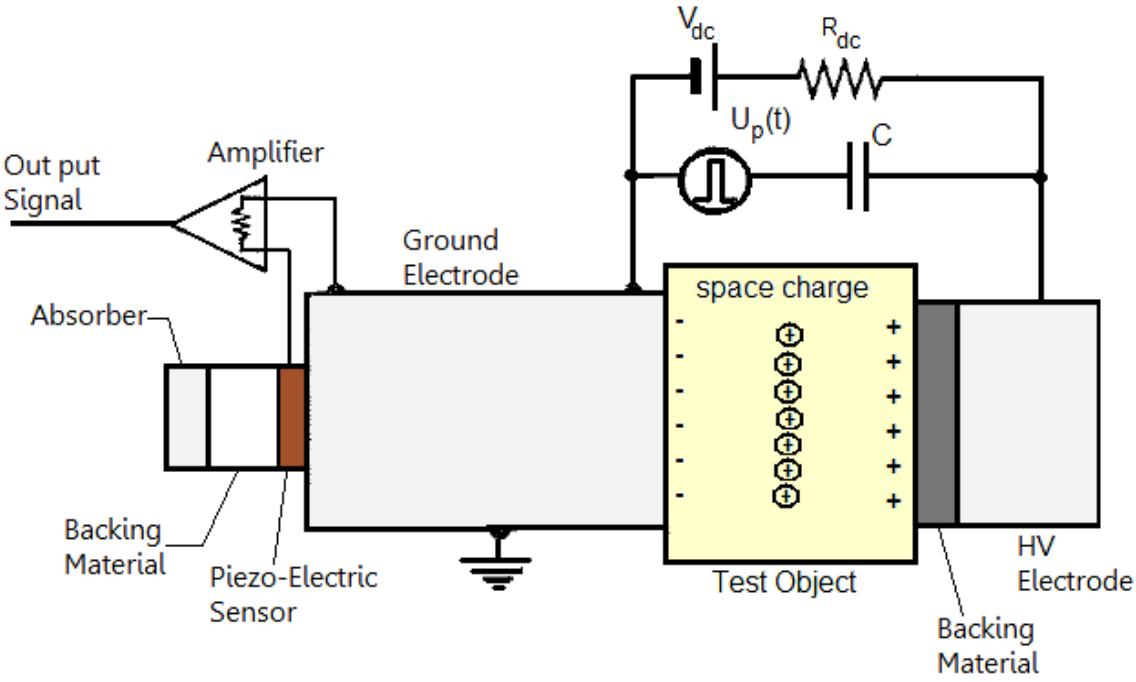

Fig. 3.3 PEA measurement setup

The DC source, V_{dc}, is the voltage applied to inject space charges. When the short duration pulse, $U_p(t)$, is applied, the resulting electric field, e(t), acts both on the space charges and charges at the electrodes and they experience a force. This force causes the charges to move slightly in their position. This perturbation causes a pressure pulse, p(t), that is proportional to the charge distribution in the sample. The pressure pulse moves in both directions to the HV electrode and ground electrodes. The ground electrode is thick and delays the acoustic waves until the disturbances caused by the firing of the impulse generator have died away. At the back of the ground electrode, a piezo-electric transducer is located that converts the acoustic wave to an electric signal which is then amplified and fed to an oscilloscope. The backing material, having the same acoustic impedance as the piezoelectric transducer but lacking piezoelectric

properties, is added to suppress the reflections of the acoustic wave which might disturb the measurement.

The generated pressure pulse can be calculated using equation 3.2 [25].

$$p(t)=\frac{Z_{Al}}{Z_{sa}+Z_{Al}}\left[\sigma(0)e(t)+u_{sa}\int_{-\infty}^{\infty}\rho(\tau)e_p(t-\tau)d\tau+\sigma(d)e(t-\frac{d}{u_{sa}})\right] \quad (3.2)$$

Where, Z_{Al} and Z_{sa} represent the acoustic impedances of aluminum and the sample respectively. $\sigma(0)$ and $\sigma(d)$ represent the surface charges at the ground and HV electrodes respectively. u_{sa} stands for the acoustic velocity in the sample, d for the thickness of the sample, and ρ for the space charge density. The generated acoustic waves then travel in two directions: some part towards the ground electrode and the other part towards the HV electrode. Every time the acoustic wave encounters an interface, some of the signal is transmitted to the next medium and the other part is reflected back. The fraction of the signal transmitted and reflected is determined by the transmission and reflection ratios respectively. Fig. 3.4a shows the numerical details. Fig. 3.4b illustrates the effect of using a backing material in suppressing multiple reflections. In the figures, $P_o(t)$ represents the original acoustic wave, and Z_p stands for the acoustic impedance of the transducer. In practice, however, it is not possible to completely avoid reflections. Thus, a need for numerical compensation is mandatory.

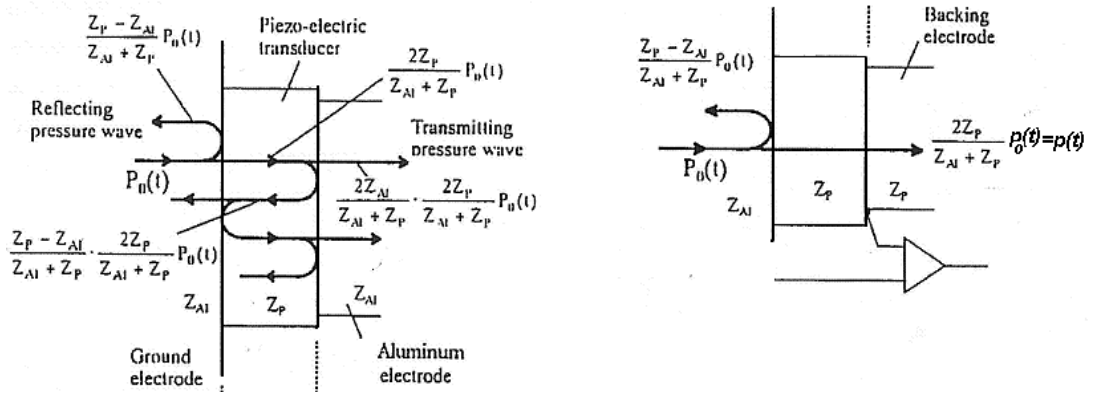

Fig. 3.4 (a) Multi reflections of the acoustic waves at the both interfaces, **(b)** Improving multiple reflections using a backing material [25]

The sensor converts the acoustic signal p(t) into a voltage V(t). This conversion is frequency dependent giving favor to the higher frequency signals. Besides, the sensor has a certain capacitance which acts a high pass filter together with the input resistance of the amplifier. To account for the cumulative effects, a deconvolution process is implemented in the signal processing. In effect, this process does the following; a transfer function is obtained for a signal of a known shape. The transfer function is then used to calculate the processed signal from a received signal using the deconvolution process. This deconvolution in time domain is equivalent to division of the output signal by the transfer function in frequency domain. Two

problems might arise hindering the well functioning of the transfer function. For some high frequency values, the frequency content of H(f) might contain zeroes, thus creating an invalid division by zero, or contains very small values, thus amplifying the high frequency noise in the signal. These two problems can be addressed using a *Wiener filter* and a *Gaussian filter* respectively [30]. The deconvolution process is explained in fig. 3.5 and the associated equations.

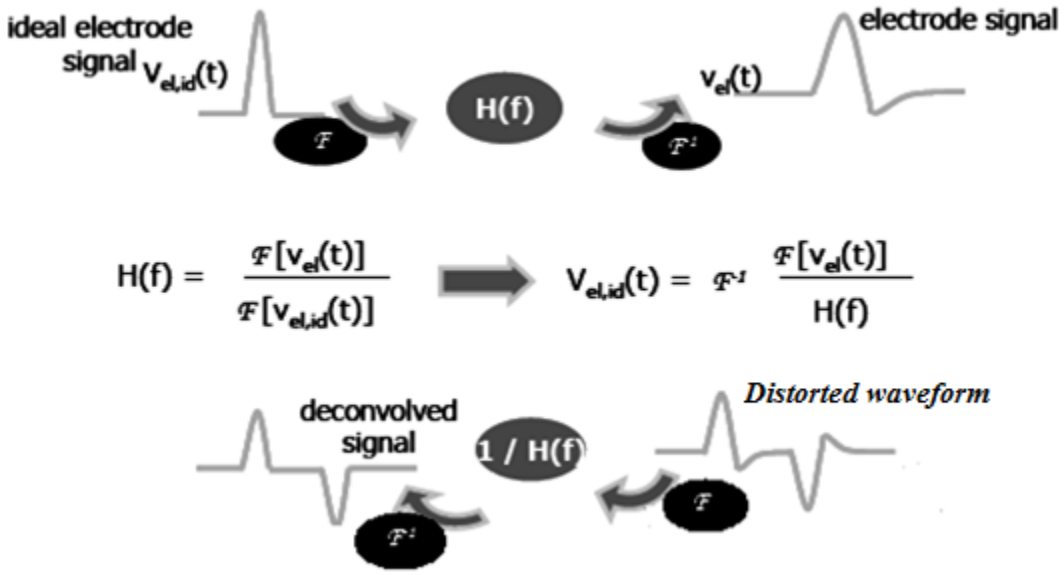

Fig. 3.5 Illustration of the deconvolution process (Adopted from lecture notes of Dr. Morshuis for the course HVDC, TU Delft)

As the acoustic signals travel through the sample, energy is dissipated due to elastic losses. The acoustic wave is, therefore, attenuated. The attenuation is seen in the decreasing amplitude of the signal as it travels through the sample. The signal is also dispersed; where, high frequency components are attenuated more than the low frequency components [31]. The dispersion[4] affects the signal such that it gets broader as it travels along the sample. These two effects should therefore be accounted for during the mathematical processing.

For the PEA method, and some other space charge measuring methods, calibration is needed before quantitative space charge density can be obtained [29]. The deconvolved voltage output, in mV, obtained above must be converted into units of charge density C/m^3. A DC voltage, U_{DC}^{cal}, is put across an initially space charge free sample. The electrode surface charge σ can then be computed using equation 3.3.

[4] Dispersion: is the broadening of the signal in time resulting from the different speeds at different frequencies

$$\sigma=\varepsilon\frac{U_{DC}^{cal}}{d} \tag{3.3}$$

Where, ε and d stand for the permittivity and thickness of the sample respectively.
From the fact that the voltage after deconvolution, V_s, is proportional to the space charge [30], equation 3.4 shows the relation. The calibration constant is represented by k.

$$V_s=k\cdot\rho(x)=k\cdot\frac{\sigma}{b} \tag{3.4}$$

Where $b=u_{sa}.\Delta t$, u_{sa} being speed of sound in the sample and Δt the pulse width. From equations 3.3 and 3.4, the calibration constant is evaluated in 3.5.

$$k=\frac{V_s db}{\varepsilon U_{DC}^{cal}} \tag{3.5}$$

It was indicated that the calibration process is necessary to get a numerical value of the space charge. Equally important is the calculation of the electric profile from the space charge distribution. This is done using the Poisson equation 3.6. As can be seen in equation 3.7, the integration of the field gives the potential distribution throughout the thickness of the sample.

$$E(z)=\int\frac{\rho(z)}{\varepsilon}dz \tag{3.6}$$

$$V(z)=-\int E(z)dz \tag{3.7}$$

In the above equations, z represents the distance from the HV electrode, ε and ρ(z) stand for the permittivity of the material and the position dependent charge density respectively.

3.4. Space charge measurement protocol (for this thesis)

The physical PEA set up used for the space charge measurement on the nanocomposite samples is shown in fig. 3.6 and the characteristics of the setup are presented in table 3.2.

a. **b.**

Fig. 3.6 PEA set up used in this thesis: **a.** closed **b.** Opened view

Table 3.2 Some specifications of the PEA setup [32]

Amplifier:	Gain= 60dB Bandwidth= 0.1-500MHz Input impedance= 50Ω
Sensor:	PVDF= 9μm
Pulse generator:	Amplitude= 0-1kV Pulse width= 20ns
Max. Temperature**:**	70^0C
Maximum Voltage:	20kV

The measurements were done at ambient conditions where the temperature ranged from 18 to 22^0C and humidity was 37 to 52%. The samples and field strengths used for the test are shown in table 3.3.

Table 3.3 Samples used in the space charge measurement

Samples	**Nanofiller Weight Percentage**	**Field Strengths (kV/mm)**		
Al_2O_3_Epoxy nanocomposite	0.5	10	15	18
	2	10	15	18
	5	10	15	18
Al_2O_3_Epoxy conventional filler	5	10	15	18
AlN-Epoxy nanocomposite	0.5	10	15	17.7
	2	10	15	18
	5	10	15	18
MgO-Epoxy nanocomposite	0.5	10	15	18
	2	10	15	18
	5	10	15	18
BN-Epoxy nanocomposite	0.5	10	15	18
Pure Epoxy	0	10	15	18

Before performing the measurements, the electrodes, the sample, and the rubber overlaying the sample were thoroughly cleaned using alcohol and they were allowed to dry for some time. After assembling the test setup and before the application of the poling voltage, V_{dc}, a narrow pulse with duration of 20 ns and pulse amplitude of 300 V, was applied across the sample. The system response was saved in this step. Then the sample was stressed at10 kV/mm for 1 hour during which time space charge was measured continuously (voltage-on measurement). Then the poling voltage was turned off and the sample short-circuited for discharging (voltage-off measurement). The depoling procedure lasted for about 1 hour until all space charge was depleted. Then the poling field was raised to 15 kV/mm and similar procedures were followed. Finally, the procedure was repeated for a poling field of 18 kV/mm.

The diameter of the samples was around 50 mm, trimmed from their original 56 mm diameter to avoid the bevels at the edges. This rendered the occurrence of surface discharges at a voltage of around 13 kV and the current limiter turned the voltage off. This was addressed by putting a thin, large diameter flat rubber, approximately the size of the diameter of the ground electrode, with a hole at its center rendering contact of the semicon and the sample between the HV electrode and a sample. This step, in effect, increased the creepage length and avoided the discharges observed (see fig. 3.5). This step worked fine and measurements were made effectively.

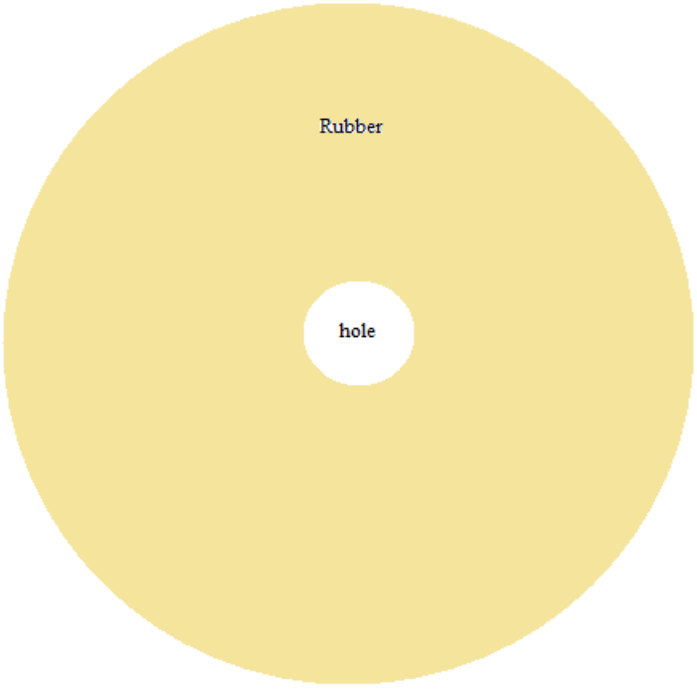

Fig. 3.5 Schematic of the rubber sheet used to prevent flash over

On the other hand, the thickness of the samples varied from 0.6 mm to 1.13 mm from sample to sample. The thick samples brought in a limitation for the maximum field to be applied. For comparison purposes, a set of field intensities were required, the maximum of which was determined with the highest voltage that can be allowed with the set up, which was 20 kV. Hence, the field stresses selected for analysis were, 10 kV/mm, 15 kV/mm, and 18 kV/mm. For samples, whose DC ramp breakdown strength can easily go beyond 160 kV/mm, the considered field strengths might not tell as much as they should. Liable to this fact, the procedure was taken as a preliminary space charge measurement for low field strengths and a consensus was reached to perform higher field strength space charge measurements separately from this thesis.

3.5. Processing of the oscilloscope signals

The signals saved to the oscilloscope picked up noise, were attenuated, and dispersed. Besides, they were not calibrated. Hence, the saved voltage profiles needed processing. The processing phase was done using a code written in MATLAB which basically contained the steps of denoising, deconvolution, correction of the attenuation and dispersion, calibration, and two integration steps that had electric field and potential distribution as outputs. Besides, two MATLAB codes were written where one was used to calculate the average space charge and the other one for surface plotting the space charge growth/ depletion with time.

Space charge profiles obtained after one hour of poling were copied to the MATLAB workspace for analysis. Each file was an average of 500 *sweeps*[5]. Taking the average of the sweeps was necessary to avoid some unsystematic noise that might be picked up during the measurement. Besides, it reduces memory size and speeds up analysis. The files were raw voltage files, where the first one was the response of the system to the application of the pulse only. During the processing stage, this system response was subtracted from all the signals. A sequence of steps like, denoising, deconvolution, calibration, correction of attenuation and dispersion were later on performed on the signals. After obtaining the space charge profile, a *print step*[6] of 10 was chosen where only 16 files were taken out of the 160 files that were obtained. This step was important to keep track of the space charge growth at some intervals in time which simplified the comparison between different samples. Besides, it was also important to reduce the number of files, with a print step of 10, so that the calculation of the average of space charges is performed easily. After obtaining the space charge profiles, (C/m^3), two integration steps were included in the code that calculated the electric field distribution (kV/mm) and the voltage profile (V). Apart from this, a separate code was written that calculated the average space charges at intervals of 4 min for the whole duration of poling, which in most cases was 1 hour. The first space charge profile, which represents an electrode charge due to the voltage only and hence, space charge free case, was then subtracted from all the 15 space charge signals. This step was necessary to clearly follow the homocharge growth in time without being shielded by the surface charge. This step was not necessary for the case of depoling as the voltage is turned off and the sample is short circuited.

Fig. 3.7 shows some of the basic steps undertaken to process the raw signals. Fig. 3.7a shows the raw signal with an easily perceivable attenuation and dispersion in the HV electrode. In fig. 3.7b, the system response has been subtracted and the signal has been denoised with a low pass *Butterworth filter*. Passing the steps of deconvolution, correction for the attenuation and

[5] One sweep represents a full trace of a dot on the oscilloscope screen.

[6] Print step refers to the interval where small data are picked from a big set of data. With a print step of 10, data roll numbers 1, 10, 20… will be picked from the bigger set that goes like 1, 2, 3,....

dispersion, fig. 3.7c shows a two space charge profiles; one after 1 min of poling (no space charges) and the blue one at the end of 1 hour of poling. The difference of the two signals is displayed in fig. 3.7d, which clearly shows the accumulation of homocharges in front of the ground electrode of sample by the end of 1 hour. Fig. 3.7e shows the *Poissonian integration* step, equation 3.8, of the space charge profile in fig. 3.7c.

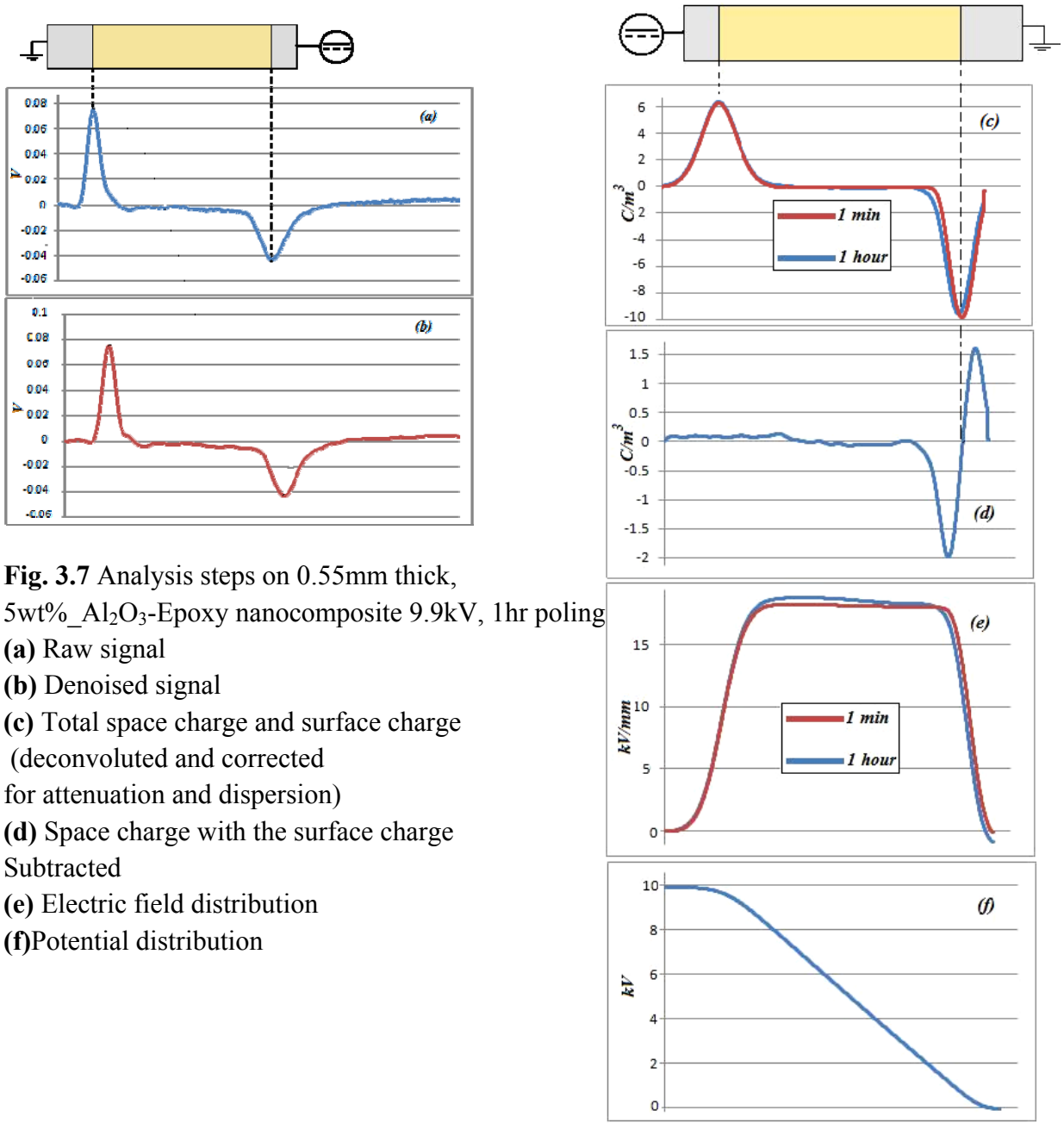

Fig. 3.7 Analysis steps on 0.55mm thick, 5wt%_Al_2O_3-Epoxy nanocomposite 9.9kV, 1hr poling
(a) Raw signal
(b) Denoised signal
(c) Total space charge and surface charge (deconvoluted and corrected for attenuation and dispersion)
(d) Space charge with the surface charge Subtracted
(e) Electric field distribution
(f) Potential distribution

$$E(z)=\int \frac{\rho(z)}{\varepsilon} dz \qquad (3.8)$$

Finally equation 3.9, gives the potential distribution as depicted in fig. 3.7f.

$$V(z)=\int -E(z)dz \tag{3.9}$$

Another important observation that can be made from fig. 3.7e is the field enhancement caused due to space charges. It can be seen from the figure that in some places, the field after one hour, blue line, is higher than the field with no space charges present, red line. This is an important point to note in the design for HVDC insulation. The percentage increase in the maximum field over the Laplacian field is termed field enhancement factor. The factor can be calculated using the relation 3.10:

$$E_{ff}=\frac{E_{max}-E_{lap}}{E_{lap}}\times 100\% \tag{3.10}$$

Where, E_{ff} stands for the field enhancement factor, E_{max} for the maximum field and E_{lap} for the Laplacian field, the field with no space charges. The field enhancement factor indicates the increase in percentage of the maximum field above the Laplacian field. The distortion of the field in general and the enhancement in some part of the insulation system add another challenge to the designer and a likely more stressed spot for the insulation. Determination of breakdown voltage at DC should therefore be accompanied with the values that also take the space charge distribution into consideration. This in turn asks for space charge measurements at fields that are high enough to approximate the space charge situation for a given breakdown voltage.

To estimate space charge accumulation, the average charge density, Q_{av}, which quantifies the absolute space charge density accumulated in the insulation bulk, can be calculated from the space charge profile according to equation 3.11 [33]:

$$Q_{av}(t)=\frac{1}{x_1-x_2}\int_{x_1}^{x_2}|\rho(x,t)|dx \tag{3.11}$$

Where x_1 and x_2 are the electrode positions and $\rho(x,t)$ is the space charge density profile measured at any given time and location along the insulation thickness. Equation 3.11 was considered while performing the calculation. Apart from this, another code was written that displayed the space charge growth with time, for the case of poling, throughout the insulator cross section.

3.6. Results and discussions

Homocharges were observed in all epoxy nanocomposites considered. All but MgO-Epoxy nanocomposites showed higher homocharges as compared to neat epoxy. After performing the signal processing steps illustrated in section 3.5, the results have to be arranged in a way that renders a basis for comparison among the nanocomposites. Hence, electric field, type of nanocomposites, weight percent of nanocomposites, and time were taken as parameters for the

comparisons outlined from (a-e) below; among the nanocomposites and base epoxy or among the nanocomposites themselves.

a. For a specific sample at a given electric field, the accumulation/depletion of space charges with time,
b. For the same sample, at a given time, the space charge accumulation/depletion at different field levels,
c. For samples of similar nanocomposites, the space charge distribution at a given time and field for varying weight percent of the nanocomposites,
d. For different types of nanocomposites, the comparison of average space charges with respect to time at a given field,
e. Comparison of the average space charges at every field by the end of poling (voltage-on case only).

3.6.1. Space charge results for voltage on measurement (Poling)

a. <u>For a specific sample at a given electric field, the growth or accumulation of space charges with time:</u>

In this section, surface plots were made that revealed the growth of space charges with time. The main stress made was on the qualitative time constant of the charge accumulation.

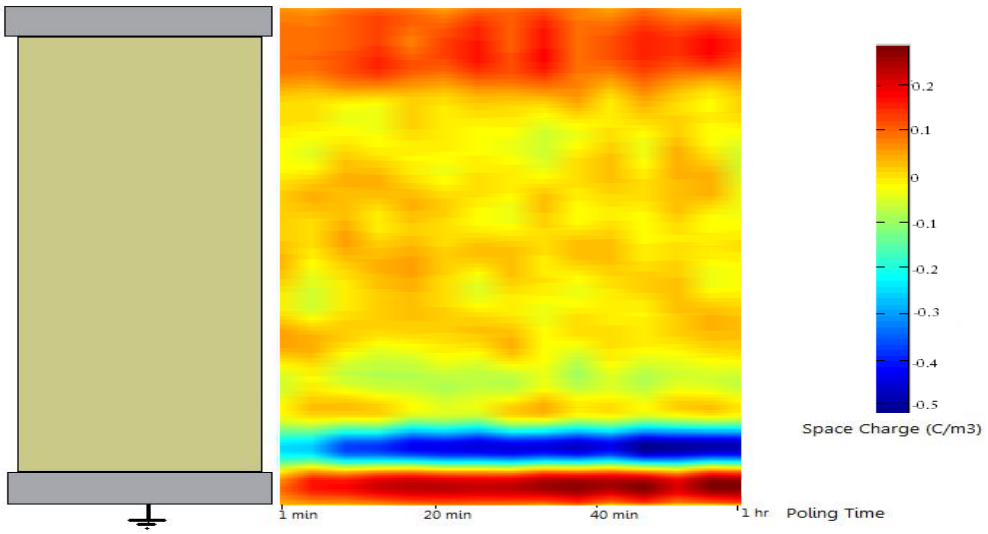

(3.8a)

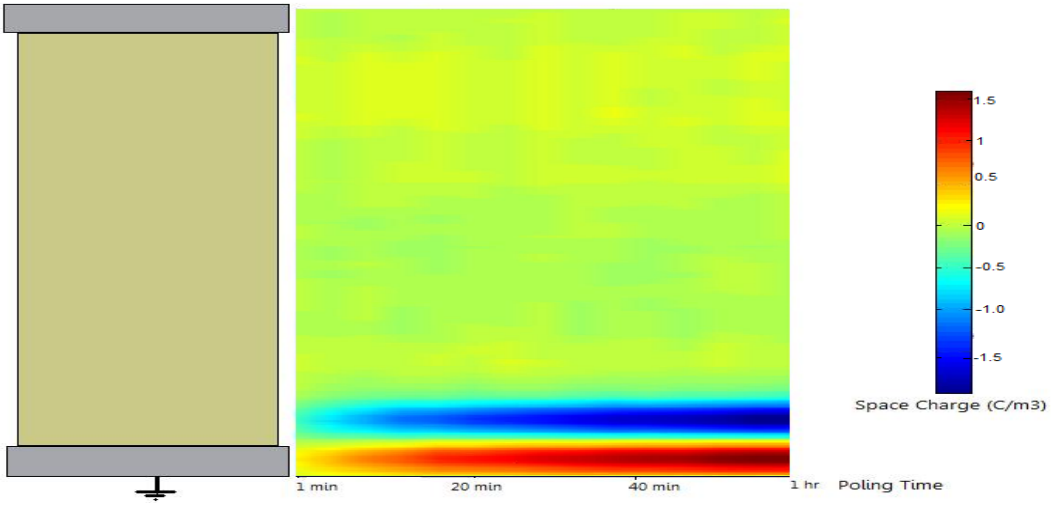
1.5
1
0.5
0
-0.5
-1.0
-1.5
Space Charge (C/m3)
1 min
20 min
40 min
1 hr
Poling Time

(3.8b)

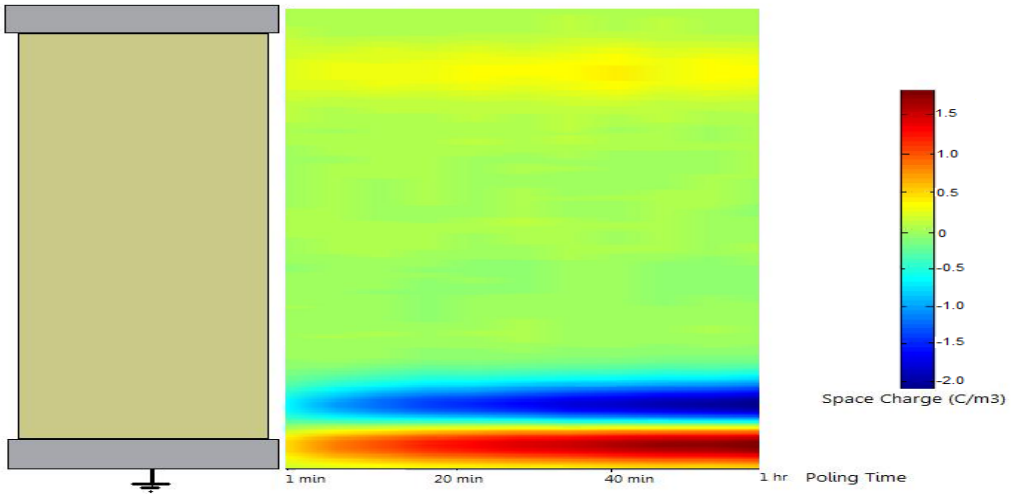
1.5
1.0
0.5
0
-0.5
-1.0
-1.5
-2.0
Space Charge (C/m3)
1 min
20 min
40 min
1 hr
Poling Time

(3.8c)

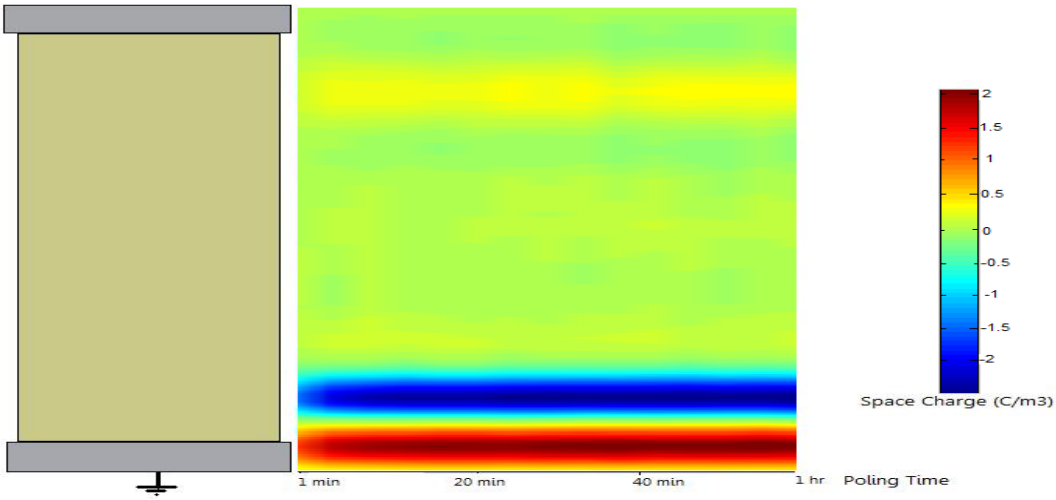
2
1.5
1
0.5
0
-0.5
-1
-1.5
-2
Space Charge (C/m3)
1 min
20 min
40 min
1 hr
Poling Time

(3.8d)

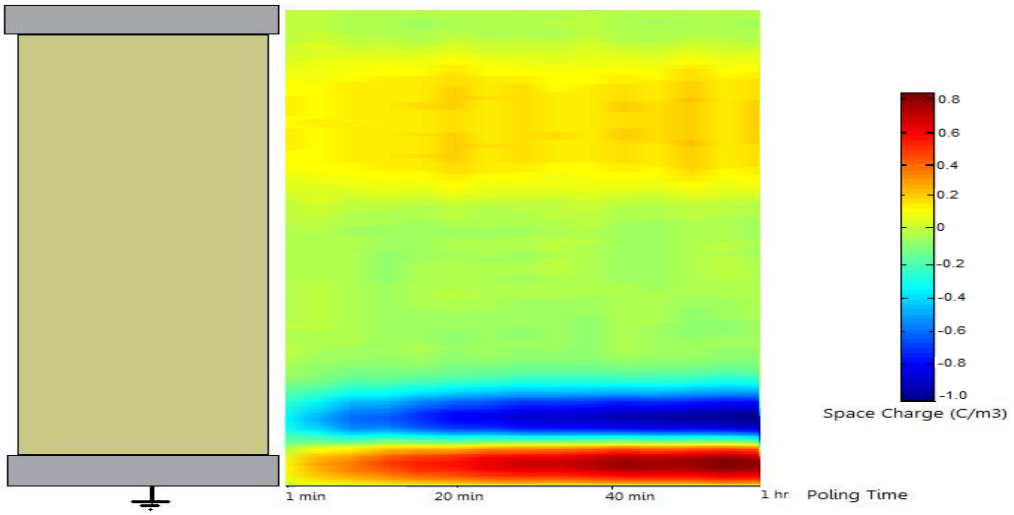

(3.8e)

Fig. 3.8 Space charge accumulation at 18 kV/mm: **(a)** 2wt%_ MgO-Epoxy nanocomposite, **(b)** 5wt%_ Al_2O_3-Epoxy nanocomposite, **(c)** 5wt%_ AlN-Epoxy nanocomposite, **(d)** 0.5wt%_BN-Epoxy nanocomposite **(e)** Neat epoxy

From fig. 3.8 (a-e) and more poling surface plots in appendix A.1, for the field levels considered, it can be seen that MgO-Epoxy (0.5wt%, 2wt%, 5wt%), AlN-Epoxy (0.5wt%, 2wt%), and BN-Epoxy (0.5wt%) nanocomposites in general, reach the charge saturation point in a time which generally was less than 20 min and a stable homocharge distribution was obtained afterwards. On the other hand, neat epoxy, Al_2O_3–Epoxy nanocomposites, and 5wt%_AlN-Epoxy nanocomposites showed a continuous increase in the level of homocharges with time at a given field, even beyond 1 hour. These results are also reflected in the average space charge plots of fig. 3.11, where the numerical values and the approximate time taken for the space charge saturation in the nanocomposites can be seen. Table in appendix B, among other details, shows the time to reach a stable space charge state for all samples at a given field. Another point that can be noted from fig. 3.11 is that the change of space charge in time was noticeable only at the interface, and almost no visible change was observed in the bulk of the insulator material. Similar observations were made by Hajiyiannis et al. [6] on epoxy-alumina nanocomposites. Observation of the little charge in the center of nanocomposite as compared to neat epoxy may be due to the fact that nanoparticles may act as recombining centers.

Generally, for low weight percent AlN-Epoxy nanocomposites (0.5wt%, 2wt%), saturation of space charges was reached shortly, whereas for 5wt%_AlN-Epoxy nanocomposites, continuous growth of space charges was observed. Although not as clear, a similar trend was followed for Al_2O_3-Epoxy nanocomposites.

b. For the same sample, at a given time, the space charge accumulation at different field levels:

To see the effect of electric field strength on the accumulation of space charge, a space charge profile is plotted for the same sample and a given time at varying fields.

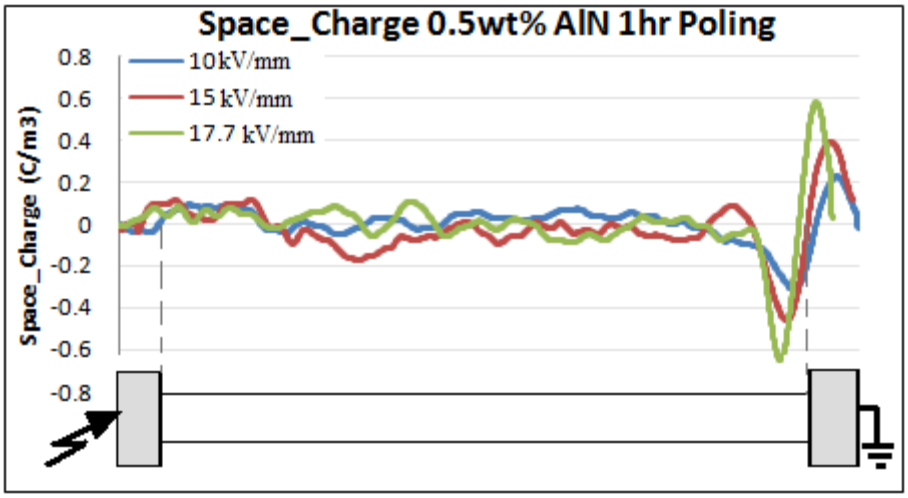

(3.9a)

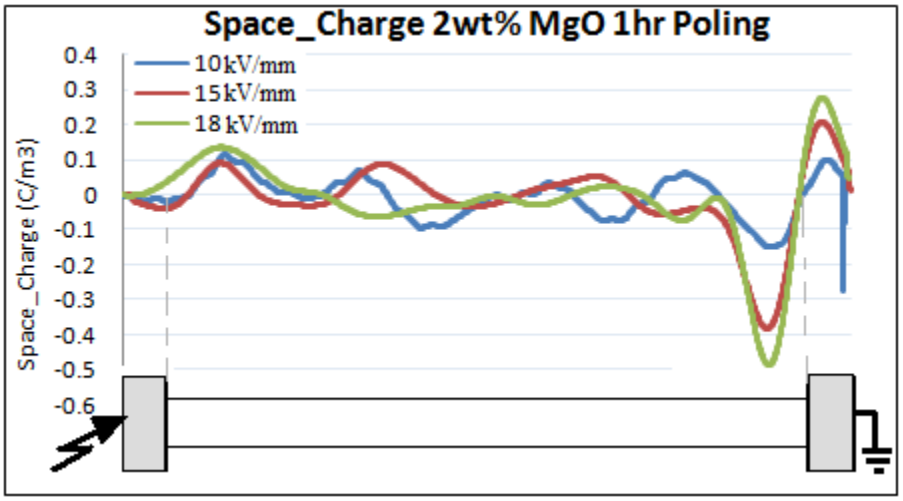

(3.9b)

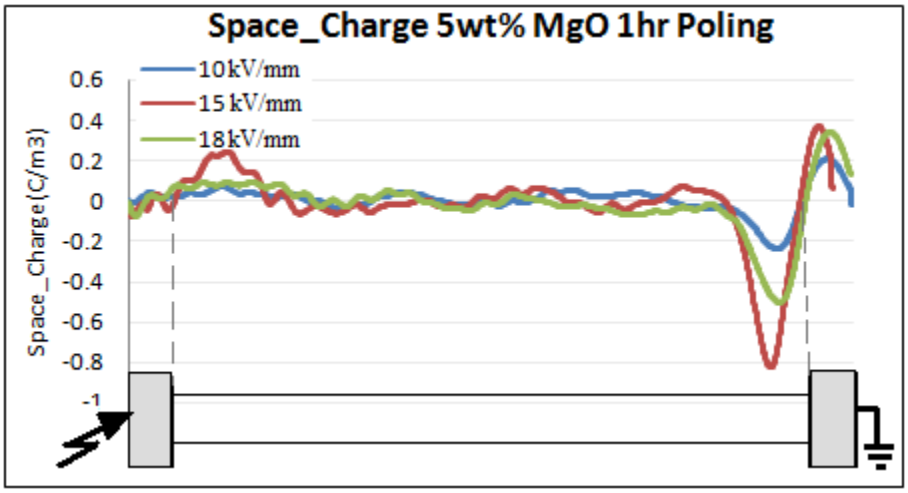

(3.9c)

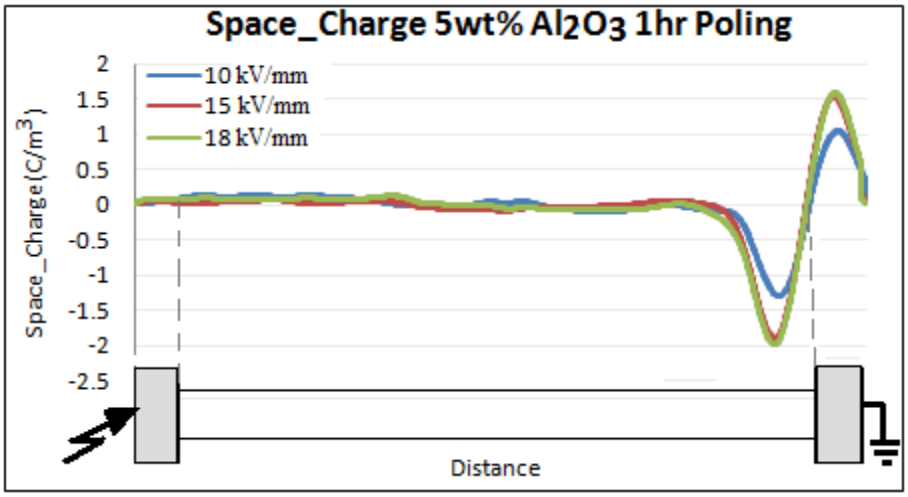

(3.9d)

Fig. 3.9 Space charge amounts of epoxy nanocomposites at three fields after 1 hour of poling: **(a)** 0.5wt%_AlN, (b)2wt%_MgO, **(c)** 5wt%_MgO, **(d)** 5wt%_Al_2O_3

As can be seen from the plots on fig. 3.9, and some more figures in appendix A.3, in most of the cases, the homocharge growth adjacent to the ground electrode increased with increasing the applied field. Above a certain threshold value of the electric field, charge accumulation starts and mostly keeps on increasing as the applied voltage increases. An interesting situation was observed for the case of 5wt%_MgO-Epoxy nanocomposites. A decrease in the value of peak homocharges was observed on the side of the samples adjacent to the ground electrode when the field was increased from 15 kV/mm to 18 kV/mm. The improved space charge properties of MgO-Epoxy nanocomposites can render overall improvement in the space charge behavior at higher field strengths. This effect could be attributed to the material changes due to the introduction of the filler [34]. To make an assertion, however, this must be accompanied with space charge measurement at higher fields and DC breakdown tests.

c. *For samples of similar nanocomposites, the space charge distribution at a given time and field for varying weight percent of the nanocomposites:*

This evaluation was included to see how the loading of a given nanofiller plays a role in the space charge characteristics. It is often found in literature that the increase in the weight percentage of the filler material beyond a certain level doesn't bring about a lot of change in the insulation behavior [16].

In this evaluation, for the same time, and electric field, space charge profiles of nanocomposites with the same filler type but different weight percentages are compared.

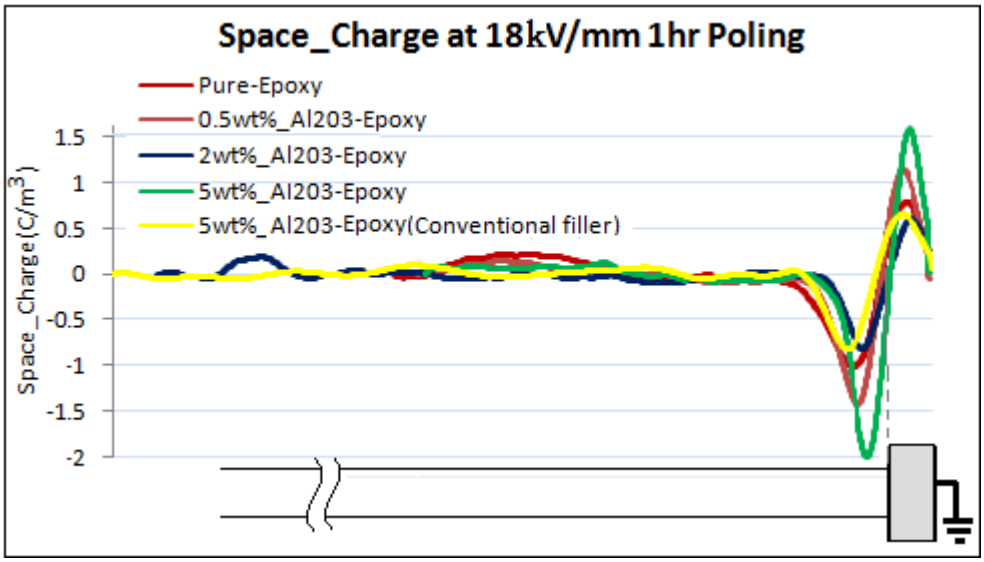

(3.10a)

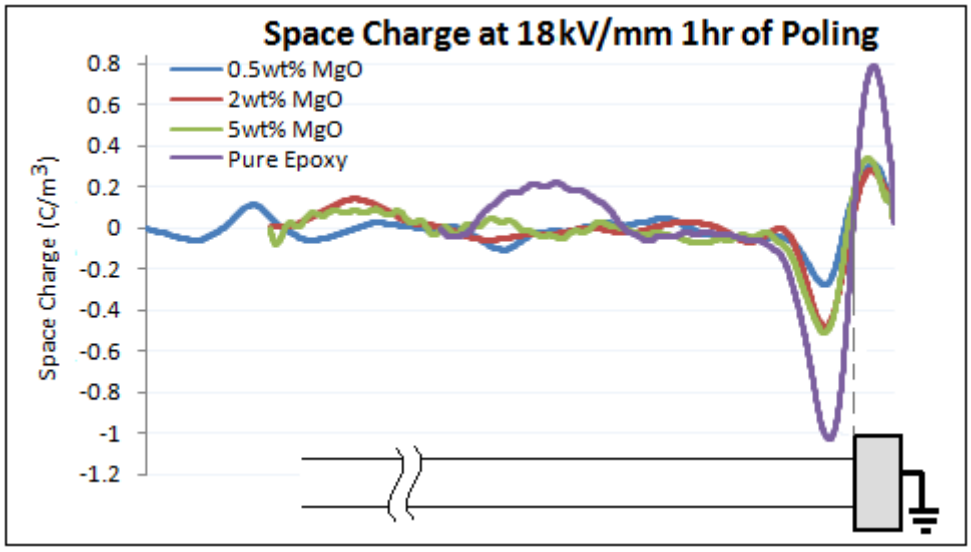

(3.10b)

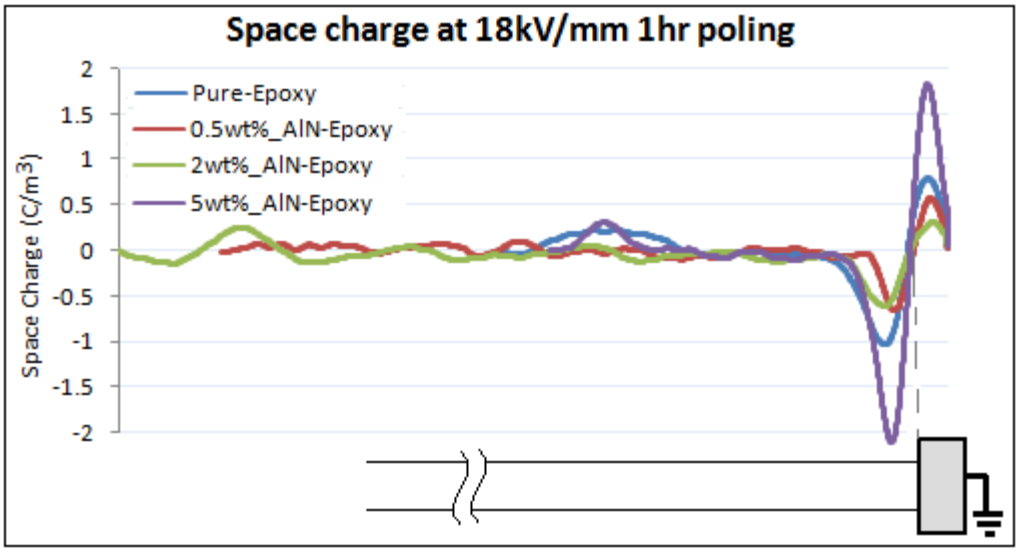

(3.10c)

Fig. 3.10 Space charge plots for the same filler material with different weight loadings[7]: **(a)** Al_2O_3-Epoxy, **(b)** MgO-Epoxy, **(c)** AlN-Epoxy

The non uniformity in the location of the homocharges is due to the difference in thickness of the samples. From each category, some of the samples showed higher homocharge concentration on their sides facing the ground electrode. Except for the case of MgO-Epoxy nanocomposites, that showed almost no difference in the value of peak homocharge with weight percentage, the AlN-Epoxy and Al_2O_3-Epoxy nanocomposites showed a high homocharge concentration for higher weight compositions, at least until 5wt%.

d. For different types of nanocomposites, the comparison of average space charges with respect to time at a given field:

Together with *e.*, this comparison is adopted to see the effect of increasing the weight percentage of nanocomposites on the value of the average space charge behavior. At a certain field, the average space charge is plotted against time for a group of nanocomposites of the same filler, with neat epoxy set as a reference.

[7] Due to the variation in thickness of the samples, the space charge profiles are drawn with the earth electrode located at the same point. This makes the location of the HV electrode different.

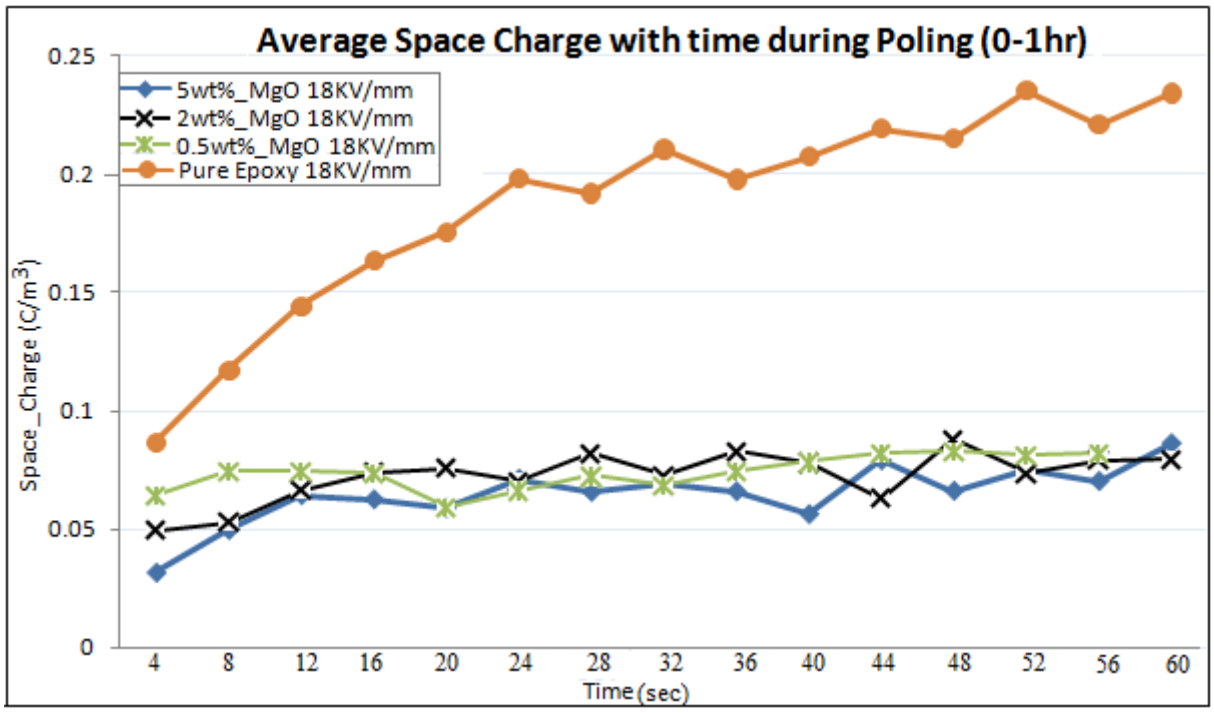
Average Space Charge with time during Poling (0-1hr)
5wt%_MgO 18KV/mm
2wt%_MgO 18KV/mm
0.5wt%_MgO 18KV/mm
Pure Epoxy 18KV/mm
Space_Charge (C/m3)
Time (sec)
0
0.05
0.1
0.15
0.2
0.25
4
8
12
16
20
24
28
32
36
40
44
48
52
56
60

(3.11a)

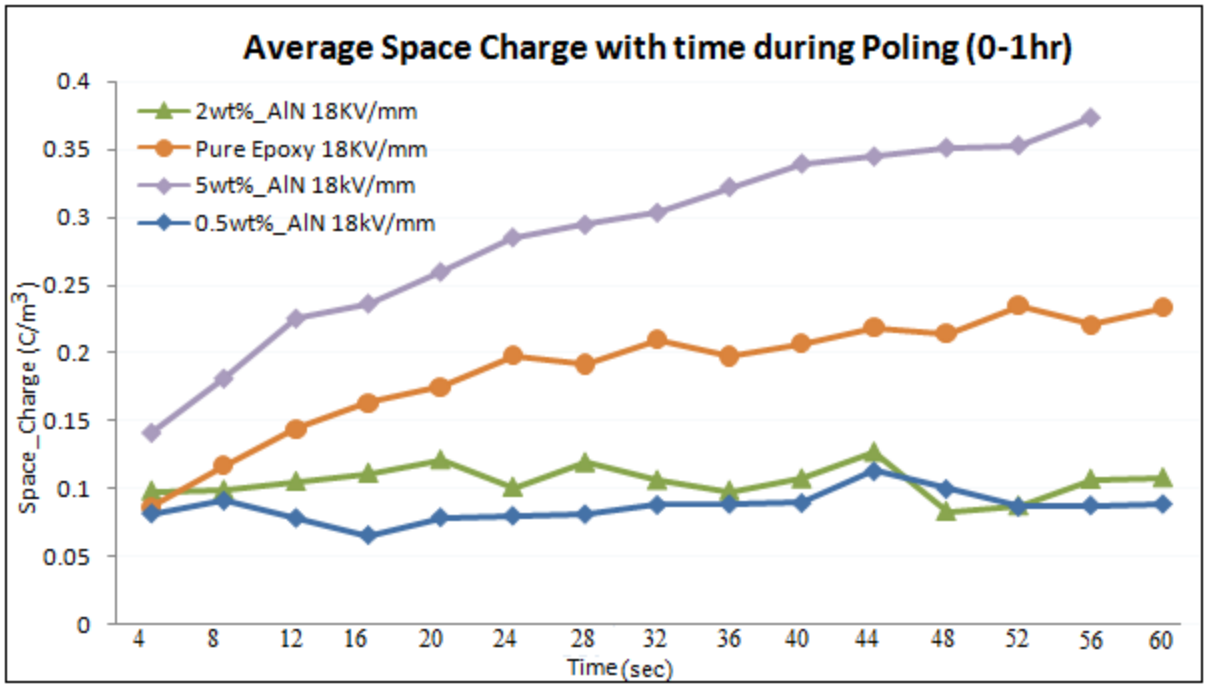
Average Space Charge with time during Poling (0-1hr)
2wt%_AlN 18KV/mm
Pure Epoxy 18KV/mm
5wt%_AlN 18kV/mm
0.5wt%_AlN 18kV/mm
Space_Charge (C/m3)
Time (sec)
0
0.05
0.1
0.15
0.2
0.25
0.3
0.35
0.4
4
8
12
16
20
24
28
32
36
40
44
48
52
56
60

(3.11b)

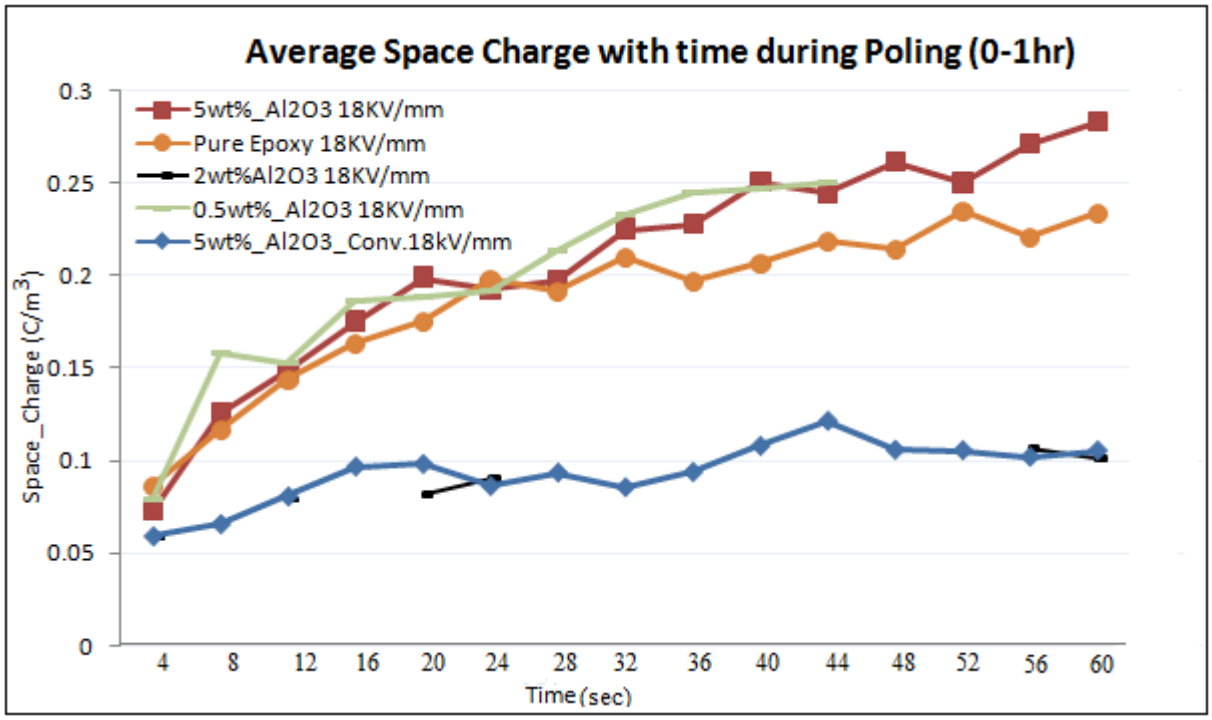

(3.11c)

Fig. 3.11 Growth of average space charge during poling **(a)** MgO-Epoxy Nanocomposites, **(b)** AlN-Epoxy Nanocomposites, **(c)** Al_2O_3-Epoxy Nanocomposites

From the results shown in fig. 3.11, the following deductions are made:

MgO-Epoxy:

It can be seen that, for the considered percentages of MgO nanofiller (0.5, 2, and 5wt%), an increase in weight proportion did not result in an observable change in the average space charge value. All the loading proportions of MgO nanofillers, at a field of 18 kV/mm, settled with an average space charge which is approximately 3 times less than neat epoxy. Besides, it was observed that the average space charge tends to saturate and reach a stable value in less than 20 min. It is mentioned that LDPE-MgO nanocomposites showed reduced space charges at high field strengths as compared to the LDPE base [16].

AlN-Epoxy:

Considering the case of the AlN-Epoxy nanocomposites, the weight proportion of the nanofiller had an effect both in the space charge saturation time and the value of the average space charge. Epoxy with lower nanofiller loadings (0.5 and 2wt%) of AlN resulted in properties that resemble to MgO nanofillers. An average space charge of 0.1 C/m^3 by the end of 1 hour and space charge saturation time less than 15 min were noticed. For the 5wt%_AlN-Epoxy nanocomposite, the average space charge was about 0.38 C/m^3 and still increasing after 1 hour.

Al_2O_3-Epoxy:

As can be seen in fig. 3.11c, Al_2O_3-Epoxy nanocomposites, the relation of the weight percentage and the average space charge density doesn't follow a trend. (0.5 and 5wt%)_Al_2O_3-Epoxy nanocomposites showed an incessant growth in average space charge until one hour. 2wt%_Al_2O_3-Epoxy nanocomposites, and Epoxy with 5wt%_Al_2O_3 conventional filler displayed properties such that the space charge saturation time was short and the average space charge by the end of one hour, ~0.1 C/m^3, was smaller than the value attained by neat epoxy and the other Al_2O_3 nanofillers. The average space charge results obtained for epoxy with microsized Al_2O_3 filler are in contradiction with literature results, e.g. [10], mentioning that a significant space charge improvement over the nanocomposite counterpart is observed with the addition of microsized filler .

e. Comparison of the average space charges at every field by the end of poling:

The average space charge of all samples has been looked into and the effect of increasing the field level on the average space charge for every nanocomposite sample was analyzed by the end of one hour of poling. The each plot shows the average space charge calculated by the end of 1hour for one type of filler material, with neat epoxy considered a reference in all cases.

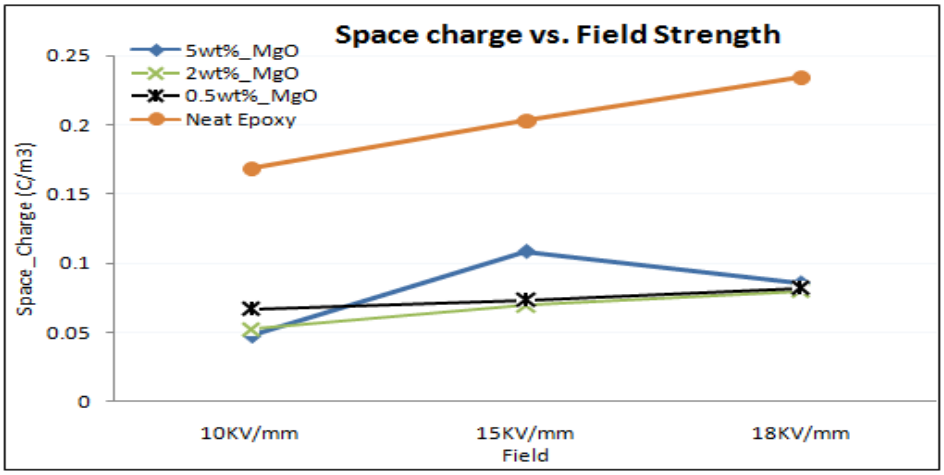

(3.12a)

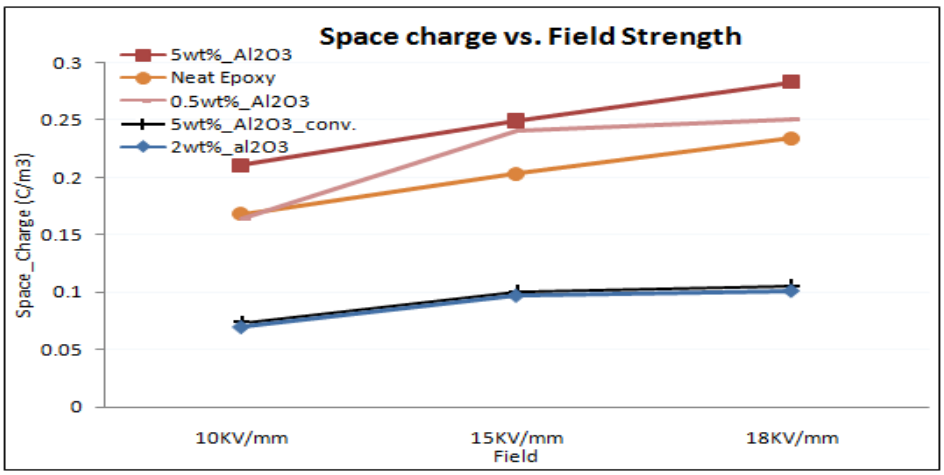

(3.12b)

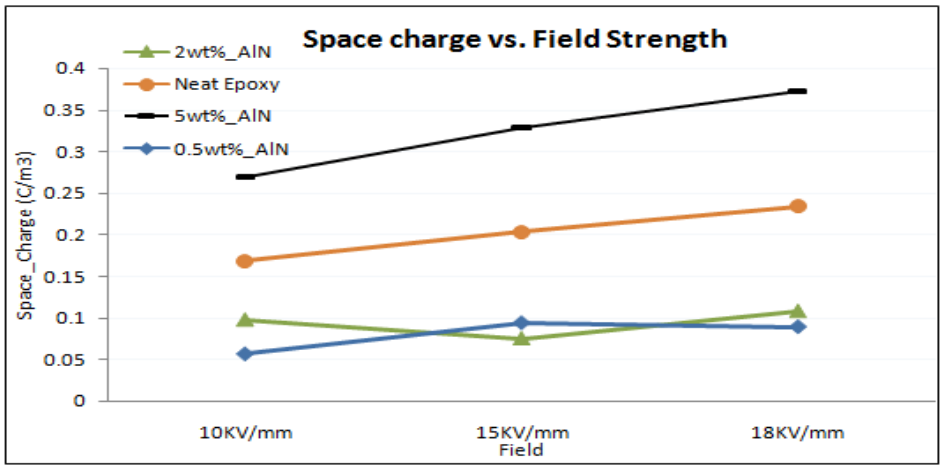

(3.12c)

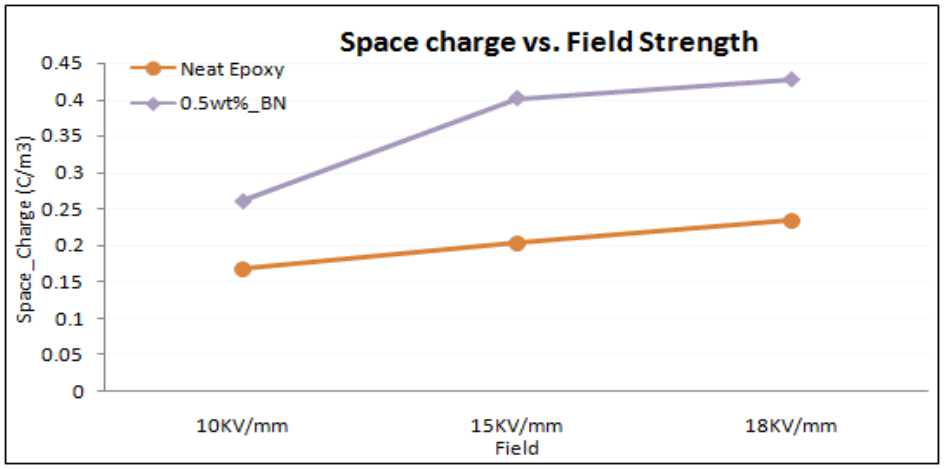

(3.12d)

Fig. 3.12 Average space charge with respect to field strength on different nanocomposite samples: **(a)** MgO-Epoxy, **(b)** Al_2O_3-Epoxy, **(c)** AlN-Epoxy, **(d)** BN-Epoxy Nanocomposites

As can be seen from the fig. 3.12 (a-d), two points are worth noting:

- How the average space charge behaves with increase in the applied voltage , and
- The effect of using nanocomposites of the same filler with different weight percentages and to observe their influence on the average space charge behavior.

In general, an increase in the applied voltage resulted in higher average space charge by the end of one hour for most of the nanocomposite samples. A behavior is exhibited by 5wt%-MgO-Epoxy nanocomposites where a decrease in the average space charge was observed when the poling field was raised from 15 kV/mm to 18 kV/mm as can be seen in fig.3.12a. Apart from this, all MgO-Epoxy nanocomposites considered during the test showed significantly less space charge characteristics than neat epoxy. Similar results are mentioned with MgO nanofiller on LDPE base [16]. Looking at the average space charge behavior of the other samples in fig. 3.12, the nanocomposites are observed to have better or worse space charge characteristics than neat epoxy depending on the weight percentage. For instance, 2wt% and 0.5wt%-AlN-Epoxy show improved space charge behavior whereas 5wt%_AlN-Epoxy nanocomposite was worse as compared to neat Epoxy. Another point worth mentioning is the nearly tripled average space charge observed in the 0.5wt%-BN-Epoxy nanocomposites as compared to neat epoxy. This result disregards the expectation that BN-Epoxy nanocomposites would coin similar space charge properties as MgO-Epoxy nanocomposites, where the fillers have similar structure [34]. A high content of B_2O_3 on the BN-particle surfaces lead to inferior behavior in every respect. Main problem was that the preparation of samples was very difficult. Due to the B_2O_3-layer, creating stable suspensions was not possible. This resulted in relatively large agglomerates of 100 nm to 500 nm in the samples [34].

3.6.2. Analysis of PEA results during voltage-off measurement (Depoling)

The depoling procedure, unlike the poling counterpart, was not performed for exactly 1 hour. Based on visual inspection of how low the remaining space charge in the samples was, the depoling time was chosen.

The following parameters were considered to characterize the discharging behaviors of the nanocomposites.

f. *For a specific sample at a given electric field, the depletion of space charges with time:*

In this characterization, the depletion of the space charges was surface plotted against time throughout the thickness of the sample including the interface with the electrodes. These plots were made with the intention of obtaining how the fast the space charge disappears when the sample is short circuited from a given voltage. Besides, the time taken for the samples to be literally free of space charges was considered as a guide line for comparison.

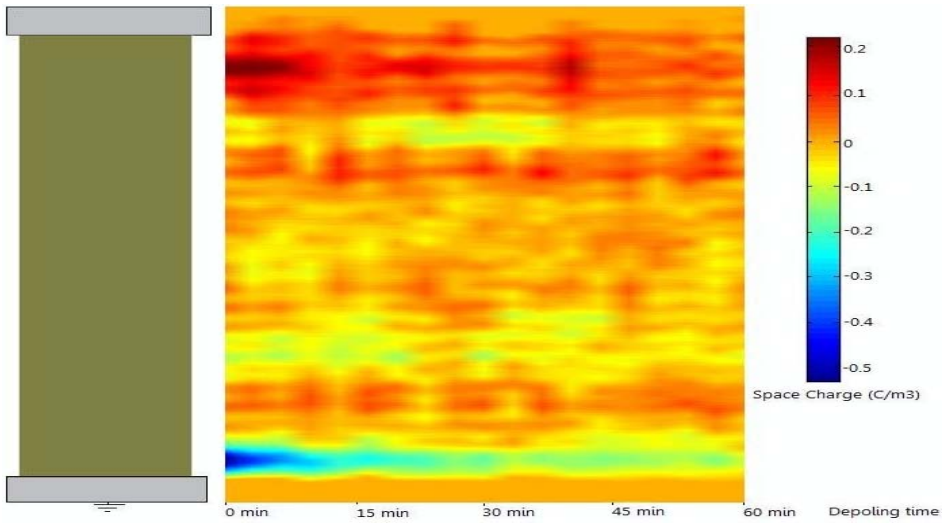
0.2
0.1
0
-0.1
-0.2
-0.3
-0.4
-0.5
Space Charge (C/m3)
0 min
15 min
30 min
45 min
60 min
Depoling time

(3.13a)

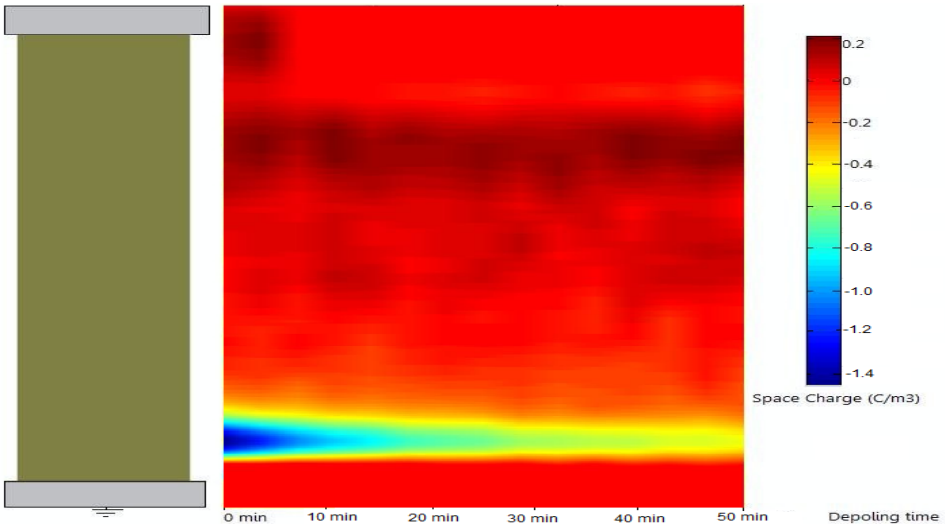
0.2
0
-0.2
-0.4
-0.6
-0.8
-1.0
-1.2
-1.4
Space Charge (C/m3)
0 min
10 min
20 min
30 min
40 min
50 min
Depoling time

(3.13b)

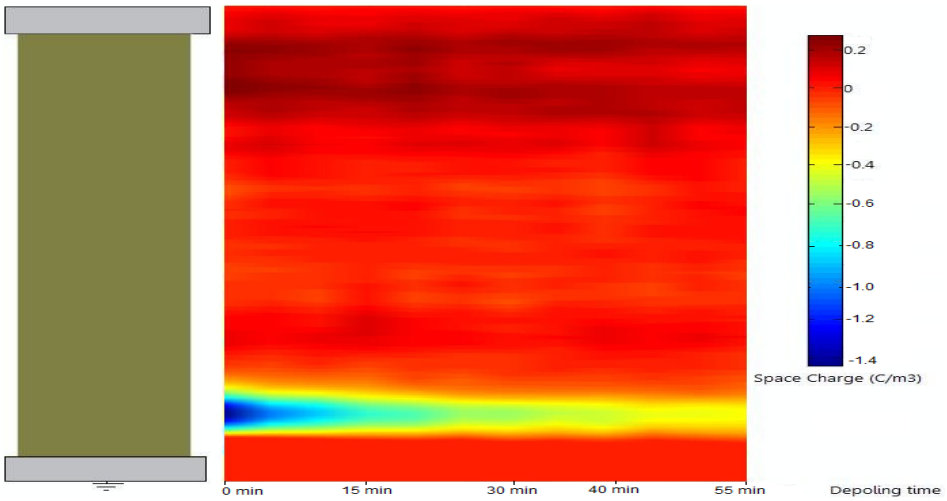

(3.13c)

Fig. 3.13 Space charge profiles for the depletion from 18 kV/mm of Epoxy nanocomposites: **(a)** 5wt%_MgO-Epoxy, **(b)** 5wt%_Al_2O_3-Epoxy, **(c)** 5wt%_AlN-Epoxy

The plots of fig. 3.13 and some more plots in appendix A.2 show the trend of depoling throughout the thickness of the material. Except for the depletion of the homocharge, as it could be observed from the figures, the change in the space charge with time in the bulk of all the samples is insignificant. With the plots in *g,* the average time for the samples to be free of space charges could be approximated. It should be noted that the time considered here is when a value less than 0.05 C/m^3 is reached for the average space charge[8]. The values are tabulated in appendix B.

[8] This value was chosen as visual inspection for 'space charge free' sample resulted in average space charge of less than 0.05C/m^3

g. For different types of nanocomposites, the comparison of average space charges with respect to time from a given field:

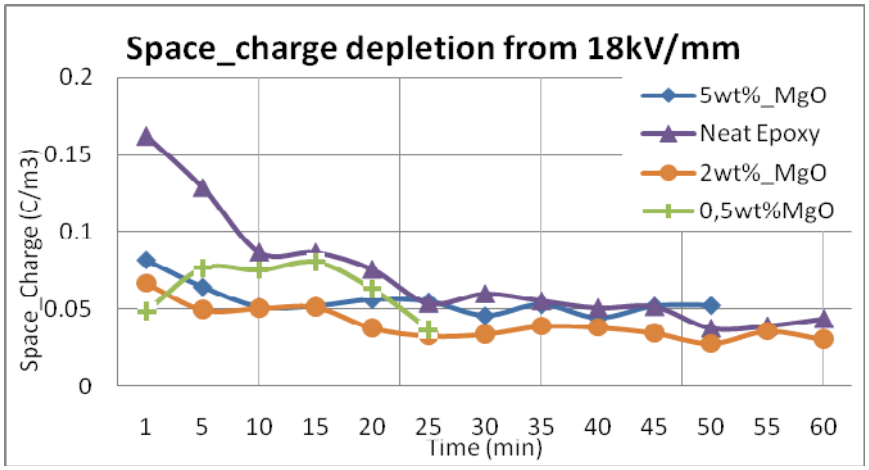

(3.14a)

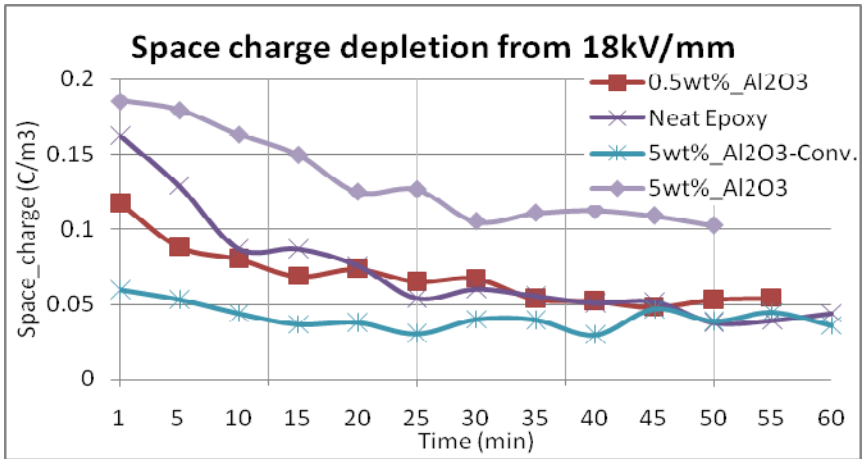

(3.14b)

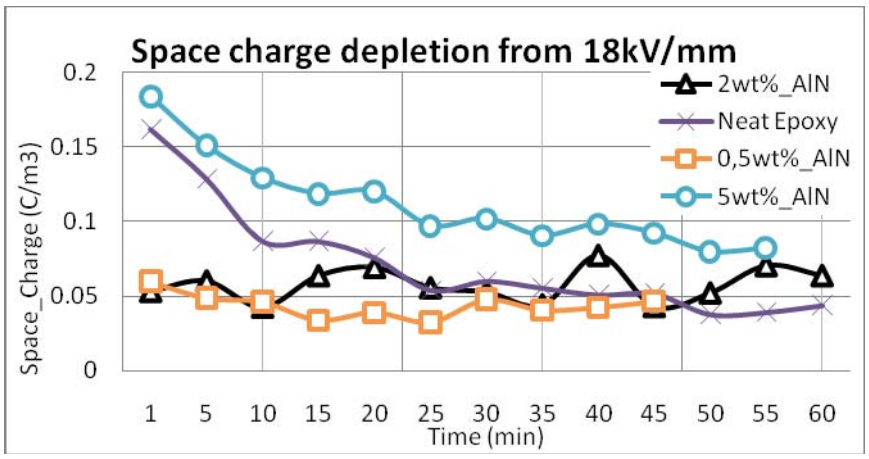

(3.14c)

Fig. 3.14 Depletion of average space charge of Epoxy nanocomposites from 18 kV/mm: **(a)** MgO-Epoxy nanocomposites, **(b)** Al_2O_3-Epoxy nanocomposites, **(c)** AlN-Epoxy nanocomposites

The discharging process was performed until the samples were almost free of space charges. The criterion observed during this procedure was how fast the samples are relieved of space charges. Samples with average space charge of 0.05 C/m^3 and less were considered to be free of space charges[9]. Fig. 3.14(a-c) show the depletion of space charges of various nanocomposites that were primarily poled at 18 kV/mm for 1 hour. MgO-Epoxy nanocomposites, that originally had very small amount of space charge, less than 0.1 C/m^3 by the end of 1hr poling at 18 kV/mm, were charge free by the end of 20 min depoling. Neat epoxy on the other hand needed about 30 min to be free of space charges. Fig. 3.14b and c show the space charge depletion with time of Al_2O_3-Epoxy and AlN-Epoxy nanocomposites respectively. An important observation made from the two plots is that, in both cases, the highest weight percentages (5wt%_Al_2O_3-Epoxy and 5wt%_AlN-Epoxy) showed a slow discharging after the samples were short circuited. Two of the samples had more than 0.05 C/m^3 of average space charge after around one hour of depoling. It is likely that space charges were deeply trapped. The results obtained during depoling showed analogous output as for the case of poling. Samples that reached the charge saturation and stabilization in short time during the poling case experienced a fast depoling that was in the same time range.

[9] This value was chosen as visual inspection for 'space charge free' sample resulted in average space charge of less than 0.05C/m^3

4. Breakdown characterization of epoxy nanocomposites

This chapter includes two major sections. The preparations for the breakdown test: conductivity measurement of samples, design and preparation of the setup used for oil conductivity measurement, design of electrodes for DC ramp breakdown tests by making use of field plots, and preparation of the electrodes are included in the first part. The preparation part was executed at TU Delft. The other section comprises of the DC short time breakdown tests on epoxy based nanocomposites, and the analysis of the results using Weibull analysis. This step was conducted at Philips Healthcare. Both DC and 600 Hz AC ramp tests were planned to be performed on the epoxy based nanocomposite samples. The realization of the setup for the AC test was not successful so only DC ramp breakdown tests took place. The tests were performed using a ramp test with a rate of rise of 500 V/s, which typically was conducted on about 5 samples in each batch. As stipulated in the IEC 60243-1 & IEC 60243-2 standards, the number of samples used from each batch should be five and the breakdown field to be the mean of the individual breakdown field values. In case any one of the 5 breakdown results shows a 15% deviation from the mean value additional 5 samples be tested and the breakdown result be evaluated as the mean of the 10 breakdown results [1, 4]. Due to the limitation on the number of the samples, this rule was not strictly followed at first. Due to the omission of AC ramp tests, the rest of the samples were used for DC ramp tests. This was an important step to perform the tests according to IEC standards. For the analysis of the breakdown data, the two parameter Weibull distribution was used. This statistical tool was chosen as it is one of the extensively used extreme value functions where the system fails when the weakest link fails [35, 36].

4.1. Short time breakdown tests (Step-up and Ramp)

These are tests that are practiced at a field higher than the permissible field strength or they can be performed such that the voltage is increased discretely or continuously until breakdown takes place. In this thesis the latter was considered and a choice was made between step-up and ramp tests. Step-up tests are such that, the voltage starts at approximately half the estimated breakdown strength of the material and the voltage is raised in steps. In the case of ramp tests, however, the voltage is automatically elevated with a desired rate of rise. According to IEC 60243-1, it is possible to perform any of the tests. For this thesis, ramp test was chosen over step-up test due to the following reasons:

- Since the system is automated, it is easy to monitor
- Increased accuracy than the manual step-up test

It should be noted, however, that the ramp voltage test represents a convenient preliminary test to determine whether a material merits further consideration, but it falls short of a complete evaluation in two important respects. First, the condition of a material as installed in apparatus is quite different from its condition in this test, particularly with regard to the configuration of the electric field and the area of material exposed to it, partial discharge (corona), mechanical

stress, ambient medium, association with other materials, and effect of space charges. Second, in service there are deteriorating influences, heat, mechanical stress, partial discharge (corona) and its products, contaminants, etc., which may reduce the breakdown voltage far below its value as originally installed [37].

4.2. Preparation for DC ramp tests

While performing breakdown tests, the sample can be stressed to a level where an external flashover may occur before breakdown. This being not a desired outcome, the following list mentions the important points worth considering before carrying out any breakdown test.

1. *Designing electrodes that avoid field enhancements:*

This determining step favors smooth edged electrodes. If the electrodes are well designed, the field distribution can be shaped so that the maximum field occurs at the center and breakdown takes place there. The breakdown electric field can then be estimated using the relation E=V/d, where V is the breakdown voltage and d the thickness of the sample at the location of breakdown. It should, however, be noted that this doesn't incorporate the field enhancement due to space charges in the sample.

2. *Sample should be as thin as possible:*

This helps to stress the samples with higher fields without the peril of surface discharges or, even worse, flashover. If the samples are thin, the voltage that needs to be applied for the samples to breakdown will be comparatively small and the interference of surface discharges and/or flashover in the measurement can be greatly influenced. Besides, the thinner the samples are, the better the reproducibility of the breakdown results.

3. *Determination of the resistivity of oil and the epoxy nanocomposites:*

DC field distribution is determined by the geometry of the test cell and by the conductivities of all media involved. Knowledge of conductivity of the oil and nanocomposites is, therefore, important.

4. *Arrangement of the HV electrode and ground:*

The electrodes needed to be aligned such that flashover doesn't occur in the oil. The mechanism employed to avoid this was to arrange a set up where the supply to the electrodes enter the oil in different directions; thus placing them as far as possible from each other. The HV lead enters the oil from above and the ground lead enters from the bottom part of the container.

5. *No flashover occurs between electrodes:*

Performing any kind of DC breakdown test, the test sample can be stressed with a very high field. It must be noted that while the normal field increases, the field tangent to the electrode sample interface also increases. This is the field responsible for surface discharges and flashover

in extreme cases. The tangential field thus sets the limit to the voltage we can apply to the sample.

4.2.1. Conductivity measurement of samples

It was mentioned earlier that for DC field plots, apart from the configuration and dimensions of the samples, the conductivity of the samples and the surrounding medium is important.

An existing test setup, at TU Delft, was used for the measurement of the conductivities of the samples. The set up is well shielded and a sensitive electrometer was used for current measurement. Measurements were done at ambient conditions: typical temperature of 20^0C and humidity of 40%. The measurement procedure lasted for about 24 hours, when the current is expected to have reached a steady state value. Table 4.1 shows the samples that were considered during the conductivity measurement at a specified Electric Field and given atmospheric conditions. After obtaining the steady state current, the conductivity (σ) of the samples was calculated.

$$\sigma = \frac{4Il}{\pi V d^2} \tag{4.1}$$

In equation 4.1, I is the current, l represents the sample thickness, V is the voltage, and d stands for the diameter of the measuring electrode which is 28 mm in this case.

Table 4.1 conductivity of Epoxy nanocomposites at ambient[10] conditions

Sample	Thickness (mm)	Measurement Duration (hr)	Voltage (kV)	Field (kV/mm)	Current (pA)	Conductivity $(\Omega m)^{-1}$
Neat Epoxy	0.57	17	5.0	8.8	$9.2\cdot10^{-1}$	$2.14\cdot10^{-16}$
0.5wt%_MgO-Epoxy	1.13	17	5.0	4.4	$5.3\cdot10^{-2}$	$2.44\cdot10^{-17}$
5wt%_MgO-Epoxy	1.0	20	5.0	5	$1.3\cdot10^{-1}$	$5.18\cdot10^{-17}$
2wt%_AlN-Epoxy (dried)	1.04	24	3.5	3.4	$2.3\cdot10^{-1}$	$3.21\cdot10^{-17}$
2wt%_AlN-Epoxy	1.12	22	3.5	3.1	$3.5\cdot10^{-3}$	$2.27\cdot10^{-17}$
5wt%_AlN-Epoxy	0.563	23.5	5.0	8.9	$4.0\cdot10^{-4}$	$5.18\cdot10^{-17}$
2wt%_Al2O3-Epoxy	0.932	17.5	5.0	5.4	$6.0\cdot10^{-4}$	$2.28\cdot10^{-19}$
5wt%_Al2O3-Epoxy	0.523	17	5.0	9.6	$1.6\cdot10^{-3}$	$3.30\cdot10^{-19}$

[10] Temperature of about 20^0C and humidity of around 40%

The results show that almost all of the nanocomposites showed lower conductivity as compared to neat epoxy. In [3], a conductivity value of neat epoxy (CY1300/HY956) is reported to be $1.4 \cdot 10^{-16}$ /Ωm. This value is very close to the value of neat epoxy used for this thesis, (CY231/HY925). In the same reference, however, the conductivity of Al_2O_3-Epoxy nanocomposites is about three orders of magnitude higher than what is obtained for this thesis.

4.2.2. Oil conductivity measurement

Concentric cylinder aluminum electrodes with an insulating bottom were prepared for oil conductivity measurement. The oil, Shell Diala B, was filled in levels so that the effect of the leakage current due to the insulating bottom can be seen. If the calculated conductivity of oil doesn't show much of a change, for the different volumes of oil used, it will be deduced that the leakage current is not significant and the calculated value of conductivity is a good result at that value of electric field.

Although, the conductivity of oil is dependent on the level of electric field, a value of the conductivity at a low value was enough. This is because the oil is stressed at low fields compared to the sample.

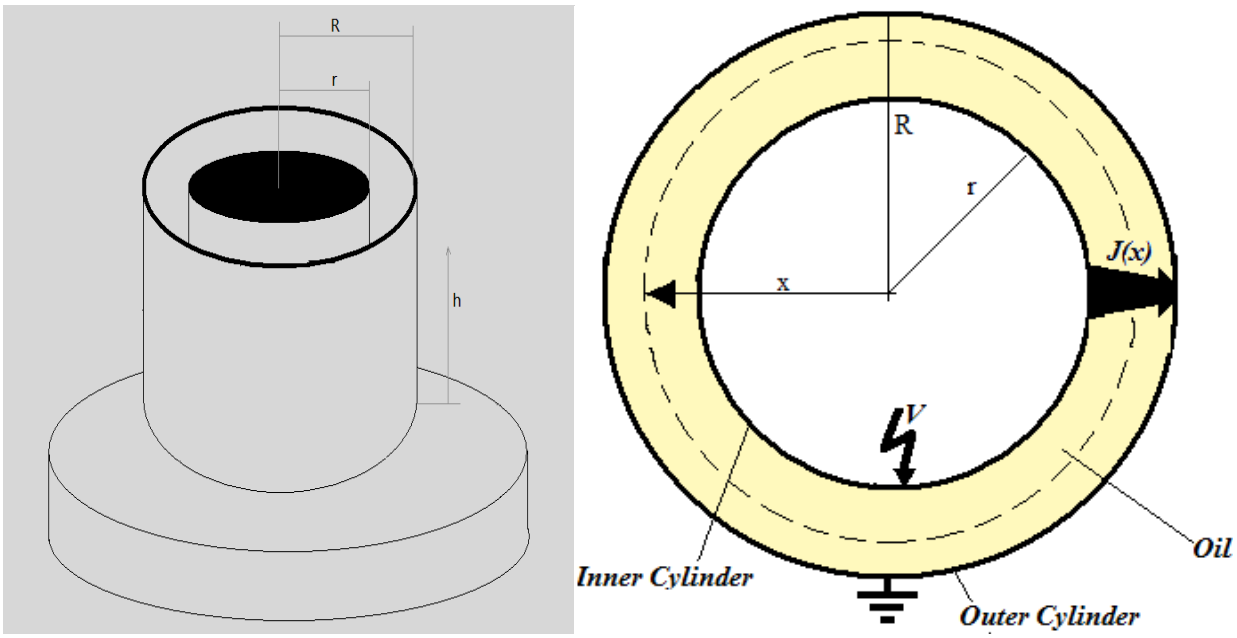

(a) **(b)**

Fig. 4.1 Setup used to measure the conductivity of oil: **(a)** Schematic **(b)** Cross-section

To increase the sensitivity of the measurement, the gap between the two cylinders should be as small as possible. This however, accentuates the probability of surface discharges and/or flash over which interfere(s) with the current measurement. This dictates the calculation of the tangential electric field at the interface between the oil and air. Besides, a potential point for

flashover, the field enhancement at the edge of the electrodes was addressed by round finishing the top of the cylinder.

The following sets of equations were used to calculate the value of resistivity and the field levels.

$$J(x)=E(x).\sigma$$

$$I=J(x).2\pi hx$$

$$\int_0^V dV=\int_r^R E(x)dx$$

$$V=\int_r^R \frac{I}{2\pi\sigma hx}dx$$

$$V=\frac{I}{2\pi\sigma h}\ln\frac{R}{r}$$

$$\sigma = \frac{I}{2\pi hV}\ln\frac{R}{r}$$

(4.2)

In equation 4.2, x represents the radial distance from the center of the inner cylinder, σ represents the conductivity of oil and J(x) represents the position dependent current density.

Important figures can also be obtained from the above set of equations: the electric field at any point between the electrodes and the maximum value, for instance.

$$E(x)=\frac{I}{2\sigma\pi hx}$$

$$E(x)=\frac{V}{x\ln\frac{R}{r}} \quad (4.3)$$

The maximum electric field occurs at x=r.

$$E_{max}=\frac{V}{r\ln\frac{R}{r}} \quad (4.4)$$

In estimating the dimensions of the cylinder, the maximum electric field of 4.4 should be less than 1 kV/mm, the permissible field strength of air along interface [24].

To realize a good sensitivity, the spacing between the electrodes was taken to be as small as possible. The dimensions of the cylinder, therefore, were taken as follows: radius of the outer cylinder R=50 mm, radius for the inner one r=37 mm, height of the cylinder, h=60 cm. The space between the cylinders was filled with oil with the following heights: 188 mm, 238 mm, 393 mm, and 528 mm and measurements were made in open air at a temperature of 20^0C and a humidity of 40%. Table 4.2 shows the levels of oil (h), as measured from the bottom of the cylinder and the values of the current and hence the conductivity calculated according to equation 4.2.

Table 4.2 Oil conductivity for different levels of oil

Level of oil h, (mm)	*Voltage (kV)*	*Current (nA)*	*Conductivity* $(\Omega m)^{-1}$
188	1	2.85	$4.11 \cdot 10^{-13}$
238	1	2.5	$5.03 \cdot 10^{-13}$
393	1	1.82	$3.04 \cdot 10^{-13}$
528	1	1.6	$2.60 \cdot 10^{-13}$

Taking the median value from table 4.2, the conductivity of oil was approximately taken to be $3.5 \cdot 10^{-13}$ $(\Omega m)^{-1}$. The conductivity of Shell Diala B according to test method IEC 60247 at, 24^0C, was $1.6 \cdot 10^{-12}$ $(\Omega m)^{-1}$ which shows a difference by a factor less than 5. The actual oil that was used for the test at Philips Healthcare was Shell Diala GX where the conductivity value obtained from the shell lubricants technical support group stating a test method of IEC 60247 at 24^0C was $4.3 \cdot 10^{-13}$ $(\Omega m)^{-1}$. This value was therefore used as the conductivity of the oil in the field plot. The conductivities of the samples ranged from $2.14 \cdot 10^{-16}$ $(\Omega m)^{-1}$ for pure epoxy to about $3.3 \cdot 10^{-19}$ $(\Omega m)^{-1}$ for 5wt%_Al_2O_3-Epoxy nanocomposite. Considering the conductivity of Shell Diala GX and the sample conductivity values from table 4.1, it can be seen that the ratio of the conductivities of the oil and samples is at least 10^3 and field plots were made for this ratio.

4.2.3. Electrode design for DC breakdown tests

Considering the dimensions of the samples that were about 0.6 mm thick and 56 mm in diameter, an electrode configuration was designed with a value of the tangential field along the electrode sample interface, shown as line1 in fig. 4.2, as small as possible. The choice started from two extremes: the first one was sphere-sphere electrodes, and the other extreme was parallel plate electrodes with round edges. The sphere-sphere configuration was discarded due the problems of aligning the electrodes perfectly. This setup is mostly used when the electrode is casted into the insulating material [1]. The parallel plate of electrodes, the second extreme, was discarded as the samples had a thickness gradient due to problems in the preparation. Hence, an intermediate configuration was sought that combats the shortcomings of the above two configurations, fig. 4.2. The electrodes were made of stainless steel. The dimensions were

chosen such that the field along line1, which is responsible for surface discharges and/or flashover, is minimized.

The DC field plot in fig. 4.3 is obtained for the configuration of fig. 4.2. The following values were considered: conductivity of oil $4.3 \cdot 10^{-13}$ $(\Omega m)^{-1}$, sample conductivity $2.14 \cdot 10^{-16}$ $(\Omega m)^{-1}$, sample thickness to be 1 mm, and an applied voltage of -150 kV .

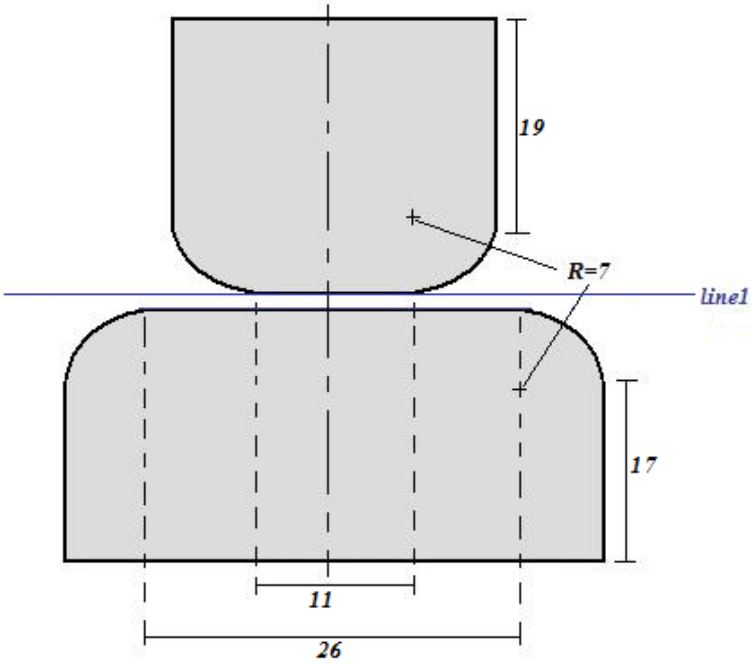

Fig. 4.2 Dimensions of the electrodes used for DC ramp test

As a thought, for the possible level of voltage applied, the equivalent interfacial field was to be estimated and matched against a value found in literature for the permissible field along solid-oil interface. The interpolated maximum tangential field would then be matched against the permissible tangential filed and made sure it stays lower. But as this data was not easy to obtain, preliminary test was performed to check levels of voltage that can be applied and primarily if the set up is prone to surface discharges and flashover.

Two points can be noted from the field plots. The maximum horizontal field, along line1, occurs at the periphery of the samples and the Laplacian field at the center is fairly perpendicular and the value can be well approximated using the relation E=V/d. It should be noted, however, that this value doesn't consider the effect of space charges.

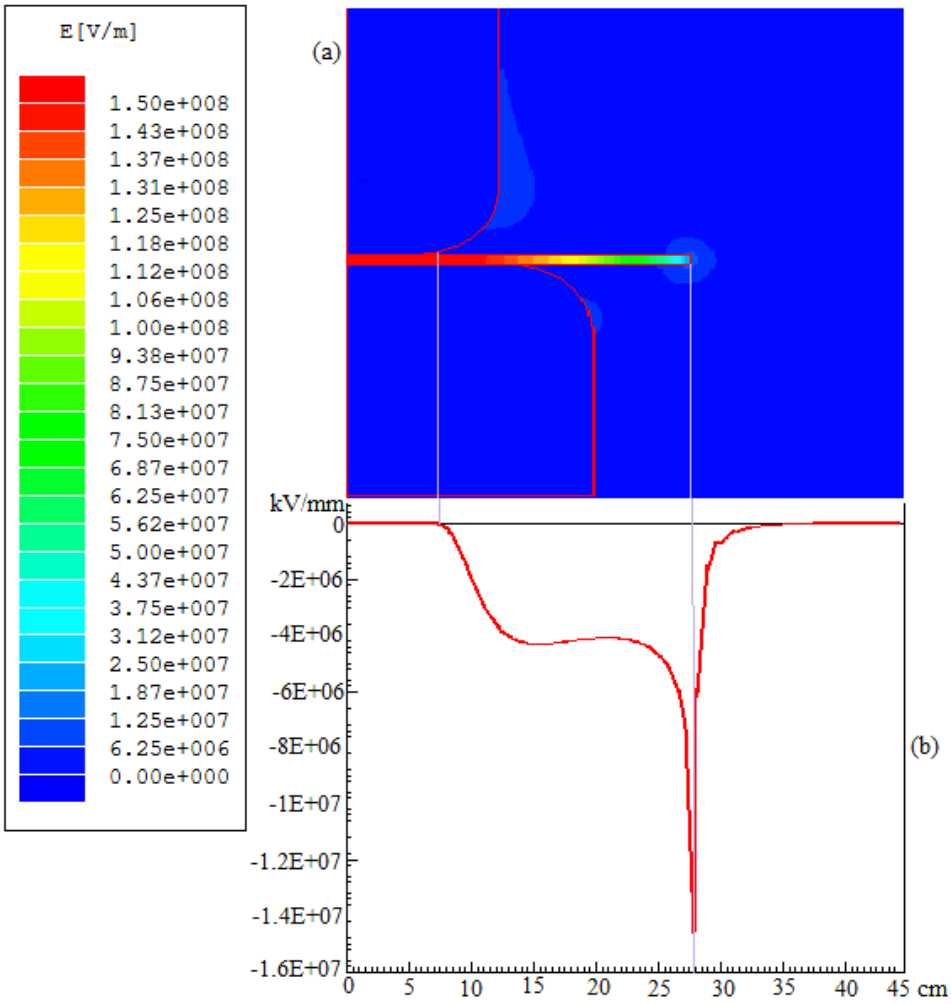

Fig. 4.3 DC field plot for conductivity ratio of 10^3: **(a)** Total Electric Field, **(b)** Electric Field along line1

4.2.4. Verification of electrode design using DC step-up test

After the electrodes were designed and prepared, they were checked using a DC step-up test at TU Delft. For this check, a 5wt%_Al_2O_3-Epoxy nanocomposite sample, with a thickness of 0.55 mm was considered. The sample and electrode setup were immersed in Shell Diala-B oil. The HV electrode was connected in series with a 350 MΩ resistance, to protect the measuring equipment in case of breakdown, and positive DC voltage was applied. Starting from 10 kV/mm with a step of 2 kV/mm and duration of 2 min per step, voltage was increased until breakdown. The Laplacian field stress during breakdown was 106 kV/mm. Discharges were not observed and the electrodes were validated.

4.3. DC ramp breakdown test protocol

4.3.1. HV source and control circuit

Fig. 4.4a and b show the setup used to do DC step-up breakdown tests. As per the requirement of the standard, D 3755 [37], a voltage source with voltage-control, voltage-measuring, and circuit-interrupting equipment and a provision for retaining the breakdown voltage reading after breakdown was necessary and arrangements were made accordingly. A resistance of 400 kΩ was used in series with the sample and a negative voltage was applied to the samples. Starting from -10 kV, the voltage was automatically increased with a rate of rise of -500 V/s until the sample breaks down. When breakdown occurs, the current limiter automatically stops the voltage increase and a dedicated program, which also has features to input the ramp level and initial voltage, records the breakdown voltage;

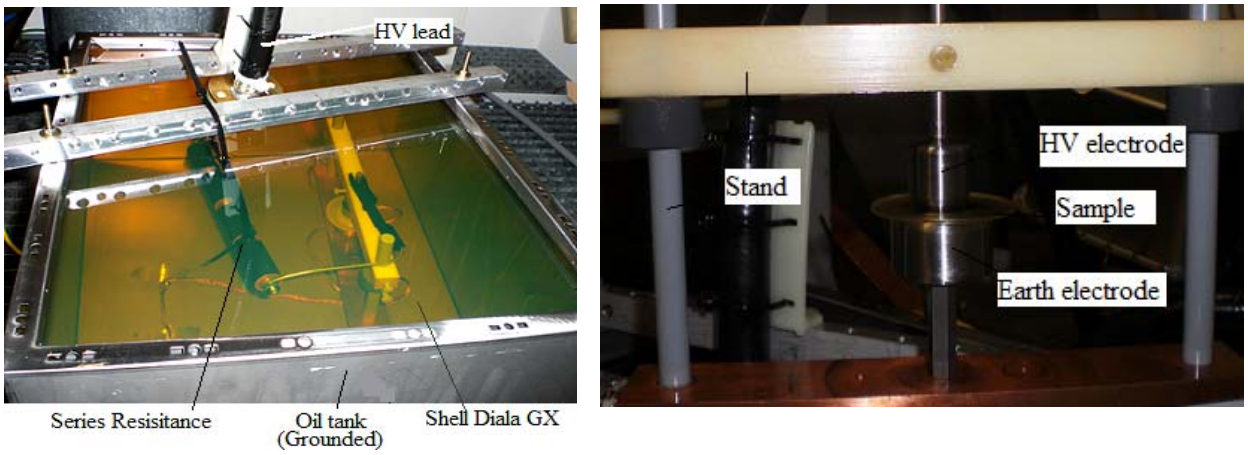

(a) **(b)**

Fig. 4.4 (a) Test setup, **(b)** Electrode setup

4.3.2. Test samples

Type of epoxy nanocomposites, their weight compositions, and the number of samples in each batch used during the breakdown tests can be singled out from table 4.3. For the test, about 173 samples were considered. The thickness of the samples ranged from 0.39 mm to 0.80 mm. More than 90% of them were, however, between 0.5 mm to 0.6 mm.

Initially, only 5 or less samples were tested from each batch. When of any one of the breakdown fields deviates from the mean value by more than 15%, that value was discarded and analysis made on the rest of the results. This was not correct according to the stipulation of the IEC standard, that dictates to test 5 more samples in case of the aforementioned situation [1, 4].

Since the AC ramp tests were not performed, however, the samples were later used for DC ramp tests. This step played an important role in augmenting the amount of DC breakdown data.

4.3.3. Data capture

For each of the samples, the voltage breakdown was recorded. The samples were then taken out of the oil tank and visually analyzed for breakdown channels. In some cases, where the visual inspection was not assuring, microscope investigation was done to look for the breakdown channel(s), if any. The thickness of the samples was then measured at the location of breakdown. The electric field during breakdown, the parameter used for comparison, was then calculated from the breakdown voltage and thickness using the relation E=V/d. In most of the cases, the breakdown took place around the center. A few of breakdown channels emanated from the edge of the high voltage electrode.

4.4. Analysis of breakdown results using the Weibull distribution

As mentioned above, the breakdown data obtained were analyzed using the two-parameter Weibull and the distribution of the breakdown field strength values were displayed on Excel scatter diagrams.

The Weibull distribution is one of the extreme value functions which is the most common for solid insulation breakdown data analysis [36]. It bases the analysis such that the system fails when the weakest link fails [35].
The expression for the cumulative density function for the two-parameter Weibull distribution is shown in equation 4.5.

$$F(E;\eta,\beta)=1-\exp\left(-E/\eta\right)^{\beta} \tag{4.5}$$

Where:

E	is the breakdown voltage,
$F(E;\eta,\beta)$	is the probability of failure at a voltage E.
η	is the scale parameter and is positive, and
β	is the shape parameter and is positive.

The scale parameter η represents the electric field for which the failure probability is 63.2%. The unit of η is the same as E. On the other hand, the scale parameter β is a measure of the range of the breakdown field. The larger the value of β is, the smaller the range of breakdown fields. It is analogous to the inverse of the standard deviation.

If the same experiment involving the testing of many specimens is performed a number of times, the values of the parameters from each experiment differ. This variation in estimates results from the statistical nature of insulation breakdown, [38]. Therefore, any parameter estimate differs from the true parameter value that is obtained from an experiment involving an infinitely large number of specimens. Hence, it is common to give with each parameter estimate a confidence interval that encloses the true parameter value with high probability. For this thesis, each of the parameters is presented with their bilateral 90% confidence interval. As an example, fig. 4.5 shows the breakdown distribution of 0.5wt%_AlN-Epoxy nanocomposite with 90% confidence bound. The actual value of η being 188 kV/mm, the lower and upper bounds of η are 161 kV/mm and 221.3 kV/mm respectively. Thus, there is 90% probability that the true value of η lies between 161 kV/mm and 221.3 kV/mm.

For this thesis, the trial version of Weibull++ software was used to calculate the parameter values and make plots.

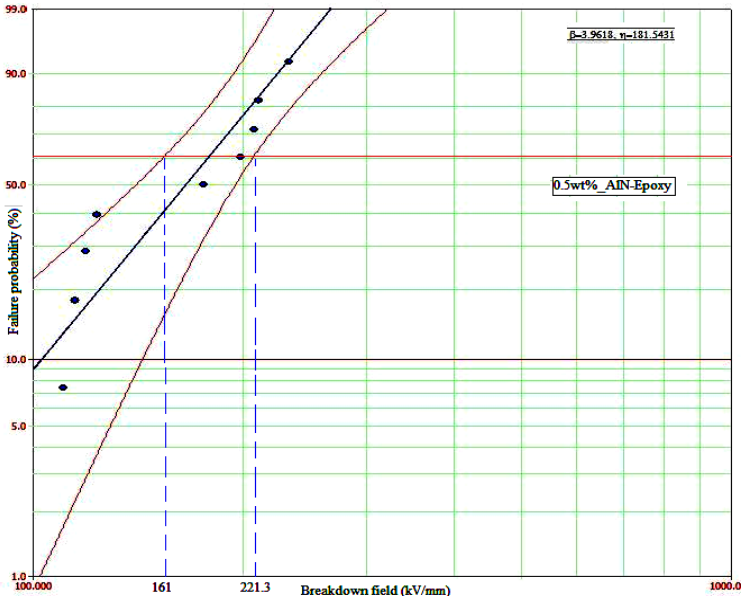

Fig. 4.5 Weibull plot with 90% confidence bound

4.5. Results and discussions

Fig. 4.6(a-f) shows Weibull plots of the breakdown field distribution for the samples considered. The nanocomposites are compared according to their weight percentages taking neat epoxy as a reference (0wt% of the respective nanofiller). Scatter plots of the breakdown distribution are presented in appendix C and the shape and scale parameters, with their limits for 90% confidence bound, for each batch of samples is tabulated in table 4.3.

It can be generalized that most of the epoxy nanocomposites showed improved DC ramp breakdown field strength compared to neat epoxy, fig. 4.7. The scale parameter (η) showed

higher value for filler loading of 0.5wt% for most of the nanocomposites considered. Increase in filler loading above 2wt% displayed no change in the value of η. For Nanopox, however, an increase in the value was observed when increasing filler content from 10wt% to 15wt%.

Table 4.3 Parameters for DC ramp breakdown tests and confidence bound

Nanocomposite	***Filler wt%***	***Number of samples***	***Parameters with 90% Confidence Bounds***					
			Lower	***β***	***upper***	***Lower*** *(kV/mm)*	η^{11} *(kV/mm)*	***Upper*** *(kV/mm)*
Neat Epoxy	--	8	6.64	***10.2***	15.8	153	***162.6***	172.8
Al_2O_3-Epoxy	0.5	8	2.3	***3.8***	6.4	214.06	***252.3***	297.4
	2	9	6.81	***10.5***	16.3	207	***218.6***	230.9
	5	6	6.73	***10.4***	16	206.18	***218.0***	230.4
	10	9	2.53	***4.2***	7.1	174.6	***202.5***	234.9
	5 (Conv.)	5	6.75	***12.3***	22.3	207.48	***221.0***	235.3
AlN-Epoxy	0.5	9	2.35	***3.8***	6.3	161.06	***189.0***	221.3
	2	7	3.09	***5.1***	8.4	199.08	***226.4***	257.5
	10	7	5.59	***9.3***	15.3	178.4	***191.5***	205.6
MgO-Epoxy	0.5	7	4.38	***6.7***	10.3	192.0	***214.4***	239.4
	2	6	3.91	***6.4***	10.6	150.5	***168.1***	187.9
	5	7	4.31	***7.3***	12.2	168.3	***184.1***	201.3
Nanopox (SiO_2-Epoxy)	0.5	6	8.81	***15.3***	26.7	283.2	***296.5***	310.4
	2	7	2.7	***4.4***	7.3	204.1	***236.6***	274.2
	5	5	6.32	***11.4***	20.5	194.9	***208.7***	223.3
	10	8	2.13	***3.4***	5.3	183.6	***220.7***	265.2
	15	7	3.91	***6.5***	10.4	249.8	***276.4***	305.9
(Al_2O_3+SiO_2)-Epoxy	0.5+0.5	5	21.76	***38.6***	68.4	260.2	***265.4***	270.8
	2.5+2.5	7	2.42	***4.3***	7.5	204.5	***239.5***	280.6
(AlN+SiO_2)-Epoxy	0.5+0.5	7	1.98	***3.5***	6.1	147.5	***179.6***	218.6
	2.5+2.5	8	2.38	***3.9***	6.3	202.6	***238.0***	279.6
10wt%_BN-Epoxy	***Filler size (nm)***							
	70	7	3.19	***5.39***	9.1	204.1	***230.6***	260.5
	500	6	4.45	***7.5***	12.7	178.5	***196.3***	215.8
	1500	6	2.67	***4.8***	8.7	155.3	***180.3***	209.2
	5000	6	3.33	***5.77***	10.0	152.4	***172.3***	194.9

[11] The scale parameter, mathematically, should be a positive value as is presented in the results. It should, however, be kept in mind that for the tests in this thesis the samples were stressed with a negative voltage, hence a negative breakdown field strength.

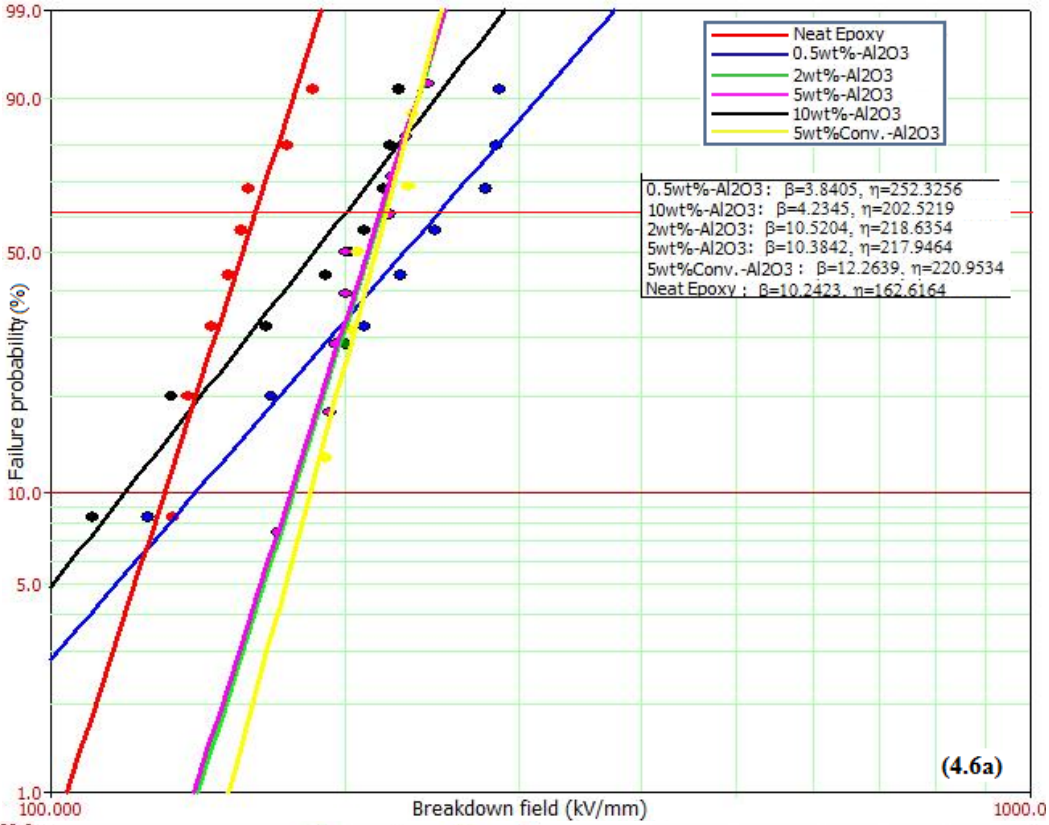
99.0
90.0
50.0
10.0
5.0
1.0
Failure probability (%)
100.000
Breakdown field (kV/mm)
1000.0
Neat Epoxy
0.5wt%-Al2O3
2wt%-Al2O3
5wt%-Al2O3
10wt%-Al2O3
5wt%Conv.-Al2O3
0.5wt%-Al2O3: β=3.8405, η=252.3256
10wt%-Al2O3: β=4.2345, η=202.5219
2wt%-Al2O3: β=10.5204, η=218.6354
5wt%-Al2O3: β=10.3842, η=217.9464
5wt%Conv.-Al2O3 : β=12.2639, η=220.9534
Neat Epoxy : β=10.2423, η=162.6164
(4.6a)

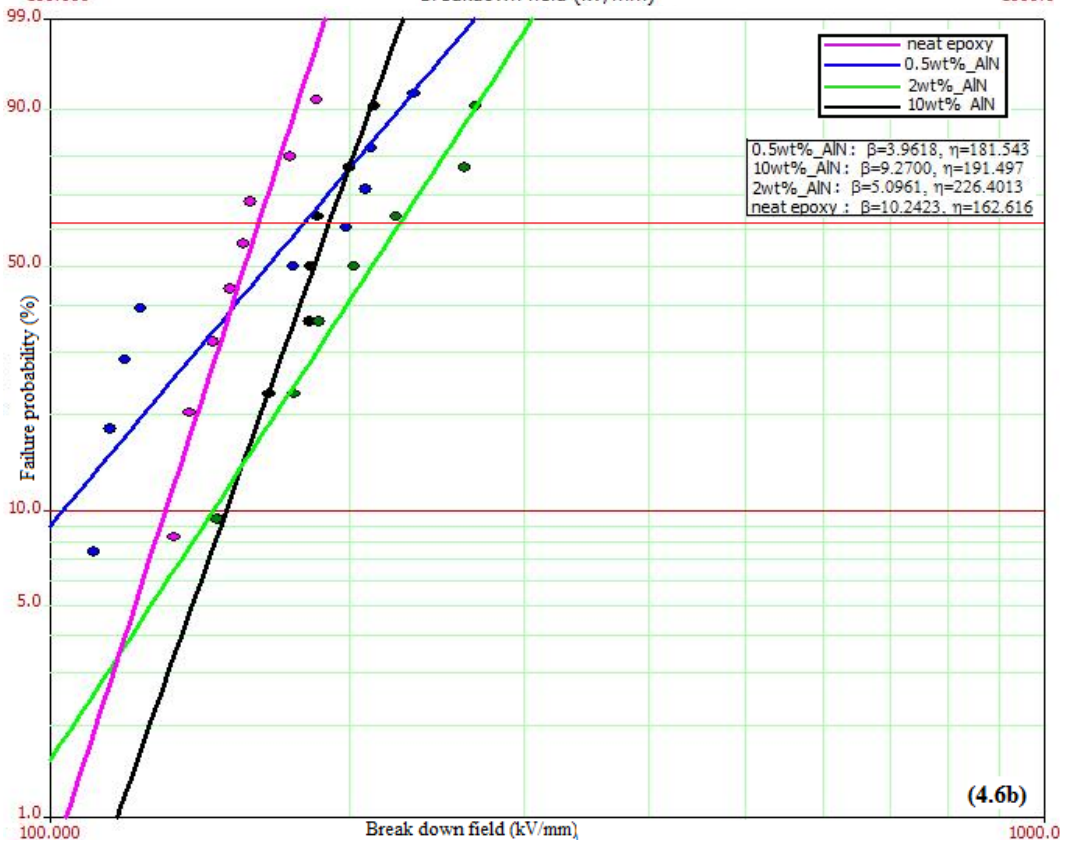
99.0
90.0
50.0
10.0
5.0
1.0
Failure probability (%)
100.000
Break down field (kV/mm)
1000.0
neat epoxy
0.5wt%_AlN
2wt%_AlN
10wt% AlN
0.5wt%_AlN: β=3.9618, η=181.543
10wt%_AlN: β=9.2700, η=191.497
2wt%_AlN: β=5.0961, η=226.4013
neat epoxy : β=10.2423, η=162.616
(4.6b)

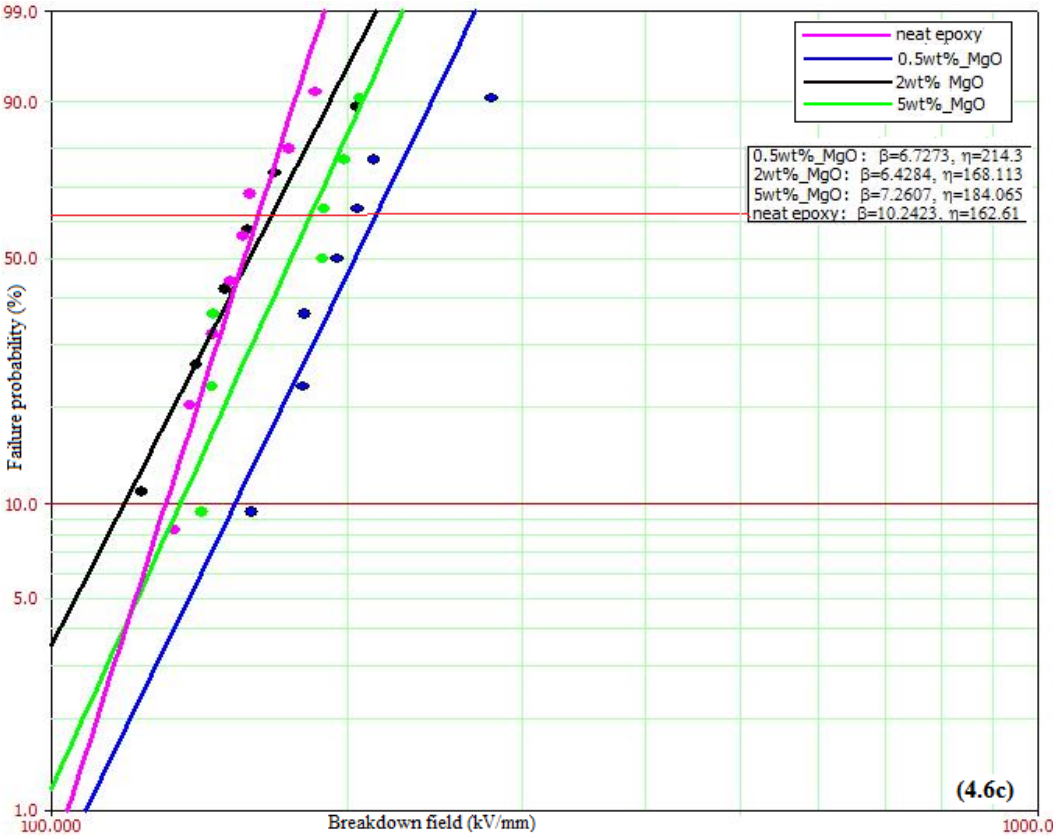
99.0
90.0
50.0
10.0
5.0
1.0
Failure probability (%)
100.000
Breakdown field (kV/mm)
1000.0
neat epoxy
0.5wt%_MgO
2wt% MgO
5wt%_MgO
0.5wt%_MgO: β=6.7273, η=214.3
2wt%_MgO: β=6.4284, η=168.113
5wt%_MgO: β=7.2607, η=184.065
neat epoxy: β=10.2423, η=162.61
(4.6c)

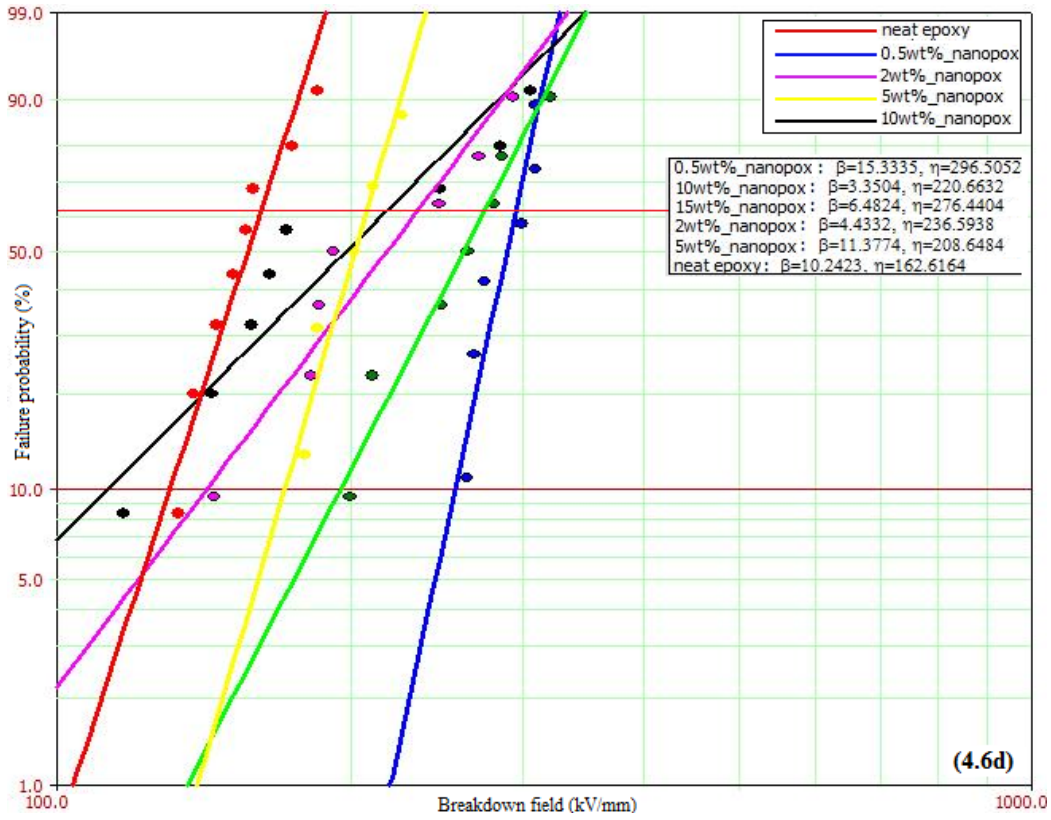
99.0
90.0
50.0
10.0
5.0
1.0
Failure probability (%)
100.0
Breakdown field (kV/mm)
1000.0
neat epoxy
0.5wt%_nanopox
2wt%_nanopox
5wt%_nanopox
10wt%_nanopox
0.5wt%_nanopox : β=15.3335, η=296.5052
10wt%_nanopox : β=3.3504, η=220.6632
15wt%_nanopox : β=6.4824, η=276.4404
2wt%_nanopox : β=4.4332, η=236.5938
5wt%_nanopox : β=11.3774, η=208.6484
neat epoxy: β=10.2423, η=162.6164
(4.6d)

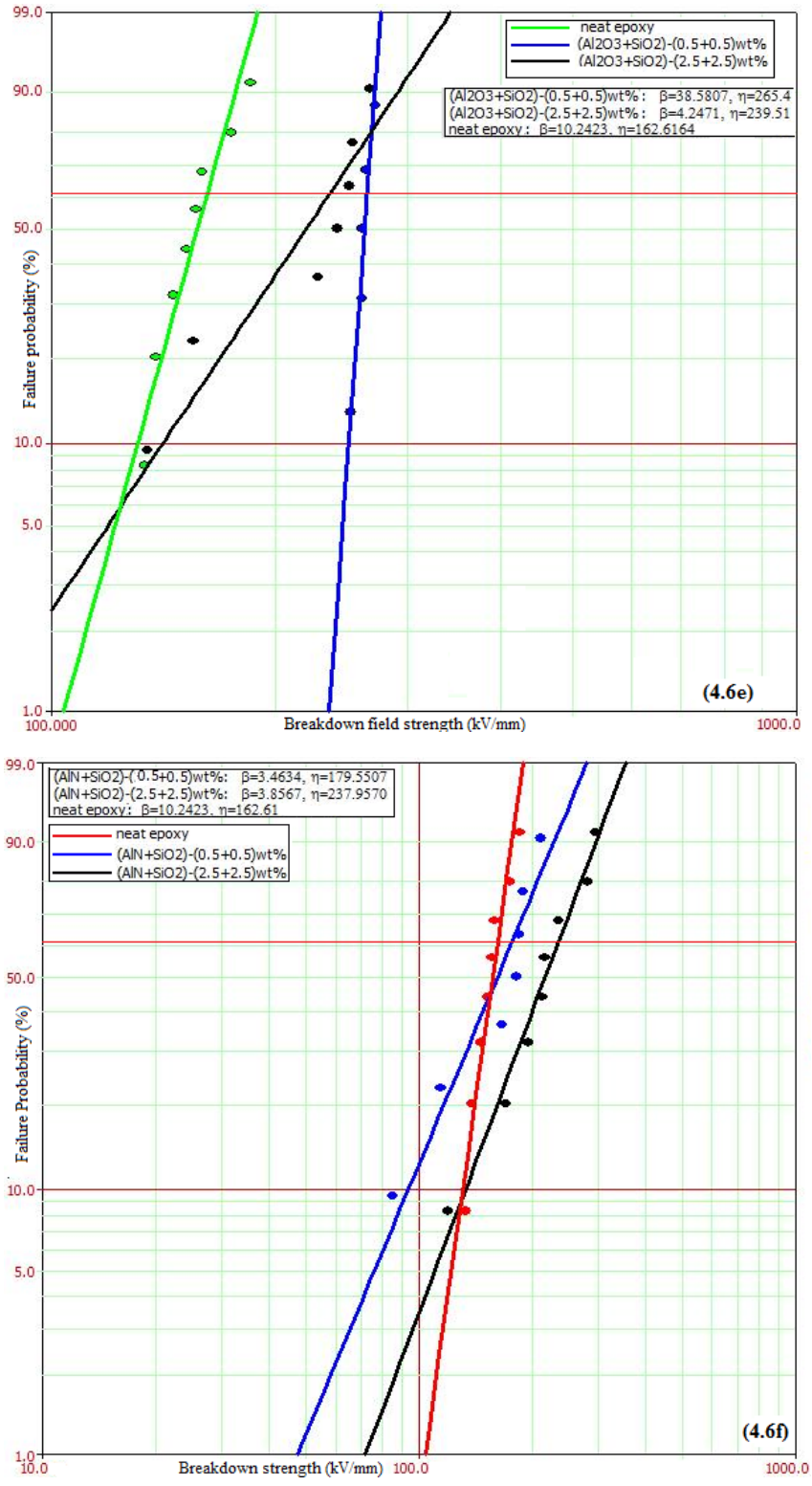

Fig. 4.6 Weibull plots for the breakdown distribution of epoxy nanocomposites with various fillers: **(a)** Al_2O_3-Epoxy, **(b)** AlN-Epoxy, **(c)** MgO-Epoxy, **(d)** Nanopox, **(e)** (Al_2O_3+SiO_2)-epoxy, **(f)** (AlN+SiO_2)-Epoxy

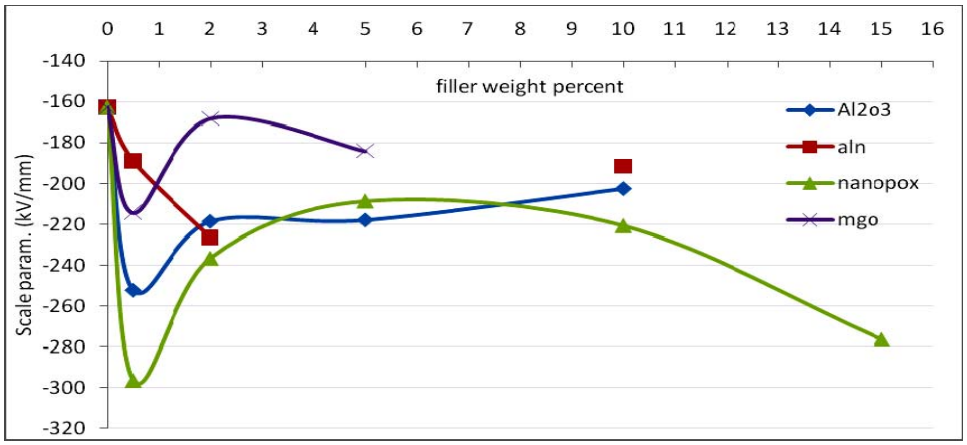

Fig. 4.7 Scale parameter against filler loading

Al_2O_3 filler:

As can be seen from the fig. 4.6a, fig. 4.8, and the parameters in table 4.3, all Al_2O_3-Epoxy nanocomposites showed better DC ramp breakdown strength as compared to neat epoxy. The Weibull shape parameter β, except for (0.5 & 10) wt%_Al_2O_3-Epoxy nanocomposites, is greater than 10, showing good distribution of the breakdown data. As can be seen especially from fig. 4.8, increasing the filler loading above 2wt% showed no change in η. It should be noted however, that the highest DC ramp breakdown strength is observed for 0.5wt% Al_2O_3 filler. 5wt%_Al_2O_3 Conventional filler, despite a few literature reports claiming no improvement of microfiller on the breakdown strength of the base material, a breakdown value comparable to nanofiller of the same weight loading was recorded, and about 50% higher η was obtained as compared to neat epoxy.

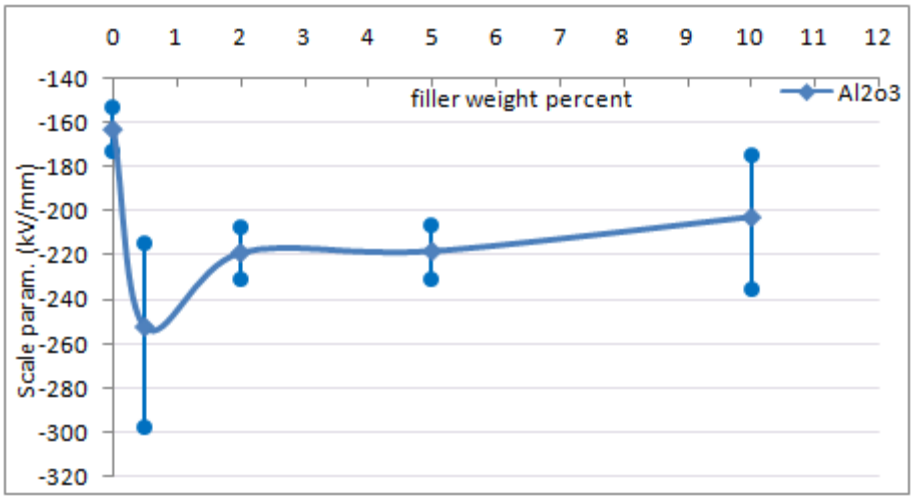

Fig. 4.8 Scale parameter vs. filler loading with limits of 90% confidence bound (Al_2O_3-Epoxy)

AlN filler:

For the DC ramp breakdown strength of AlN-Epoxy nanocomposites, loadings of 0.5wt%, 2wt%, and 10wt% were considered. 5wt%_AlN-Epoxy nanocomposites had major preparation problems and were disregarded lest they would lead to wrong conclusions. For this group of nanocomposites, higher breakdown field strengths were obtained as compared to neat epoxy, fig. 4.9. An increase in the scale parameter was observed when increasing the weight percentage from 0.5 to 2, with similar values of the shape parameter, β.

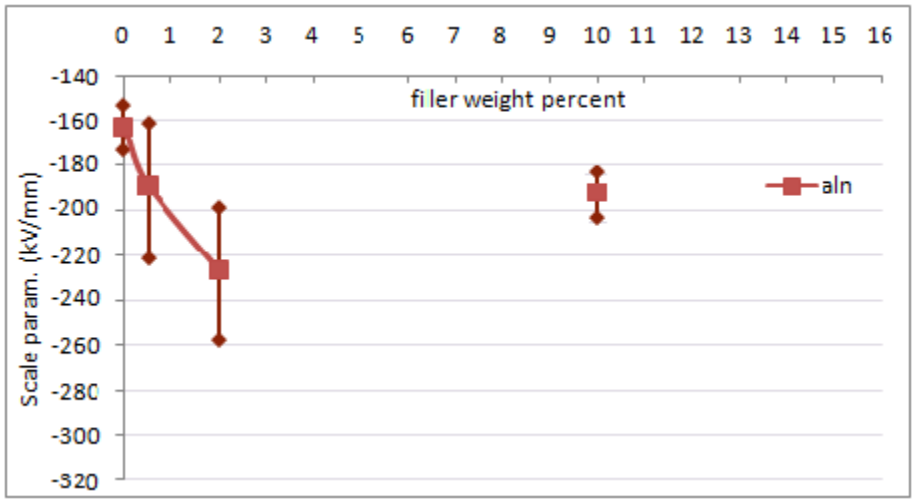

Fig. 4.9 Scale parameter vs. filler loading with limits of 90% confidence bound (AlN-Epoxy)

MgO filler:

In this category, MgO-Epoxy nanocomposites with MgO filler contents of 0.5wt%, 2wt%, and 5wt% were considered. For all fill grades, the shape parameter was less than 10. Similar to Al_2O_3 and SiO_2 nanofillers, highest value of η was obtained for 0.5wt% filler. For (2 and 5)wt%_MgO-Epoxy, the scale parameter was more or less close to that of neat epoxy.

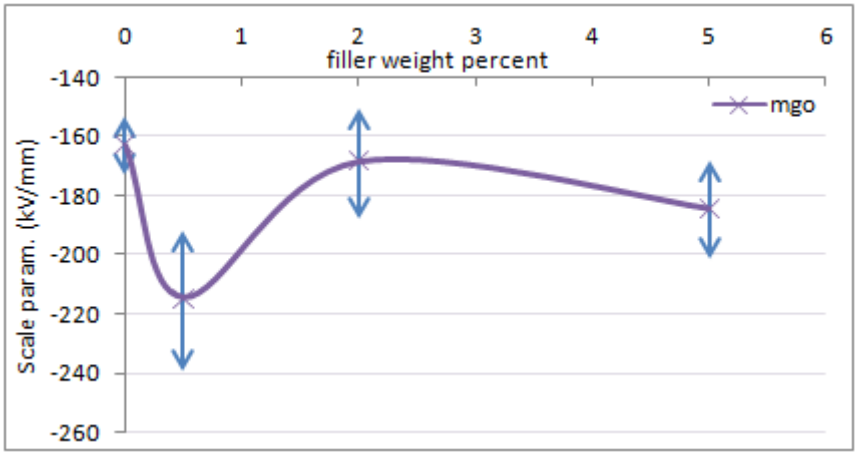

Fig. 4.10 Scale parameter vs. filler loading with limits of 90% confidence bound (MgO-Epoxy)

Nanopox:

Higher DC ramp breakdown strengths were obtained for nanopox compared to neat epoxy or the other nanocomposites considered. As can be seen from fig. 4.7 the highest breakdown field was filed for 0.5wt% of SiO_2, η value of 296.5 kV/mm and β of 15.3 with narrow 90% confidence bound were scored. Though lower than the 0.5wt% filler, higher η values as compared to neat epoxy were exhibited by the 2wt% and 5wt%-Nanopox with a fair reproducibility. Unlike the other nanocomposites, where a decrease in the scale parameter was observed for higher filler content, 15wt%-Nanopox scored the second highest score parameter of all the nanocomposites considered for this thesis.

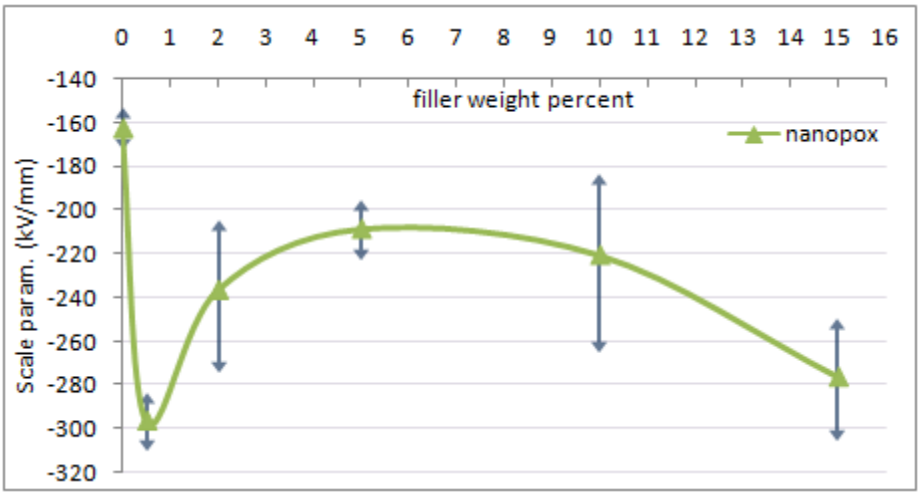

Fig. 4.11 Scale parameter vs. filler loading with limits of 90% confidence bound (Nanopox)

Another group of nanocomposites that were considered for the DC ramp breakdown test were those with two types of nanofillers in the epoxy base. Two groups of fillers (SiO_2+Al_2O_3) and (SiO_2+AlN) were considered.

(SiO_2+Al_2O_3)-filler:

For (0.5+0.5)wt% (SiO_2+Al_2O_3) a breakdown strength about 60% higher than neat epoxy and a value of β of 38.6 was recorded, which is a large value and displays excellent reproducibility of the data. For (2.5+2.5)wt% of similar filler, a higher value of breakdown strength with low value of β=4.3 is obtained. This increase in scatter of the data with increase in the fill grade is well reflected in the scope of the 90% confidence bounds in fig.4.12. The dramatic fall of the shape parameter, i.e. the scatter in the breakdown results, with increase in the filler content could be due to the possibility of presence of agglomerations at higher weight proportions of the filler(s).

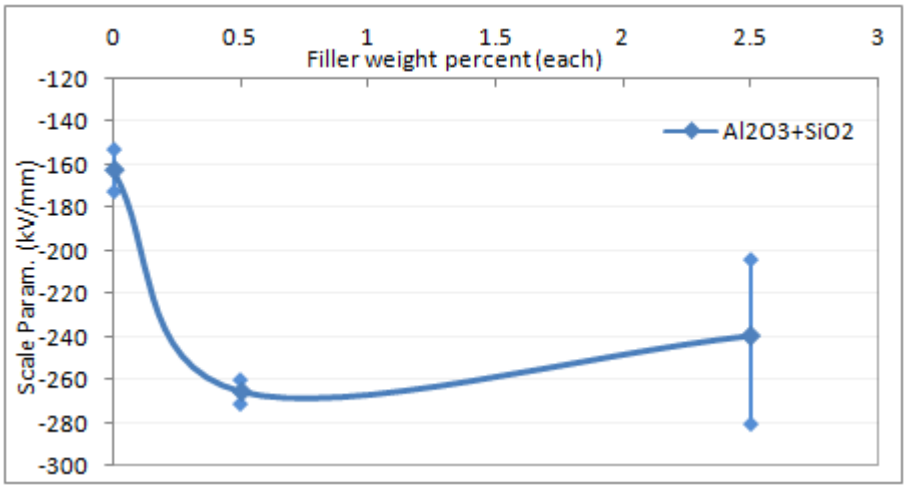

Fig. 4.12 Scale parameter vs. filler loading with limits of 90% confidence bound (SiO_2+Al_2O_3)

(SiO_2+AlN)-filler:

In this group, fig. 4.12, η increases with increase in fill grade. The scatter of the data, however, is very high for both the (0.5+0.5)wt% and (2.5+2.5)wt% of (AlN+SiO2)-Epoxy nanocomposites. The small value of β, and hence wide confidence bound, could be related to the problems in dispersing the AlN filler in the presence of SiO_2, where agglomerates of AlN filler with a size of 500 nm were observed.

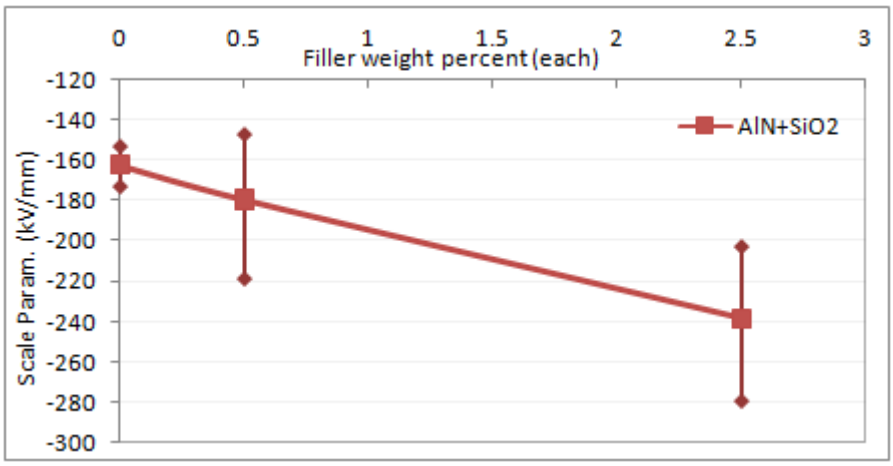

Fig. 4.12 Scale parameter vs. filler loading with limits of 90% confidence bound (SiO_2+AlN)

BN-filler:

For the case of BN-Epoxy nano/microcomposites, different filler sizes of the same weight percentage (10wt%) were considered. The filler sizes considered are 70 nm, 500 nm, 1500 nm, 5000 nm. This was intended to see the effect of breakdown strength when the filler size goes from nano to micron level. In fig. 4.13(a,b) the filler size is displayed in logarithmic scale. The shape parameter was close to 10 in all cases. η being the highest for 70 nm filler size (about 45% higher than neat epoxy), it decreased with increase in filler size. At 5000 nm, the scale parameter was close to the value of neat epoxy.

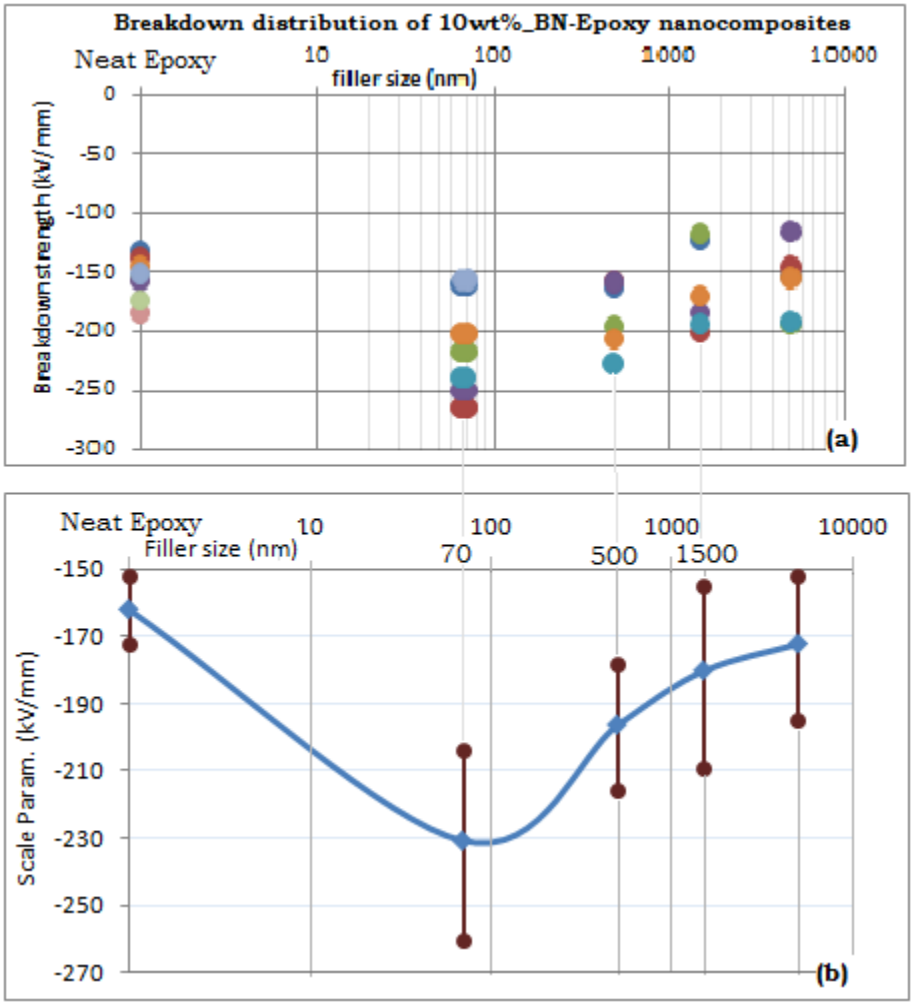

Fig. 4.13 (a) DC ramp breakdown strength scatter plot 10wt%_BN-Epoxy **(b)** Scale parameter vs. filler size with limits of 90% confidence bound (10wt%_BN-Epoxy)

4.6. Breakdown results in relation to space charge results

Apart from distorting the Laplacian field, space charges can create field enhancements in some parts of the insulation. Depending on the test, duration of the voltage application, and the type of charge accumulated on the sample electrode interface the accumulation of space charges can affect the breakdown strength either positively or negatively. Especially for applications that may encounter polarity reversals, such as HVDC cables, the electric field could be enhanced due to superimposition of space charge field and applied field. In x-ray systems, tube flashovers may also result in temporary reversal of voltage polarity [39].

The DC breakdown tests performed for this thesis are short time breakdown tests, where most of the samples broke down in the range of 3-5 minutes. It has been discussed in chapter 3 that the samples that reached a stable space charge accumulation after voltage application needed typically 15-20 minutes.

The short time for voltage application added to the continuous increase in voltage, a direct relationship between the space charge behavior and the breakdown field is not easily found. Besides, the space charge measurements were performed at field levels far lower than the field strength at DC ramp voltage application.

For this thesis, more types of nanocomposites were considered for the breakdown tests than the space charge measurements. Epoxy with Al_2O_3, AlN, and MgO nanofillers were involved both in the space charge measurements and breakdown tests. As has been mentioned in the previous paragraph, it is difficult to relate the space charge behavior and short time breakdown tests. In general, MgO-Epoxy nanocomposites showed lower DC ramp breakdown strength as compared to the other nanocomposites. It is to be recalled that they scored the least average space charge by the end of 1 hour, at 18 kV/mm, in comparison to the other nanocomposites. On the other hand, Al_2O_3 nanocomposites, that had the highest homocharge in front of the cathode by the end of poling at field strength of 18 kV/mm, recorded among the highest DC ramp breakdown field strengths.

5. Concluding remarks and recommendations

In this chapter, conclusions will be drawn based on the space charge measurement and breakdown test results. The observation on the short time breakdown characteristics of the nanocomposites will then be assessed for relationship with the space charge observations. The chapter is then finalized with recommendations and a mention of possible further research.

5.1. Space charge measurements

The space charge measurements, although performed at relatively low field strengths, i.e. 10 kV/mm, 15 kV/mm, and 18 kV/mm, allow some conclusions to be made. Conclusions on the space charge characteristics will be made based on the average space charge, time constants for poling and depoling, and the space charge behavior with increasing poling voltage.
In general:

- The observation of homocharges in all the epoxy nanocomposites might be explained by enhanced charge injection due to the addition of nanofillers to epoxy [40].
- It was observed that an increase in the applied voltage resulted in an increase of the amount of accumulated charge. This is attributed to enhanced charge injection with increase in voltage.
- Due to the large homocharge accumulation compared to the space charge in the bulk of the nanocomposite, the average space charge was mainly determined by the homocharge accumulation.
- Observation of the little charge in the center of nanocomposite may be due to the fact that nanoparticles may act as recombining centers [6].
- Samples reaching fast charge saturation during poling experienced fast depletion of charges during depoling.

Al_2O_3-Epoxy nanocomposites:

These nanocomposites showed a large amount of space charge by the end of poling. The samples with the highest weight percentage of the filler, 5wt%, showed highest peak homocharge and the average space charge had not even reached saturation after 1 hour. The large amount of homocharge was attributed to the increased charge injection due to the introduction of the Al_2O_3 nanofillers. Hence, it is assumed that, a higher weight percentage of Al2O3 nanofiller in epoxy enhances charge injection. This could also be the reason for the high resistivity values measured for 5wt%_Al_2O_3-Epoxy nanocomposite at 9.6 kV/mm to be $3.0 \cdot 10^{18}$ Ωm, which is three orders of magnitude higher than that of neat epoxy, table 4.1. It is mentioned [6] that higher homocharges can act as a barrier to the charge injection in the sample.

AlN-Epoxy nanocomposites:

A similar behavior, though not as distinct, was observed for these nanocomposites. For the highest weight percentage of the filler, 5wt%, large homocharge accumulation was observed

and the space charges didn't saturate after 1 hour of poling. Hence, it can be deduced that increased in the weight percentage of AlN nanofiller to epoxy increases charge injection. Lower weight percentages of AlN nanofiller (0.5wt% and 2wt%) in epoxy showed low average space charge by the end of poling and saturation of space charges in less than 20 minutes at 18 kV/mm.

MgO-Epoxy nanocomposites:

For all the weight percentages of MgO nanofiller, very low average space charge, hence low peak homocharge, in comparison to neat epoxy was observed. Besides, all the MgO nanocomposites reached space charge saturation in less than 15 minutes. The observation of lower homocharge could be the result reduced charge injection due to the introduction of the nanofiller.

Further, for 5wt%_MgO-Epoxy nanocomposites, an increase in the poling field from 15 kV/mm to 18 kV/mm resulted in a reduction of the charge accumulated in the sample by the end of poling.

0.5wt% -BN-Epoxy nanocomposite:

The molecular structure of the BN filler is quite similar to MgO. The BN samples, however, showed very high average space charge as compared to neat epoxy and MgO nanocomposites. This can be attributed to the problems of preparing BN-Epoxy nanocomposite where agglomerations of 100-500 nm were observed. These agglomerations might act as charge traps and deteriorate the space charge management of the base material.

5.2. DC ramp breakdown tests

For almost all the nanocomposites considered during the short time breakdown tests, higher breakdown strengths were obtained with respect to neat epoxy. It is to be recalled that epoxy nanocomposites, except for MgO-epoxy nanocomposites, accumulated more homocharge by the end of poling. Hence, apart from the value of the average space charge at a certain poling field, specifying the type of interface charge, homo- or hetero-, would be very important if space charge behavior is to be associated with DC breakdown results. Since hetero-charge gives rise to increased, and homo-charge to decreased electric fields at the electrodes, where breakdown is most likely to initiate, homocharge is generally felt to be preferable to hetero-charge under DC conditions [21]. If the space charge characteristics observed for the nanocomposites under consideration happens to follow a similar trend for higher electric field values, for the cases where higher homocharge concentration were observed, the improved DC ramp breakdown field strength, among others, could be the result of the homocharge. However, as space charges might damage or deform the material locally, and hence facilitate the ageing of the material, it should be noted that higher homocharge accumulation might result a different effect when endurance tests are considered.

For epoxy nanocomposites with Al_2O_3, MgO and SiO_2 fillers, highest breakdown strengths were observed for 0.5wt% of the filler. A fall in breakdown field strength was observed when increasing the weight percentage to 2wt% and the breakdown strength didn't change with increasing the weight percentage. It could be concluded that lower filler percentages of the aforementioned fillers increase the DC ramp breakdown strength. This observation might be associated with the increase in agglomerations with increase in filler proportions.

For the 10wt%_BN-Epoxy nanocomposites considered, the breakdown strength decreased when the filler size was increased from 70 nm to 5000 nm. Besides, for a filler size of 5000 nm, breakdown field strength close to the value of neat epoxy was observed. This observation asserts the fact that when the filler size exceeds 100 nm, the interfacial interactions decrease and no significant improvements over the base materials are observed. Besides, it can be said that micro sized BN filler doesn't improve the DC ramp breakdown strength.

For the AlN+SiO_2 nanofiller mixture introduced to epoxy, the breakdown strengths observed showed very high dispersion, and hence, a low value of β=3. It was noticed that 500 nm sized AlN agglomerates were present in the samples. Hence, the dispersion in the breakdown field strengths observed was linked to the presence of these agglomerations.

5.3. Recommendations and further research

In this thesis, space charge measurements and short time breakdown tests were performed to reach the goal, characterization of epoxy nanocomposites. Based on the results of the work, some conclusions on the behavior of the nanocomposites can be drawn. What has been done, however, remains short of full explanation and further work is highly recommended.

5.3.1. Recommendations

Samples thickness:

Samples used for space charge measurement were of different thicknesses 0.6 mm to 1.3 mm. The large samples put the limit on the maximum electric field that could be applied to the samples as the voltage was limited to only 20 kV. Even though a standard thickness of 0.6 mm was chosen for the breakdown tests, the samples made later varied from 0.4 mm to 0.8 mm. It is specified [35] that, as far as possible, specimens should be identical, have the same history prior to testing, and be tested under the same conditions. The variation in thickness of the samples gives results that are not directly comparable with each other [1, 4]. This is attributed to the volume effect, where more defects are expected when the sample thickness increases. For tests that will be performed in the future, therefore, the sample preparation should be practiced so that samples with the same thickness are obtained.

Variable thickness within a sample:
Most of the samples considered had different thickness at different locations. This mostly was caused due to the slanting of the molds when they were put in the oven for curing. In determining the breakdown field, as the thickness was measured at the location of breakdown, no problem could be mentioned. This, however, posed some problems while aligning the electrode sample setup. This made the tests time consuming.

More than one sample for the space charge measurement:
Only one sample of each type of nanocomposite was considered during the space charge measurements. Although the space charge measurement procedure was well followed, sample defects can cause some errors in the results. It is advisable, therefore, to consider more than one sample for future measurements.

5.3.2. Proposed further work

Space charge measurement at higher fields:
For complete characterization of the epoxy nanocomposites, the use of higher poling fields than are considered for this thesis is very important. This would especially be important for the identification of the threshold field for space charge accumulation. 5wt%_MgO-Epoxy nanocomposite, for example, showed a decrease in the value of the average space charge when the poling field was increased from 15 kV/mm to 18 kV/mm. Higher field measurements, therefore, could be very helpful in understanding the mechanism behind this effect. Besides, this would also play a role in understanding the possible effect of homocharges in the breakdown characteristics of the samples.

Performing duration tests:
The space charge measurements have revealed that for the samples that reached space charge saturation during poling, at least 15 minutes were needed. A number of the samples, on the other hand didn't show saturation even by the end of 1 hour poling. The short time breakdown tests, performed in less than 300 seconds, would thus not incorporate the effect of space charges on the breakdown results. It is therefore important to perform longtime DC breakdown tests for the characterization of the nanocomposites. The effect of space charges on duration test could be different from DC ramp tests. This is because of the association of space charges to the ageing of the material.

Performing AC ramp tests:
It was planned to perform both DC and AC ramp breakdown tests. Problem of preparation of the AC setup limited the scope of this thesis to performing only DC ramp tests. To see the effects of switching and transients on the epoxy nanocomposites, it is important to perform

short time AC tests. In general, tests on the samples, depending on the intended application are necessary. Such tests might include temperature cycles, polarity reversals, ageing tests etc.

Introducing nanofillers to the hybrid material[12] *and performing space charge measurements and breakdown tests:*

The hybrid material (syntactic foam) is an insulating material of hollow glass spheres, with a size of 60 μm, introduced into epoxy resin. It is applied in the transformer part of the Philips CT scans. Using this hybrid material highly reduces the weight of the HV generator on the rotating part of the system. 50% -60% of the volume of the hybrid system is usually covered by the glass spheres. This proportion dramatically reduces the breakdown strength, where short time DC breakdown strengths of 23.4 kV/mm were noted for 60 vol.% of the glass content. Details about this material, can be found in [41].

Introducing nanofillers to this material and observing the space charge properties and DC breakdown characteristics sounds very important at this point. Improved breakdown strength could further reduce the weight of the HV generator and associated merits that come afterwards. As almost all epoxy nanocomposites showed higher short time DC breakdown strength than neat epoxy, similar properties might be observed for the case of the hybrid nanocomposites.

[12] Hybrid material and syntactic foam are interchangeably used.

Appendix A. Surface plots of space charge profiles

A.1. Plots for space charge growth with time

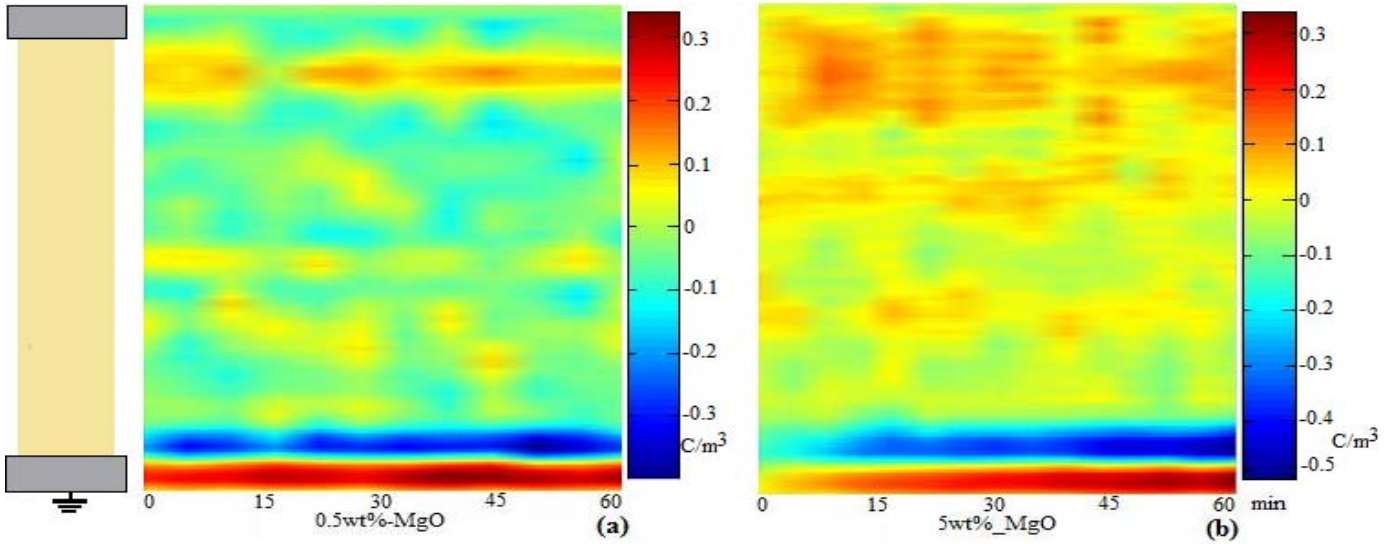

Fig. A.1 Poling profile (18kV/mm): **(a)** 0.5wt%_MgO-Epoxy, **(b)** 5wt%_MgO-Epoxy

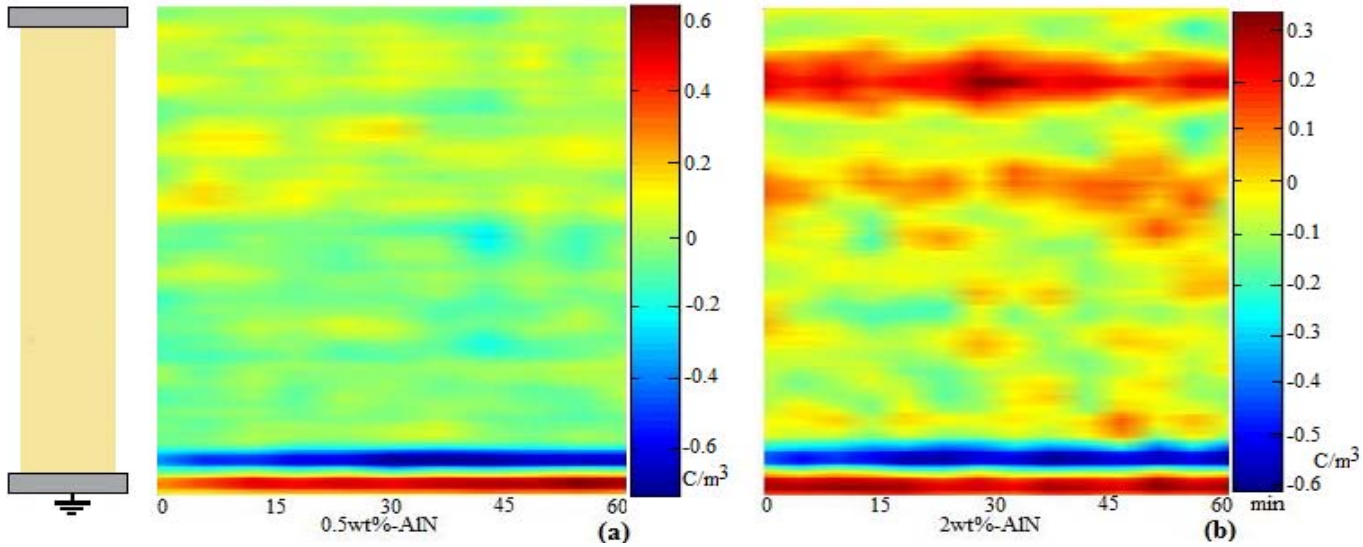

Fig. A.2 Poling profile (18kV/mm[13]): **(a)** 0.5wt%_AlN-Epoxy, **(b)** 2wt%_AlN-Epoxy

[13] O.5wt%_AlN-Epoxy was poled at 17.7kV/mm

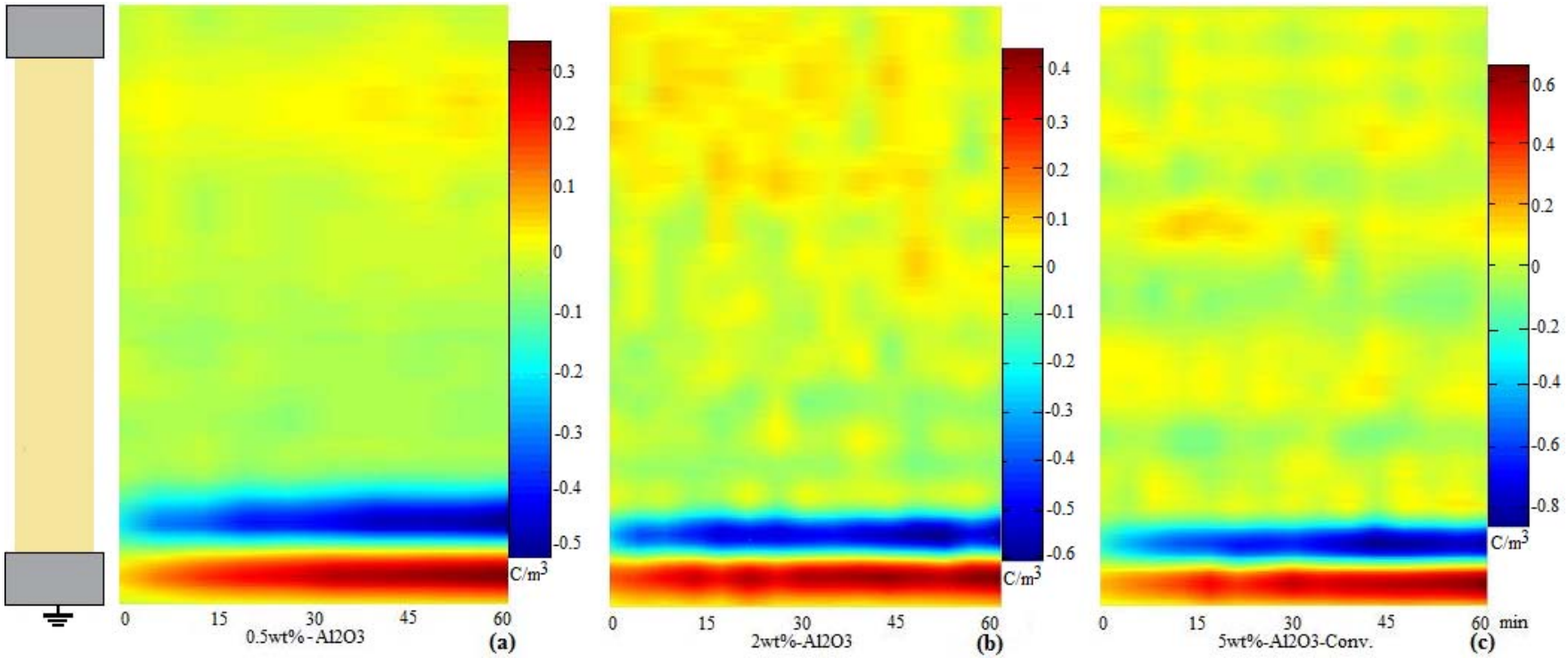

Fig. A.3 Poling profile (18kV/mm)**: (a)** 0.5wt%_Al_2O_3-Epoxy, **(b)** 2wt%_Al_2O_3-Epoxy, **(c)** 5wt%_Al_2O_3 Conv.-Epoxy

A.2. Plots for space charge depletion with time during depoling

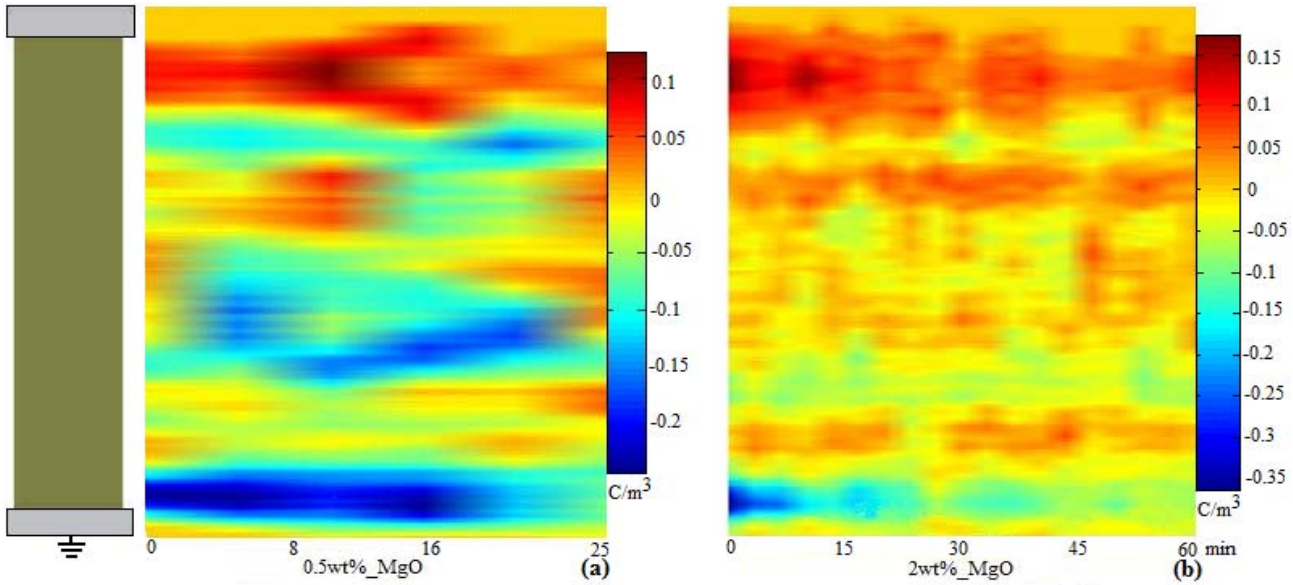

Fig. A.4 Depoling profile (from 18kV/mm): **(a)** 0.5wt%_MgO-Epoxy, **(b)** 2wt%_MgO-Epoxy

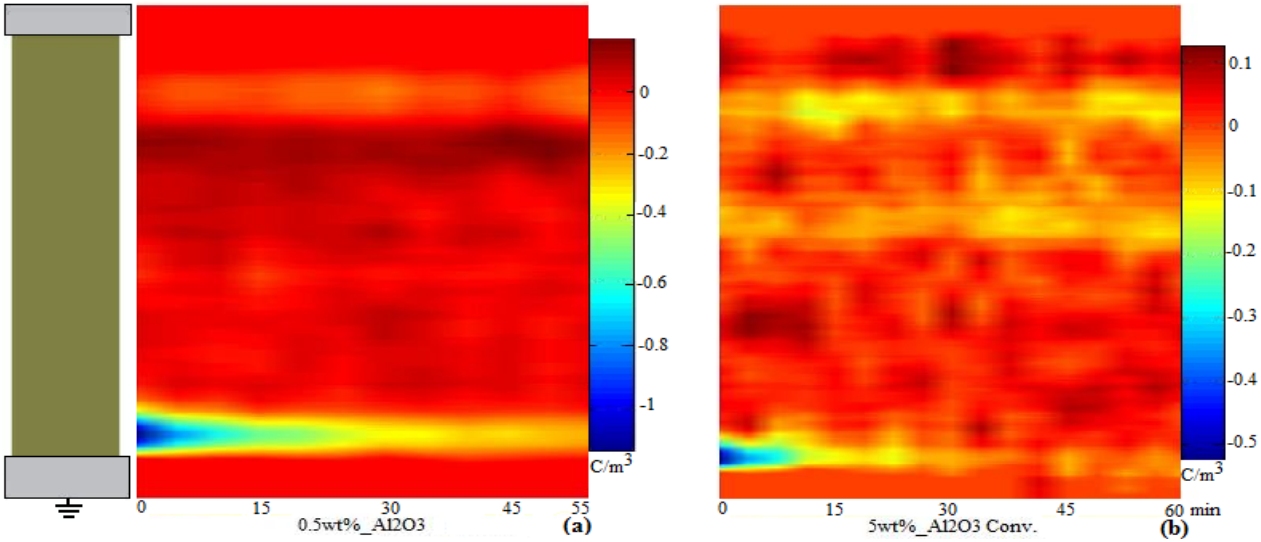

Fig. A.5 Depoling profile (from 18kV/mm): **(a)** 0.5wt%_Al_2O_3-Epoxy, **(b)** 5wt%_Al_2O_3 Conv.-Epoxy

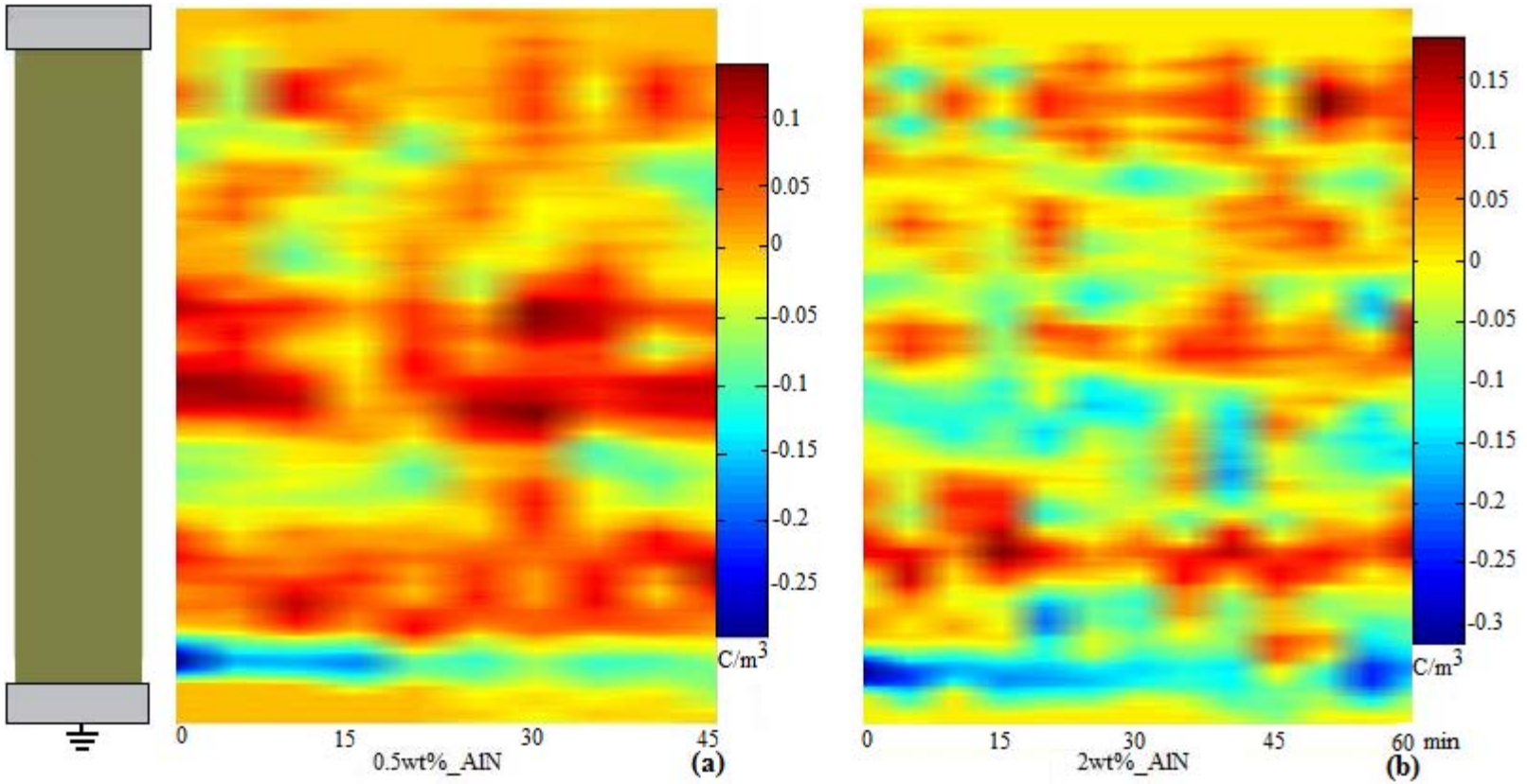

Fig. A.6 Depoling profile (from 18kV/mm[14]): **(a)** 0.5wt%_AlN-Epoxy, **(b)** 2wt%_AlN-Epoxy

[14] O.5wt%_AlN-Epoxy was depoled from 17.7kV/mm

A.3. Plots for space charge accumulation at different field levels

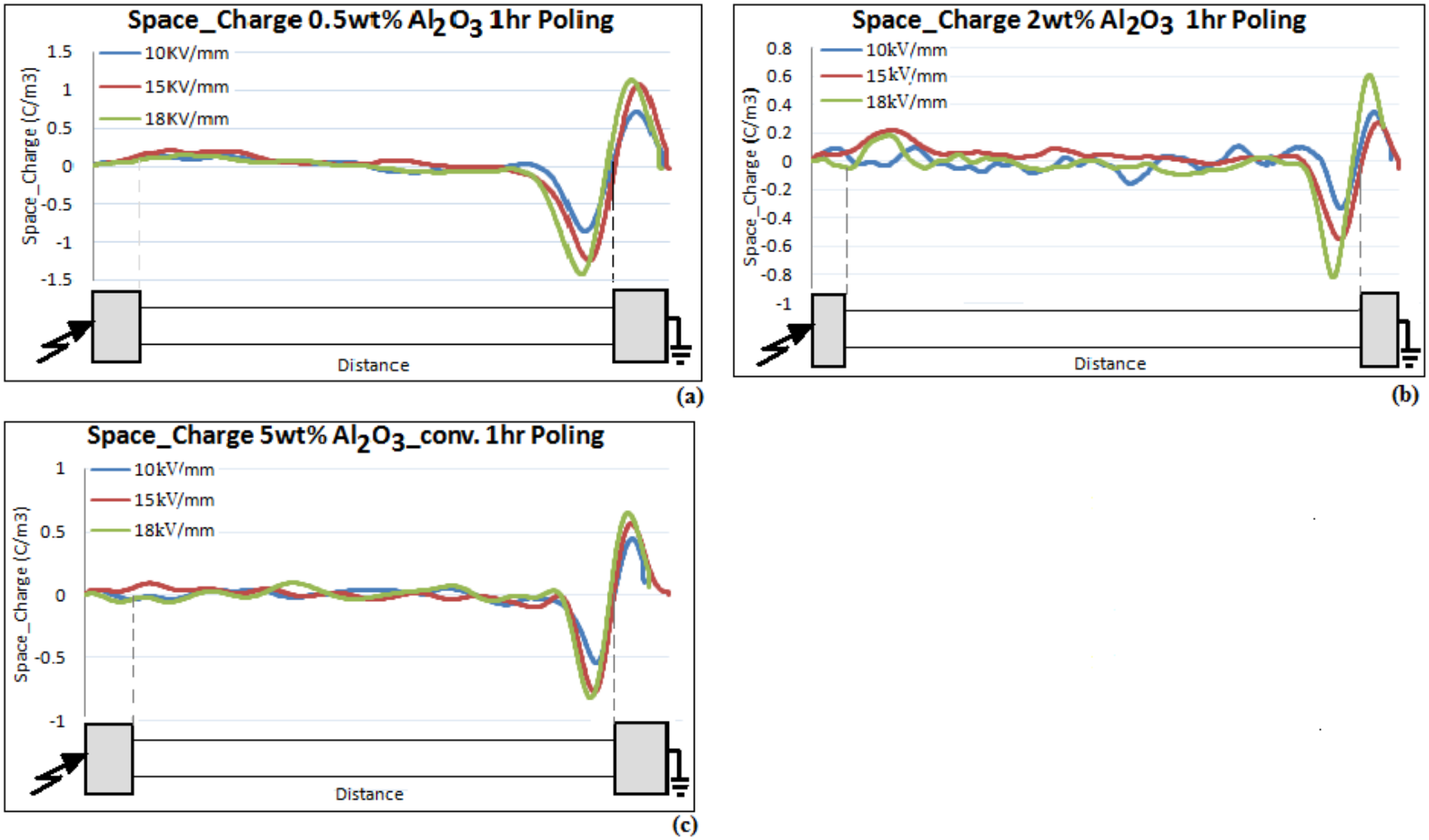

Fig. A.7 Space charge at different by the end of poling **(a)** 0.5wt%_Al_2O_3-Epoxy, **(b)** 2wt%_Al_2O_3-Epoxy, **(c)** 5wt%_Al_2O_3 Conv.-Epoxy

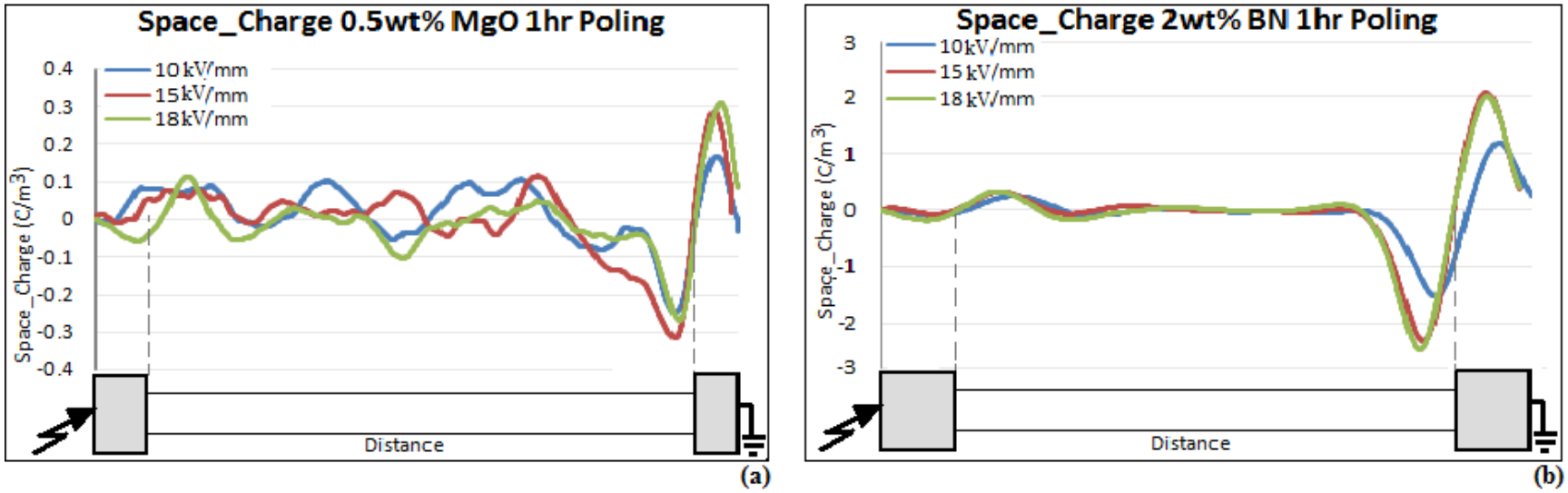

Fig. A.7 Space charge at different by the end of poling **(a)** 0.5wt%_MgO-Epoxy, **(b)** 2wt%_BN-Epoxy

Appendix B. Table for results

Table B.1 Numerical results of space charge measurements and breakdown tests

Nanocomposite	*Wt%*	*Field*	*Size of nanofiller (nm)*	*App. Time to level off charge growth (min.)*	*Avg. space charge end of 1hr(C/m^3)*	*Time to be free of charge (min)*	*Conductivity (Ωm)*	*Peak homocharge cathode (C/m^3)*	*DC ramp BD results*	
									η (kV/mm)	*β*
Al_2O_3	0,5	*10*	25 nm (ranging between some nm up to 200 nm)	30	0,164				252.3	3.8
		15		-	0,24					
		18		-	0,25	15		-1.35		
	2	*10*	25 nm (ranging between some nm up to 200 nm)	10(possibly)	0,07		$2.28\cdot10^{-19}$		218.6	10.5
		15		20(possibly)	0,1					
		18		- (possibly)	0,105			-0.78		
	5	*10*	25 nm (ranging between some nm up to 200 nm)	-	0,211		$3.30\cdot10^{-19}$		218.0	10.4
		15		-	0,25					
		18		-	0,283	-		-1.88		
	5 Conv.	*10*	4μm	5	0,073				221.0	12.3
		15		10	0,1					
		18		15	0,105	10		-0.76		
AlN	0,5	*10*	60 nm	5	0,057				189.0	3.8
		15		15	0,094					
		18		10	0,089	5		-0.62		
	2	*10*	60 nm	Unclr~5	0,098		$3.21\cdot10^{-17}$		226.4	5.1
		15		20	0,076					
		18		20	0,109	15~unclr		-0.5		
	5	*10*	60 nm	-	0,27		$5.18\cdot10^{-17}$			
		15		-	0,33					
		17,7		-	0,372	-		-1.93		
MgO	0,5	*10*	22 nm	5	0,067		$2.44\cdot10^{-17}$		241.4	6.7
		15		5	0,073					
		18		5	0,082	20		-0.25		
	2	*10*	22 nm	5	0,052				168.1	6.4
		15		15	0,069					
		18		15	0,08	5		-0.46		
	5	*10*	22 nm	15	0,048		$5.18\cdot10^{-17}$		184.1	7.3
		15		15	0,109					
		18		15	0,086	10		-0.47		
BN	0,5	*10*	20 nm (agglom. 100-500nm)	10	0,26					
		15		10	0,401					
		18		10	0,427			-2.4		
Neat Epoxy	-	*10*	-	50	0,168		$2.14\cdot10^{-16}$		162.6	10.2
		15		-	0,203					
		18		-	0,234	50		-0.98		

Appendix C. Breakdown scatter plots

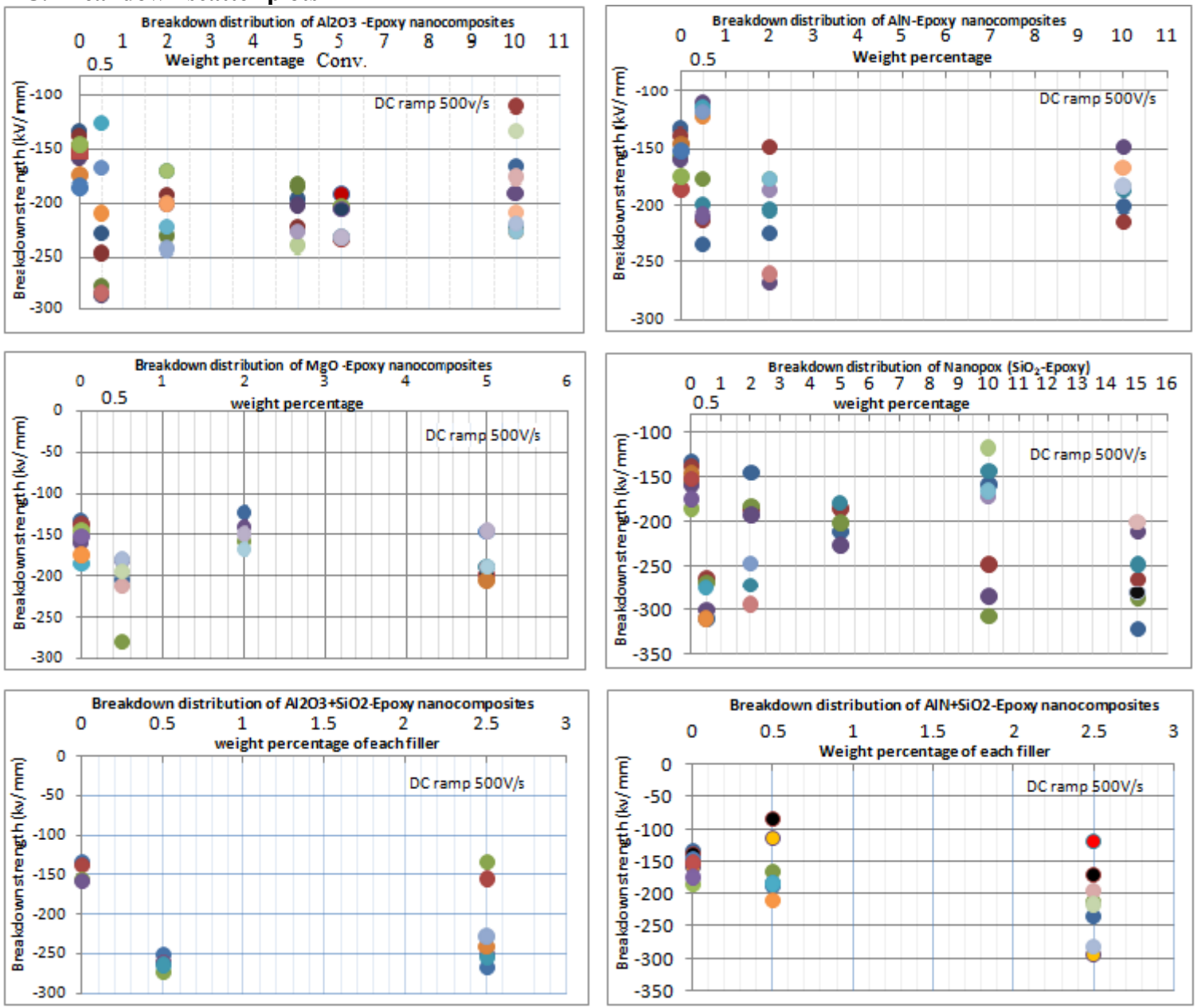

Fig. C.1 Scatter plots for DC ramp breakdown results

Bibliography

1. IEC60243-1:1998, *Electrical strength of insulating materials-Test methods Part 1: Test at power frequencies*. 1998.

2. Tesoro, G., *Epoxy resins-chemistry and technology.* Journal of Polymer Science Part C: Polymer Letters, 1988. **26**(12): p. 539.

3. S. Singha, M.J.T., *Dielectric Properties of Epoxy Nanocomposites.* IEEE transactions on Dielectrics and Electrical Insulation, February 2008. **15**(1): p. 12-23.

4. IEC60243-2:1998, *Electrical strength of insulating materials- Test methods part 2: Additionsal requierements for testing using direct voltage*. 1998.

5. P.M. Ajayan, L.S.S., P.V. Braun, *Nanocomposite science and technology*. July 2003: Wiley-VCH.

6. A. Hajiyiannis, G.C., C. Zhang, G. Stevens. *Space Charge Formation in Epoxy Resin Including Various Nanofillers*. in *Annual Report Conference on Electrical Insulation Dielectric Phenomena*. October 2008. Canada.

7. T. Andritsch, P.H.F.M., *Nanotechnology for HVDC Applications- Literature Survey Tailored Insulation Material*, in *Truimvirate IV, Report 1*. January 2007, TUDelft.

8. Nanocompositech. *Commercial nancomposites and nanoclays*. 2005; Available from: http://www.nanocompositech.com/commercial-nanocomposites-nanoclays.htm.

9. R.M. Laine, J.W.C., I. Lee, *Organic-Inorganic Nanocomposites with Completely Defined Interfacial Interactions.* Advanced Materials, 2001. **13**(11): p. 800-803.

10. M. Roy, J.K.N., R.K. MacCrone, L.S. Schadler, C.W. Reed, R. Keefe, W. Zeneger, *Polymer Nanocomposite Dielectrics – The Role of the Interface.* IEEE Transactions on Dielectrics and Electrical Insulation, August 2004. **12**(4): p. 629-643.

11. Lewis, T.J., *Interfaces are the Dominant Feature of Dielectrics at the Nanometric Level.* IEEE Transactions on Dielectrics and Electrical Insulation, October 2004. **11**(5): p. 739-753.

12. F. Sawa, T.N., T. Ozaki, T. Shimizu, M. Kozako, T. Tanaka,, *Effects of nano- and Micro-filler Mixture on Electrical Insulation Properties of Epoxy based Composites.* IEEE Transactions on Dielectrics and Electrical Insulation February 2006. **13**(1): p. 319-326.

13. M. Roy, J.K.N., L.S. Schadler, C. Zou, J.C. Fothergill. *The influence of physical and chemical linkage on the properties of nanocomposites*. in *Annual Conference Report on Electrical Insulation and Dielectric Phenomena, CEIDP*. October 2005. UK.

14. M. Kozako, S.K., T. Imai, T. Shimizu, T. Tanaka. *Surface erosion due to partial discharges on several kinds of epoxy nanocomposites*. in *Annual Conference Report on Electrical Insulation and Dielectric Phenomena, CEIDP*. October 2005. Japan.

15. M. Kozako, N.F., K. Shibata, N. Hirai, Y. Ohki, T. Okamoto, T. Tanaka. *Surface change of polyamide nanocomposite caused by partial discharges*. in *Annual Conference Report on Electrical Insulation and Dielectric Phenomena, CEIDP*. October 2003.

16. Y. Murata , Y.M., M. Nemoto, Y. Sekiguchil, Y. Inoue, M. Kanaokal, N. Hozumi, M. Nagao. *Effects of Nano-sized MgO-filler on Electrical Phenomena under DC Voltage Application in LDPE*. in *Annual Conference Report on Electrical Insulation and Dielectric Phenomena, CEIDP*. October 2005. Japan.

17. G.C. Montari, D.F., F. Palmieri, D. Kaempfer, R. Thomann, R. Mulhaupt, *Modification of electrical properties and performance of EVA and PP insulation through nanostructure by organophilic silicates.* IEEE transactions on Dielectrics and Electrical Insulation, October 2004. **11**(5): p. 754-762.

18. US Environmental Protection Agency, E.P.A., *EPA Nanotechnology White Paper*. February 2007.

19. RJ Aitken, K.C., CL Tran, *Nanoparticles: An occupational hygiene review*. 2004, Institute of Occupational Medicine: Edinburgh.

20. T. Tanaka, G.C. Montari, and R. M¨ulhaupt, *Polymer Nanocomposites as Dielectrics and Electrical Insulation-perspectives for Processing Technologies, Material Characterization and Future Applications.* IEEE transactions on Dielectrics and Electrical Insulation, October 2004. **11**(5): p. 763-784.

21. J.C. Fothergill, J.K.N., M. Fu. *Dielectric properties of epoxy nanocomposites containing TiO_2, Al_2O_3, and ZnO fillers*. in *Annual Conference Report on Electrical Insulation and Dielectric Phenomena, CEIDP*. 2004. UK.

22. T. Andritsch, P.H.F.M., *Nanotechnology for HVDC applications*, in *Truimvirate IV, Report IV*. 2007, TUDelft.

23. J. Xu, C.P.W. *High-K Nanocomposites with Core-Shell Sturctured Nanoparticles for Decoupling Applications*. in *Proceedings of the 55th Electronic Components and Technology Conference,* . June 2005. Florida, USA.

24. Kreuger, F.H., *Industrial High DC Voltage*. 1995, Delft: Delft University Press.

25. T. Takada, J.H., A. Toureille, J. Densley, N. Hampton, J. Castellon, R. Hegerberg, M. Henriksen, G.C. Montanari, M. Nagao, P. Morshuis, *Space charge measurement in dielectrics and insulating materials*. February 2006, CigreTask Force D1.12.01.

26. N. Adachi, X.Q., Y. Tanaka, T. Takada, *Comparison between the PEA Method and The PWP Method for Measuring Space Charge Distributions*. IEEE transactions on Dielectrics and Electrical Insulation, December 1998. **5**(6): p. 944-951.

27. S. Bamji, A.F., A. Bulinski and M. Abou Dakka, *Space Charge Distribution with the Phase Resolved PEA Method in XLPE Subjected to a 50 mHz AC Field.* IEEE transactions on Dielectrics and Electrical Insulation, October 2007. **14**(5): p. 1110-1112.

28. Y. Li, M.Y., T. Takada, *Pulsed Electroacoustic Method Measurement of Charge for Accumulation in Solid Dielectrics.* IEEE transactions on Dielectrics and Electrical Insulation, April 2004. **1**(2): p. 188-195.

29. G. Chen, Y.L.C., M. Fu, *Calibration of the pulsed Electroacoustic technique in the presence of trapped charge.* Measurement Science and Technology, 2006. **17**(7): p. 1974-1980.

30. Jeroense, M.J.P., *Charges and discharges in HVDC cables, in particular in mass impregnated HVDC cables*. 1997, TUDelft: Delft.

31. Y. Li, K.M., Y. Tanaka, T. Takada, M. Aihara. *Space Charge Distribution Measurement in Lossy Dielectric Materials by Pulsed Electroacoustic Method*. in *Proceeding of the 4th International Conference on Properties and Application of Dielectric Materials*. July 1994. Australia.

32. Bodega, R., *Space Charge Accumulation in Polymeric High Voltage DC Cable Systems* 2006, Delft University of Technology: Delft.

33. D. Fabiani, G.M., C. Laurent, G. Teyssedre, P. H. F. Morshuis, R. Bodega, L. A. Dissado, A. Campus, U. H. Nilsson, *HVDC Cable Design and Space Charge Accumulation. Part 1: Insulation/ Semicon Interface.* IEEE Electrical Insulation Magazine, November/December 2007. **23**(6): p. 11-19.

34. T. Andritsch, R.K., Y. Gebrekiros, U. Lafont, P.H.F. Morshuis, J.J. Smit, *Space charge accumulation in epoxy based magnesium oxide and boron nitride nanocomposites*, in *To be published at ISH*. 2009: Cape Town, South Africa.

35. DEIS, *IEEE std 930TM-2004: IEEE Guide for the Statistical Analysis of Electrical Insulation Breakdwon Data*. 2005.

36. C. Chauvet, C.L., *Weibull statistics in short-term dielectric breakdown of thin polyethylen films.* IEEE transactions on Electrical Insulation, 1993. **28**(1): p. 18-19.

37. ASTM, *D 3755-97: Standard Test Method for Dielectric Breakdown Voltage and Dielectric Strength of Solid Electrical Insulating Materials Under Direct-Voltage Stress*. 2004.

38. Len A. Dissado and J.C. Fothergill, *Electrical Degradation and Breakdown in Polymers*, ed. G.C. Stevens. 1992: Peter Peregrinus Ltd. on behalf of IEE.

39. Lunding, A., *Tube Arcing*, Y.T. Gebrekiros, Editor. 2003: Hamburg.

40. Lewis, T.J., *A Model for Nano-composite Polymer Dielectrics under Electrical Stress*, in *IEEE International Conference on Solid Dielectrics, ICSD*. 2007: Winchester, UK. p. 11-14.

41. T. Andritsch, A.L., P.H.F. Morshuis, H. Negle, J.J. Smit, *A lightweight alternative to conventional insulation materials: Synatactic Foam*, in *21st Nordic Insulation Symposium*. 2009: Gothenburg, Sweden. p. 59-62.